A Thesis Entitled

A DISCHARGE-FLOW STUDY OF SOME FUNDAMENTAL RECOMBINATION REACTIONS OF OXYGEN ATOMS IN THE GASEOUS PHASE

by

MICHAEL JOHN BALL

Submitted to the Faculty of Science
for the Degree of Doctor of Philosophy
in the University of London

Department of Chemistry
Bedford College,
London N.W.1

December 1978

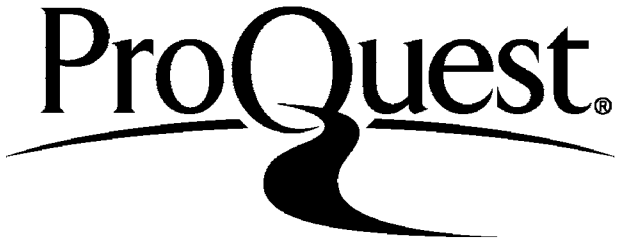

ABSTRACT

A chemiluminescence discharge-flow method was used to determine the rate constant $k_{1,M}$ in the reaction:

$$O(^3P) + O_2 + M = O_3 + M$$

for M=O_2, Ar, He, N_2, CO and CO_2 at 295 K and for M=O_2, Ar and CO_2 in the range 196-500 K at pressures in the region of 1-15 torr. The kinetic method developed enabled wall recombination coefficients, in the presence and absence of added reactant oxygen gas, to be determined individually. The use of the 'blank method' at temperatures above 300 K helped solve the discrepancy in rate constants as determined by earlier static (pulse radiolysis, flash photolysis etc.) and flow methods. The allowances for wall recombination depend on the gas phase composition (blank corrections were not made by earlier workers). In addition, in earlier flow experiments, the temperature dependence was determined for a constant mole fraction of O_2 in the presence of a third body. This work shows how an accurate, reliable determination of $k_{1,M}$ is needed.

1) for calculations on catalytic destruction of ozone in the stratosphere.

2) to supply accurate data on theoretical 'computer model' calculations of $k_{1,M}$ based on classical RRKM theory, and

3) to set up a cheap, reliable, sensitive and alternative

experimental technique to expensive and more modern ones.

The results in the range 196-500 K can be written in the form:

$$k_{1,Ar}/cm^6\ mol^{-2}\ s^{-1} = (1.49 \pm 0.04) \times 10^{14} (T/300)^{(1.5 \pm 0.3)}$$

$$k_{1,CO_2} = (6.28 \pm 0.29) \times 10^{14} (T/300)^{(1.7 \pm 0.3)}$$

$$k_{1,O_2} = (2.79 \pm 0.51) \times 10^{14} (T/300)^{(2.2 \pm 0.5)}$$

This thesis comprises a report of full time research undertaken by the author in the Physical Chemistry Laboratories of Bedford College, University of London, from October 1971 to December 1974.

ACKNOWLEDGEMENTS

I would like to express my sincere thanks to Dr. F. S. Larkin who suggested the project, supervised the earlier work and discussed the experimental results, also to Professor A. M. James, M.A., D.Phil., D.Sc., F.R.I.C., for his help and encouragement, which has made this work most satisfying.

I am indebted to Bedford College for a Tutorial Research Studentship and to the Science Research Council for an equipment grant.

I thank the academic and technical staff of the Department of Chemistry, Bedford College and my research colleagues for their help and co-operation. Thanks are also due to those at Bedford College computer terminal, and to Mr. E. Roberts at University College, London for glass-blowing assistance.

SECTION 1

Introduction

Section 1. Introduction

1.1 General Concepts

Any exothermic reaction of the type $A + B \longrightarrow \overset{*}{AB}$ (where A, B are atoms and $\overset{*}{AB}$ is a stable molecule in a vibrational (or electronically excited) state) cannot occur by a simple binary collision[1a] since the species $\overset{*}{AB}$ so formed would possess total energy ≃ 1 kT higher than the dissociation of ordinary AB molecules. A permanent recombination of the two atoms will only take place when energy is removed during the short time during which the potential energy is smaller than at infinite separation. This time is of the order of a period of one vibration, i.e. about 10^{-13} seconds.

The removal of energy may occur in one of two ways:- either by collision with a third particle during the collision time (recombination by 3-body collision) or by radiation of the energy (recombination by 2-body collision). For the case of homonuclear molecules formed by recombination, e.g. O_2^*, N_2^*, etc. in the ground state, vibrational radiation is forbidden by selection rules. In the case of heteronuclear molecules, e.g. NO*, vibrational radiation is very slow. Also, if molecules are formed in an excited electronic state from ground state atoms, then the probability of electronic transition is usually very low.

Recombination by the 2-body process is very rare, since the time that elapses on the average before an excited molecule radiates (about 10^{-8} sec.) is very large compared to the duration of the collision (10^{-13} sec.), during which the electron jump must take place in order to lead to a

recombination. Therefore, a maximum of only 1 in 10^{-5} collisions can lead to recombination by a 2-body process.

On the other hand, recombination by 3-body collision is a much more frequent process, at high or medium pressures. If τ is the average duration of a collision and Z is the collision frequency of the atoms, then the 3-body process will predominate when $Z\tau > 10^{-5}$. This is the case for most atoms such as O, N, H etc., and the 2-body process is only dominant at very low total pressures (< 0.1 torr).

This thesis contains an account of a modified discharge flow method for the study of the kinetics and rate of recombination of oxygen atoms with O_2 and with SO_2 by 3-body collisions viz.,

$$O + O_2 + M \xrightarrow{1} O_3 + M$$

$$O + SO_2 + M \xrightarrow{3} SO_3 + M$$

Sections 5 and 7 contain the experimental results for the rate constants of reactions (1) and (2) at 295K, and chapter 6 describes a determination of the temperature coefficient of reaction (1) for various M. A complete discussion of the experimental system, flow rates, pressures etc. used in this study is given in section 2.

1.2 Early Studies of Oxygen Atoms

Very early ($\sim$1922) experimental atomic recombination studies were restricted to those of hydrogen atoms. Wood[2] and Bonhoeff[3] first developed the discharge-flow method (see sections 2.2 and 2.3 for a discussion) and produced atomic hydrogen in an electrical discharge and pumped them along a cylindrical tube. However, no quantitative studies of oxygen atoms were made until the 1950's.

Many workers[7,8,11] have studied the air-afterglow (the emission resulting in the region beyond ionization from discharging air) and it's use in the study of reactions of atomic oxygen since it's discovery in 1910 by Lord Rayleigh. He demonstrated that nitric oxide was a necessary constituent of the glow but wrongly assumed that ozone was the second species necessary. Spealman and Rodebush[4] (1935) later showed that atomic oxygen and not ozone was the second constituent, and chemiluminescence was attributed to the reaction

$$\overset{*}{NO}_2 = NO_2 + h\nu \qquad \text{(emission range = 400 - 900 nm)}$$

following formation of electronically excited NO_2 assumed via a second order process (later shown to be third order)[8]. Gaydon[5] (1944) studied the role of atomic oxygen in combustion. He showed that the yellow-green continuous spectrum emitted by some flames containing nitrogen oxides was identical with the air-afterglow spectrum and was thus due to a reaction between atomic oxygen and nitric oxide. Thus the glow could be used as a qualitative test for atomic oxygen in various flames and this led to quantitative applications in CO/O_2 and H_2/air flames.

Later, McGrath and Norrish[6] (1957) studied the flash-photolytic decomposition of ozone. Under isothermal conditions in the presence of an inert gas, they identified the absorption spectrum of vibrationally excited oxygen ($\overset{*}{O}_2$) in the ground electronic state, assumed to be formed by the rapid reaction (2) below. They were able to obtain relative efficiences of various gases in promoting the rate of ozone formation viz.,

$$O + O_2 + M \underset{-1}{\overset{1}{\rightleftharpoons}} O_3 + M$$

$$O + O_3 \xrightarrow{2} {}^{*}O_2 + O_2$$

Kaufman[7] (1958) established the kinetics of the afterglow in a discharge flow system and showed that the afterglow obeyed the relation

$$I = I_o [O][NO]$$

where I_o was a constant. He thus used this relation as a quantitative measure of oxygen atom concentration (section 2.4) in the presence of a comprehensive range of reactants (which included SO_2, CO) and third bodies and obtained information on wall recombination rates (also section 2.7). Clyne and Thrush[8] showed that I^o depended on the nature of M and temperature, and calculated I^o from the relative intensity measurement calibrated from the actinometric measurements of Fontyn[9,9a] et al. These facts are fully discussed in section 2.4. A full mechanism for the air-afterglow (including radiative processes, electronic transfer etc.) is also given. Many reactions of the type $O + XO + M = XO_2 + M$ have since been found to be chemiluminescent and obey an emission law

$$I = I_o [O][XO]$$

where I and I_o may be the intensity for the complete band (integrated intensity) or only part of the band. Some examples are provided by X = C and S. This law is generally valid in only limited ranges of pressure and temperature.

A summary of earlier determinations of k_{1,O_2} at 295K are given in Table 1.1. Several investigations have been made of the thermal decomposition of O_3 in the range 298 - 1000K in order to obtain rate constants for reactions

(1), (-1), and (2), although only k_{-1} and k_1/k_2 can be determined directly by this method. Benson and Axeworthy[10] studied the decomposition in the range 310 - 350K and proposed the above mechanism for O_3 dissociation and concluded that reaction (-1) is a unimolecular reaction in the low pressure limiting region, and (2) is an overall second order reaction. This kinetic mechanism was later confirmed by direct investigations of reaction (1) and (2). Using the relative efficiency of O_2 compared to O_3 of 0.44 obtained by them and also by Castellano and Schumacher[11], Benson and Axeworthy[12] later obtained $k_1 = 1.33 \times 10^{14}$ cm^6 mol^{-2} s^{-1}, and $k_2 = 8.7 \times 10^9$ cm^3 mol^{-1} s^{-1} (Ea = -5.7 Kcal. mol^{-1}). Further work[17,18,19] establishing the kinetic mechanism of (1) and (2) is discussed below. Jones and Davidson[14] pointed out the need for an accurate determination of k_2, following the question raised by McGrath and Norrish[6] that vibrationally ($X^3\Sigma_g^-$) (and possibly electronically) excited O_2 formed in relation (2) might destroy further O_3 by the reaction

$$\overset{*}{O}_2 + O_3 = 2O_2 + O \quad (6)$$

thus providing an 'energy chain'. Elias[16a] et al. showed (by O_3 flash photolysis at 7570 nm so only ground states O_2 and O were energetically accesible) that the vibrational intensity distribution of $\overset{*}{O}_2$ appeared identical to that observed by McGrath and Norrish. Thus $\overset{*}{O}_2$ formed in reaction (2) originates from $O(^3P)$. Jones and Davidson[14] showed by their shock tube thermal decomposition of O_3 study that vibrationally excited O_2 was produced also giving a Schumann-Runge absorption spectrum similar to McGrath's[6]. However, the interpretation of this shock data (given below) does not

require the rapid occurance of reaction (6). Furthermore, work by Castellano[11] and Schumacher (on the red light photolysis of O_3) provided evidence against energy chains, since an observed quantum yield of 2.0 in pure O_3 set an upper limit of 1.05 for the chain length at room temperature. This was also the conclusion of Benson and Axeworthy.

Thus, Jones and Davidson[14] studied O_3 decomposition at temperatures between 689 and 863K(M = Ar) and 769 and 910K ($M = N_2$). The combined data with data in the range 303 to 383 due to Glissman and Schumacher[15] (which was re-interpreted by Benson and Axeworthy[10,12]) gave $k_{1,N_2} = (9.4 \pm 1) \times 10^{12}$ exp $(1700 \pm 300/RT)$ cm^6 mol^{-2} s^{-1}, $k_{-1,N_2} = (5.8 \pm 0.6) \times 10^{11}$ exp $(-23150 + 300/RT)$ cm^3 mol^{-1} s^{-1} and $k_2 = (2.4 + 0.5) \times 10^{10}$ exp $(-5600 \pm 500/RT)$ cm^3 mol^{-1} s^{-1}. At room temperature (298K) this value of k_{1,N_2} gives a value of k_{1,O_2} of 1.9×10^{14} cm^6 mol^{-2} s^{-1} in fair agreement with Benson's and Axeworthy's value of $k_{1,O_2} = 1.33 \times 10^{14}$ cm^6 mol^{-2} s^{-1} if the latter worker's relative efficiency of $O_3 : N_2$ of 0.44 is used.

Zaslowsky[16] et al. studied the decomposition by a manometric method over the pressure range 11.3 - 51.8 torr at temperatures of 388 - 403K and obtained a value of $k_{-1,O_3} = 7.98 \times 10^{12}$ exp $(-24300/RT)$ cm^3 mol^{-1} s^{-1} in reasonable agreement with Benson's value ($k_{-1,O_3} = 4.61 \pm 0.25) \times 10^{12}$ exp $(-24000/RT)$ cm^3 mol^{-1} s^{-1} and a value of $k_{1,O_2} = 1.37 \times 10^{14}$ cm^6 mol^{-2} s^{-1} also in good agreement with Benson ($k_{1,O_2} = 1.33 \times 10^{14}$ cm^6 mol^{-2} s^{-1}) at 298K.

The most reliable value for k_2 has recently been determined by Kaufman[17] using a flow system under conditions of excess O_3. This value is $k_2 = 4.5 \pm 0.36 \times 10^9$ cm^3 mol^{-1}

Table 1.1

Pre-1964 rate constants for

$O + O_2 + O_2 = O_3 + O_2$ ($T=295\pm3$ K).

	Ref.	Method	$k/10^{14}$ cm^6 mol^{-2} s^{-1}
*	7	Discharged O_2, flow, afterglow	2.0
*	10	Thermal decomposition of O_3	0.73
	14	Shock tube decomposition of O_3	1.9
	16	Thermal decomposition of O_3	1.33
	16a	Discharged O_2, flow, catalytic probe	1.0
	16b	E.S.R., flow	2.5
	16c	Discharged O_2, static, afterglow	1.1
	16d	Discharged O_2, flow, afterglow	2.2

* Extraploated to 295 K from higher temperatures.

s^{-1} at 298K and is generally lower than those given above ($E_a = -4.31 \pm 0.10$ kcal. mol^{-1}).

A brief summary of the work up to 1964 on reaction (1) is given in Table 1.1. Unfortunately, the reliability of these rate constants are open to doubt following the later work of Kaufman and Kelso[47] and Larkin[18] and Thrush (1964). These workers showed that small amounts of atomic hydrogen catalyse the removal of atomic oxygen through the homogeneous reaction sequence

$$H + O_2 + M = HO_2 + M$$

$$O + HO_2 = HO + O_2$$

$$O + HO = H + O_2$$

hence accelerating oxygen atom decay rates. Kaufman[17], and Clyne and Thrush[19] showed that electronically excited O_2 molecules (e.g. O_2 ($^1\Sigma_g^+$) can react with O_3 to regenerate O atoms and thus decelerate atomic oxygen decay via processes such as

$$O_2\ (^1\Sigma_g^+) + O_3 = O\ (^3P) + 2O_2\ (^3\Sigma_g^-)$$

and similar processes can presumably occur with higher excited states of O_2. McGrath and Norrish[20] showed that O (^1D) excited atoms react with water to generate OH radicals and Clyne and Thrush[21] showed that these react rapidly with O atoms to give hydrogen atoms viz;

$$O\ (^1D) + H_2O = 2OH$$

$$O + OH = H + O_2$$

Thus, the presence of excited O atoms and H_2O impurities can lead to high rate constants. In the light of these revelations, pre-1964 work must be considered as being unreliable since excited O_2 and/or hydrogenous impurities in flow gases were not always excluded (e.g. the value of

k_{1,O_2} determined by Francis[22] is too low, probably due to the presence of O_2^* in his system). Therefore, in this work care was taken to avoid hydrogenous impurities which generate H in the discharge cavity, or O_2 in an excited electronic state, or O (^1D). (Clyne et al.[56] show O (^1D) is absent in discharged Ar/O_2. The trapping systems, distances and discharge conditions used to overcome these snags are described in section 2.

Earlier determinations of the temperature coefficient or reaction (1) were mostly obtained from work on the decomposition of O_3. Benson[12] obtained an Arrhenius activation energy (Ea = -0.89 kcal. mol^{-1} (M = O_3, 310 - 350K), Jones and Davidson[14], -1.9 ± 0.3 kcal. mol^{-1} (M = N_2, 767 - 910K) when extrapolated with data of Benson and Axeworthy. Thus serious discrepancies exist in this determination, and the determination of the temperature coefficient of reaction (1) forms the main part of this work on the reaction. Previous temperature coefficients will be compared in section 8. Comparison of the results of the present work on reaction (1) with post-1964 data will be given in section 8, table 8.1.

On the subject of surface recombination, Smith[23] (1943) developed a side-arm method in which H and HO_x species were generated in a low pressure electrical pyrex discharge, and the rate of radical disappearance was measured along a closed pyrex side-arm by means of a catalytic thermocouple-probe. (the fraction of wall collisions leading to recombination) was determined for H, and HO_x on pyrex at 773K. Linnett[24] et al. measured (by the side-arm method) for oxygen atoms

on pyrex, silica, metals, metal oxides (293 - 573K) and found recombination to be 1st order in atomic oxygen. He stated that Smith's early work on HO_2 in particular must be treated with reserve since the actual production of HO_2 was thought to be uncertain, and be always accompanied by a complex mixture of H, O and OH species.

Voevodski[25] (1949) obtained data by a different method. The surface temperature of a glass capillary coated with various substances (e.g. metal halides, hydroxides etc.) and exposed to oxygen atoms from a Wood's type discharge was observed to rise to a high value (T = 1200K) because of an increase of γ with increasing T. Similarly, at low surface temperatures, where γ is small, little heat is released in recombination at the wall and T was small. Voevodski then established the relation (p 62)

$$\gamma = \gamma_o \, e^{-E/RT}$$

the temperature dependence (E) of recombination was found to be 6.5Kcal. mol $^{-1}$, whereas Linnett found a rapidly changing activation energy, 1 Kcal. mol $^{-1}$ at 293K rising to 13 Kcal. mol $^{-1}$ at 573K. Kaufman[26] used the Wood-Bonhoeffer flow method to show a much smaller increase of γ occurred between 298K and 1000K on vycor glass (96% SiO_2). For $k_1 = 2 \times 10^{14}$ cm^6 mol $^{-2}$ s^{-1}, he obtained $\gamma = 2.4 \times 10^{-5}$ at 298K in disagreement with those of Linnett or Voevodski. A summary of recent determinations of γ can be found in section 2.7 later, and it can be seen that recombination coefficients vary by several orders of magnitude. However, an approximate order of surfaces for high values of γ is metals $\rangle$ metal oxides $\rangle$ pyrex $\rangle$ vycor $\rangle$ coated surfaces ('Drifilm' is an excellent surface poison for studying

recombination reactions of hydrogen atoms in flow systems but a poor one for oxygen atoms as shown in the present work. In the present work, the determination of surface rate constants was an important feature, since surface effects have been considered to cause serious errors in flow methods of studying atomic reactions and especially temperature coefficients.

The reaction

$$O + O + M = O_2 + M \qquad \ldots\ 3$$

is important in atmospheric photochemistry (see section 1.3) and it s rate needs to be firmly established. The reaction was studied by Krongelb and Strandberg[27] (1951) using a paramagnetic-resonance (E.S.R.) technique and obtained $k_3 = 5 \times 10^{15}$ cm^6 mol^{-2} s^{-1} and $\gamma = 3.2 \times 10^{-4}$ (M = Ar) on clean pyrex at 298K. However, this value is in error since they attributed all recombination of atomic oxygen in the presence of molecular oxygen to occur in reaction (3) without allowing for reaction (1).

Golden and Meyerson[28] (1958) reported a value of 1.0×10^{14} cm^6 mol^{-2} s^{-1} obtained by pulse-radiolysis in a static system (M = O_2, T = 300K) in exact agreement with Morgan and Schiff[29] (M = N_2) using a fast flow method (1.0×10^{14} cm^6 mol^{-2} s^{-1}). The latter workers found γ to be 1.65×10^{-5} on clean pyrex and comparison with high temperature shock-tube data[14] indicated that the recombination temperature coefficient of k_3 (M = N_2) is small and probably not greater than $T^{-0.5}$. Harteck et al.[33] passed dilute mixtures of O_2 in Ar through a discharge and used a chemiluminescent titration technique to determine O atoms, thus obtaining a high percentage dissociation resulting in

reduction of O_3 production. The value of 0.97×10^{14} cm^6 mol^{-2} s^{-1} is again in excellent agreement with references (28) and (29).

The best determination of k_3 has been made by Campbell[30] and Thrush in a discharge-flow system for (M = Ar, N_2, T = 196 - 327K). Their value of ($k_{3,Ar} = 6.0 \pm 0.6 \times 10^{14}$ cm^6 mol^{-2} s^{-1}) $k_{3,N_2} = 11.3 \pm 1.1 \times 10^{14}$ cm^6 mol^{-2} s^{-1} is about an order of magnitude higher than those of others[28,29] which probably are effected by excited O_2 formed in discharge tubes (discussed above).

The reaction

$$O + NO + M = NO_2 + M \qquad \ldots. \quad 4$$

is a very well known atomic reaction; of the earlier workers, Ford[31] and Endow photolysed NO_2 at small partial pressures (1 - 20 torr) in a large stirred-flow reactor and obtained $k_{4,N_2} = 1.8 \times 10^{16}$ cm^6 mol^{-2} s^{-1} at room temperature. Kaufman[32] and Harteck et al.[33] both using the discharge-flow method have obtained values of $2.5 \pm 0.3 \times 10^{16}$ cm^6 mol^{-2} s^{-1} (M = Ar) and $2.7 \pm 0.2 \times 10^{16}$ cm^6 mol^{-2} s^{-1} (M = Ar, T = 298K) for k_4 respectively and in good agreement. Kaufman[32] and Gerri estimated a negative activation energy of 1.5 Kcal. mol^{-1} or k_4 proportional to $T^{-1.3}$.

Clyne and Thrush[8] used the discharge-flow method to measure k_4 obtaining $2.7 \pm 0.3 \times 10^{16}$ cm^6 mol^{-2} s^{-1} (M = Ar, T = 293K) which is the best value. k_4 (M = O_2, T = 200 - 300K) was found to have a small negative temperature coefficient which can be expressed in the form

$$k_{4,O_2} = 3 \times 10^{16} (T/273)^{-3.5 \pm 0.8}\ cm^6\ mol^{-2}\ s^{-1}.$$

Reactions (3) and (4) were potentially important side reactions in this work on reaction (1), but were made

negligible by using very low concentrations of atomic oxygen and nitric oxide (see Section 3.2 for choice of experimental conditions). A brief review of other side reactions which might be importent in the present system e.g. $O_3 + NO = NO_2 + O_2$ will be presented in section 2.

Little work has been done on the reaction

$$O(^3P) + SO_2 + M = SO_3 + M \quad .... \quad 5$$

which is important in understanding photochemical air pollution. Kaufman[7] used the discharge flow method to obtain an upper limit of $k_5 = 3 \times 10^{16}$ cm^6 mol^{-2} s^{-1} (M = Ar, T = 298K). Halstead and Thrush[34] reported a value with the same method, namely $k_5 = 4.7 \pm 0.8 \times 10^{15}$ cm^6 mol^{-2} s^{-1} (M = Ar, O_2, T = 298K) although this value may have included a contribution from the reaction

$$O + SO_2 + SO_2 = SO_3 + SO_2 \quad .... \quad 6$$

Recently Mulcahy et al[35] used the stirred-flow with both E.S.R. absorption by O and chemiluminescence from O + NO (air afterglow) to determine $[O]$. $k_{5,Ar}$ was found by extrapolating to zero $[O]$ to avoid interference from wall reactions. The experiments with E.S.R. and afterglow detection gave 1.4×10^{15} and 1.0×10^{15} cm^6 mol^{-2} s^{-1} respectively for $k_{5,Ar}$, although several corrections need to be applied to this technique, which only assumes ideal mixing in the flow reactor. Attempts to determine $k_{5,M}$ (M = Ar, SO_2, T = 295K) in the present work have been made, and results of this are set out later in section 6 and discussed in section 8. The results are similar to those of Mulcahy but are interpreted in a different way.

1.3 Atomic Oxygen Reactions in the Atmosphere and in Combustion Reactions

Reactions of oxygen atoms produced in the atmosphere by photolysis of O_2 or NO_2 play an important part in the ozone balance in the stratosphere and in photochemical air pollution; reactions of O with O_2, SO_2, CO etc. are also prominent in combustion processes. A brief discussion of the roles of such O atom reactions in these systems or environments will now be presented.

1.3.1 Photochemical Air Pollution

The principal fuels contributing to urban atmosphere pollution are coal and oil, which on combustion produce mainly SO_2, NO_x, hydrocarbons and particulate matter. SO_2 (and traces of SO_3) annual world-wide emission is estimated to be 146 million tons. The principal mechanism for SO_2 removal in clean air is considered to be the photooxidation to SO_3 (M = O_2, N_2, Ar) via the reaction (5)

$$O + SO_2 + M = SO_3 + M$$

and thus the rate for this reaction needs to be well established. At the altitudes (0 - 3km) involved in air pollution, only the photolysis of NO_2 by U.V. radiation between 360 nm and the ozone 'cut off' (light of $\lambda < 300$ nm is absorbed by the O_3 shield centred at 30 km in the stratosphere) can lead to appreciable O atom formation (typically $\sim 10^5$ atom cm^{-3}). An alternative mechanism[36] requires photoexcitation of SO_2 to it's first electronic excited state by an allowed light absorption process followed by a radiationless conversion to a long lived triplet state viz;

$$SO_2 + h\nu \longrightarrow {}^1SO_2^*$$

$${}^1SO_2^* \longrightarrow {}^3SO_2^*$$

$${}^3SO_2^* + O_2 + M \longrightarrow SO_4 + M$$

$$SO_4 + SO_2 \longrightarrow 2SO_3$$

$$SO_4 + O_2 \longrightarrow SO_3 + O_3$$

Photooxidation of SO_2 also occurs by hydrocarbons, particularly olefins but the process is slow. CO is also a common pollutant but reacts slowly with O_3 or O but not with NO_2.

60% of the NO present in the lower atmosphere is produced by the internal combustion engine. It is rapidly converted to NO_2 (see below) which is the principal light absorbing species present in smog. In air, the photodissociation of NO_2 by sunlight (the quantum yield $\sim$1 between 295 and 385 nm):

$$NO_2 + h\nu(295\text{-}430\ nm) \longrightarrow NO + O(^3P)$$

yields oxygen atoms which react primarily with molecular oxygen to form ozone, reaction (1). Leighton[37] noted the paradox that although NO_2 is efficiently photodissociated (above) in the primary photochemical act, it is ultimately reformed in highly complex photooxidation processes much faster than it is destroyed, the net result being a very rapid conversion of NO to NO_2. This conversion occurs by three major paths:

(i) reaction of nitric oxide with ozone:

$$NO + O_3 \longrightarrow NO_2 + O_2$$

(ii) thermal oxidation by molecular oxygen:

$$2NO + O_2 \longrightarrow 2NO_2$$

(iii) reaction of nitric oxide with radicals such as hydroperoxy, $HO_2^{\bullet}$, alkylperoxy, $RO_2^{\bullet}$, and acylperoxy, $RCO_3^{\bullet}$, formed by hydrocarbon oxidation.

$$\begin{matrix} HO_2 & & HO \\ RO_2 & + NO \longrightarrow NO_2 + & RO \\ RCO_3 & & RCO_2 \end{matrix}$$

By themselves, the reactions of ozone and oxygen atoms with hydrocarbons and nitric oxide are insufficient to account for either the rate of conversion of NO to NO_2 or the rates of consumption of hydrocarbons observed both in smog-chamber studies[40] in the torr region, and in ambient air. Therefore, other oxidizing species must contribute importantly to the generation of photochemical smog. Radical intermediates eg. OH seem most likely. In 1970[77] the rate constant for the reaction of CO with HO was shown to be $1.1 \times 10^{11} cm^3 mol^{-1} s^{-1}$, a value 10^3 times greater than previously believed. This led to the proposal of the following chain reaction:

$$HO + CO \longrightarrow H + CO_2$$

$$H + O_2 + M \longrightarrow HO_2 + M$$

$$HO_2 + NO \longrightarrow HO + NO_2$$

This proposal was important since:

(i) it stimulated further work on reactions of HO and HO_2 in urban atmospheres;

(ii) it focused further attention on the central smog process,

$NO \rightarrow NO_2$ conversion; and

(iii) it emphasised the possible importance of other radical intermediates such as H and HO_2.

The 'relevance' of air pollution was recently dramatically reaffirmed when in June 1974, Los Angeles U.S.A., oxidant levels exceeded maximum permitted levels of 0.7p.p.m., a level reached only a few times in history. This occurred despite 20 years of air pollution control by scientists and legislation.

1.3.2 The Photochemistry and Kinetics of Ozone Formation and Destruction in the Stratosphere.

The ozone layer of the stratosphere, centred at 30 km is responsible for the absorption of much harmful, intense (for $\lambda < 300$ nm), u.v. radiation incident on the earth. It is therefore of great interest to measure and to calculate the present day concentrations of O_3 in the upper atmosphere.

The fundamental reactions which establish the ozone layer are given by the 'classical'[38] scheme for an oxygen-only atmosphere viz;

$$O_2 + h\nu = 2O \quad , \lambda < 242.4 \text{ nm} \quad \ldots\ldots\ldots(a)$$

$$O_3 + h\nu = O + O_2, \lambda < 1140 \text{ nm} \quad \ldots\ldots\ldots(b)$$

$$O + O_2 + M = O_3 + M \quad \ldots\ldots\ldots(1)$$

$$O + O_3 = 2O_2 \quad \ldots\ldots\ldots(2)$$

$$2O + M = O_2 + M \quad \ldots\ldots\ldots(3)$$

The rate constants for these reactions together with the calculated rates of dissociation of O_2 and O_3 for an overhead sun can be

combined to predict the O_3 concentration at any altitude (10-100 km) in the atmosphere. Satellites, rockets and balloon-sounding equipment have been used to determine vertical distributions of O and O_3. Hunt[39] calculated a photochemical O_3 profile for an oxygen only atmosphere and compared it with experimental results. However, based on this model, the calculated O_3 distribution was a gross overestimate of the observed atmospheric distribution. The above scheme leads to O_3 concentrations at photochemical equilibrium given by:

$$\left[O_3\right] = \left[\frac{J_a}{J_b}\cdot\frac{k_1}{k_2}\cdot\left[M\right]\right]^{\frac{1}{2}}\left[O_2\right] \qquad \ldots.(I)$$

(since reaction (3) may be neglected below 50 km). Where k_1 and k_2 are the kinetic rate constants for reactions (1) and (2) and J_a and J_b are the photolytic rate constants for reactions (a) and (b). However, any assessment of this scheme depends critically on the values of k_1/k_2 in the range 200-300 K; a reliable determination of this ratio is clearly needed.

Bates and Nicolet[57] developed a hydrogen-oxygen ('moist') only atmosphere model and Hunt[39] recalculated O_3 profiles using this model. The results showed a remarkable O_3 concentration reduction at all levels owing of the inclusion of H-atom reactions. Later, Crutzen[41] pointed out that the rate constants chosen for the chain reaction:

$OH + O_3 = HO_2 + O_2$ (4) $\quad k = 1.5\times10^{-12}T^{\frac{1}{2}}\exp(\frac{-1500}{T})\,cm^6\,molecule^{-2}\,s^{-1}$

and $HO_2 + O_3 = OH + 2O_2$ (5) (neglected)

in the 'moist' model gave closer agreement between theoretical

and observed O_3 concentrations, but stated that since two bonds must be broken in reaction(5), then this reaction must be slow. This again led to O_3 concentrations that were too large. Furthermore, the 'moist' model included no form of correction for molecular and eddy diffusion, particularly important at altitudes above 80 km.

Crutzen[41] and Johnson[42] have drawn attention to the catalytic role of nitrogen oxides (NO_x) produced by atmospheric pollution from supersonic air traffic (SST). Johnson calculated O_3 concentrations using an extensive reaction sequence involving the catalytic removal of O_3 by NO_x and HO_x. To a zero'th' approximation (ie. in the absence of NO_x and HO_x catalyses), the O_3 concentration at a given height was given by equation I above. The rates of production (P) and destruction (D) of O_3 are given by

$$\frac{d[O_3]}{dt} = 2J_a[O_2] - 2k_2C[O][O_3] = P - DC$$

where C is the catalytic coefficient (unity in the absence of catalysis) and $[O] = \frac{J_b[O_3]}{k_1[O_2][M]}$ to a satisfactory approximation.

For mean daytime concentrations and currently accepted reactions and rate constants in the stratosphere, some of the more important catalytic chains to be considered are:

chain (1) $O + NO_2 = NO + O_2$

$NO + O_3 = NO_2 + O_2$

chain (2) $O + HO_2 = OH + O_2$

$OH + O_3 = HO_2 + O_2$

$$O \quad = OH + \quad$$

$$\quad = \quad + O_2$$

chain (3) $O + OH = H + O_2$

$H + O_3 = OH + O_2$

chain (4) $OH + O_3 = HO_2 + O_2$

$O_3 + HO_2 = OH + 2O_2$

with current experimental measurements of NO_x and HO_x, the expression given above for $[O_3]$ still leads to a small over-estimate (a factor of 2-3) of peak O_3 levels.

Thus Johnson[42] calculates that the increase in NO_x from estimated SST densities in the near future could reduce the O_3 shield by a factor of about 2, thus permitting the harsh (< 300 nm) u.v. radiation to permeate the lower atmosphere. This is also supported by Hampson[43] who draws attention to the potential danger of thermonuclear warfare in that atmospherically generated NO_x could destroy the O_3 layer. In contrast, Tuck[44] pointed out that large fluxes of NO_x generated by nuclear tests during the winter of 1961-62 caused little, if any, change in O_3 levels. Johnson[42] argues that this may be due to the tests being confined to only the northerly latitudes and low altitudes used in the largest tests in the past.

It has been discovered[75] that electronically excited oxygen $O(^1D)$ atoms react with commercial fluorocarbons at rates which are essentially diffusion controlled viz:

$$O(^1D) + CFCl_3 \longrightarrow \text{products} \quad (k = 3.5 \times 10^{11}\ cm^3 mol^{-1} s^{-1})$$

(The principal products include COFCl and possibly molecular chlorine).

It has been proposed that chlorine atoms produced by photodissociation of $CFCl_3$ may initiate chain sequences which might deplete the O_3 layer (cf. NO_2) eg.

$$Cl + O_3 \longrightarrow ClO + O_2$$
$$ClO + O \longrightarrow Cl + O_2$$

The potential of this mechanism in the stratosphere depends on whether there is an appreciable vertical transport of fluorocarbons from the troposphere (where they are released as aerosols) to the stratosphere. Eggleton et al.[45] showed that O_3 and/or fluorocarbons can be transported over distances 100-1000 km in North Western Europe and can, on occasions, provide a major contribution to photochemical pollution in the U.K. However, if such transport does occur, there remains the question of whether or not fluorocarbons would compete significantly with other halogenated compounds already present, as precursors to Cl atoms.

1.3.3 Roles of Atomic Oxygen in Combustion

In recent years, much research[68] on the kinetics of reactions occuring in flames has been carried out. A flame can be considered as two 'zones', (i) the primary reaction zone - an inner cone in which intense reaction of the pre-mixed reactants occurs and (ii) the 'burned' or post flame gas. Kinetic studies[69] have been conducted on both zones. However, rather elaborate procedures are necessary to extract rate constants or Arrhenius parameters from the experimental data. Many gaseous oxidations are chain reactions involving free atoms or radicals such as O, H, OH and O_2H. Chain mechanisms can explain the existence

of sharply defined explosion limits, the influence of inert gases and the effects of small amounts of catalysts on reaction rates.

The concentration of radicals in flames can be determined by several methods. OH radicals have been measured by their absorption in the ultraviolet region. Radicals such as CH_3, C_2, CH, S_2 have been monitored in various flames by absorption photometry. Relative H concentrations can be determined from the emission intensity from CuH radicals formed in an electronically excited state when a copper salt is added to the flame. Gaydon[5] studied the yellow green continuum (see section 2.3) in flames. The colour results from radiation from an electronically excited state of NO_2, formed by reaction of atomic oxygen and nitric oxide. Thus, addition of NO to a flame served as a qualitative test for the presence of O_2 atoms. More recently[70], radical concentrations have been determined by E.S.R. spectrometry. The flame is either situated in the cavity of the spectrometer or, with more precision, it is sampled into the cavity by expanding the gases rapidly through a fine probe. The concentration of hydrogen atoms is most conveniently measured indirectly[71] by adding a trace of lithium salt to the reactants (as an aqueous mist from an atomizer). The lithium exists in the flame both as free atoms and lithium hydroxide and the species come rapidly to equilibrium with hydrogen atoms present by the reaction:

$$Li + H_2O \rightleftarrows LiOH + H$$

The lithium concentration is determined by atomic absorption photometry. The standard apparatus is the flat flame burner,

an elaborate version of a laboratory Meker burner. By varying gas flow velocities through the burner, a range of reaction temperatures can be obtained and measured by a thermocouple. This method is suitable for kinetic studies only in the post-flame region.

The reactions, however, occur under conditions whereby the temperature and the linear flow velocity as well as the concentrations of products increase steeply with time (distance). The steep concentration gradients cause the reactant molecules to diffuse rapidly forwards and product molecules backwards in the flowing medium. Thus unfortunately the concentration of a species being observed at any point is determined to a significant extent by diffusion.

Whittingham[46] studied the oxidation of SO_2 in a bunsen flame during the slow combustion of CO and concluded that oxidation took place through a termolecular addition with O as well as bimolecular addition depending on the nature and concentration of other constituents. HO radicals also play an important part in processes such as:

$$SO_2 + OH = SO_3 + H$$

but this reaction is endothermic and likely to be slow compared with:

$$O + SO_2 + M = SO_3 + M$$

The primary reaction of the methane-oxygen flame has been investigated carefully by Fristrom et al.[72] It seems certain that the endothermic reaction:

$$O_2 + CH_4 = HO_2 + CH_3 \qquad .....(c)$$

makes a negligible contribution to CH_4 consumption. Its

maximum possible rate, calculated at 1650 K is several orders of magnitude less than the rate of formation of CH_4. The likely radical attackers are H, OH and O and since the concentration of H is low in the presence of excess O_2, this leaves O and OH. Results of studies of the reactions:

$$O + CH_4 = OH + CH_3 \qquad .....(d)$$

$$\text{and} \quad OH + CH_4 = H_2O + CH_3 \qquad .....(e)$$

by flow-tube[73] and flash photolysis[74] techniques suggest that reaction (e) is an order of magnitude faster than (d) at 1650 K. Since, also, O is usually less abundant in flames than OH, then to a first approximation, reaction (e) can be considered the sole means by which methane is destroyed.

1.4 Modern Experimental Techniques

The growing and renewed interest in the chemistry of the upper atmosphere and photochemical air pollution has led to a need for accurate, reliable rate data for atomic reactions of the type described previously. Several new or modified techniques have found application in oxygen atom studies and some will now be briefly reviewed under the headings 'flow' and 'static' methods.

Since 1958 (Kaufman[7]), many atomic recombination reactions have been studied by fast-flow (or modified Wood-Bonhoeffer) methods. Flow systems are most convenient for the measurement of O-atom combination reactions, eg. the present method can be used to study reactions with third-order rate constants in the range 10^{13}-10^{17} $cm^6 mol^{-2} s^{-1}$. The flow system can be constructed

so that atomic decay profiles along the reaction tube can be determined (see section 2.4 and 5.2), and optimum conditions obtained by adjusting flow rates, pressures and mean gas flow velocities. This limits systematic errors to instrumental measurements (5-7% error) and surface reactions. The latter are the main disadvantages but are effectively eliminated by the present technique. High atomic concentrations (10^{12}-10^{14} molecule cm^{-3}) can be produced and measured absolutely, enabling reactions of various kinetic orders to be measured. However, total pressures are generally limited to 1-20 torr although the present method may make the study of reactions obeying first order kinetics in atomic concentration up to 1 atmosphere feasible.

Other techniques, based on this method have recently been developed. Kaufman and Kelso[47] have used a pyrolysis-flow tube technique in which ozonized oxygen (0.3-0.4% O_3) is dissociated in a quartz tube at 1100-1400 K. The main advantage of this is that no excited species (section 2.4) are produced. Ozone has also been dissociated using a Nernst glower.[17] One further modification of the flow-method, ie. the stirred-flow method, is discussed below.

Jennings[48] and Kaufman[26] have reviewed the various absolute and relative methods of determining atomic concentrations in flow systems. Calorimetric probes, which have mainly been applied to H[49] and O[58,16a] atoms, are sensitive and accurate when operated isothermally but not specific and thus cannot be used directly to follow reactions where several active species are formed or destroyed. Wrede-gauges are also non-specific

and lose accuracy at low atomic concentrations. Furthermore, they can be used only at fixed positions along a tube. However, both of these methods are absolute.

The 'titration' method[7,8] is analogous to analytical titrimetry in solution. A gaseous reactant is added to the flowing atomic stream to be determined, and its flow rate is increased until all the atoms are consumed. The added reactant must react rapidly, specifically and stoichiometrically so that no interference from other reactions occur. Hence, the number of molecules of reactant at the 'end point' is equivalent to the number of atoms originally present. In order to apply this technique, a reaction is needed that occurs within fewer than a hundred or so collisions. A few of these are given below in Table 1.4. The 'end point' can be determined photometrically (if the reaction is chemiluminescent) or by end-product analysis.

For example, on addition of NO_2 to O-atoms, (reaction (a))

Table 1.4

Reaction	$k/cm^3\ mol^{-1}\ s^{-1}$ at 298 K	Reference
a) $O + NO_2 = NO + O_2$	4×10^{12}	67
b) $N + NO = N_2 + O$	2×10^{13}	8
c) $H + NO_2 = HO + NO$	3×10^{13}	68
d) $O + Br_2 = OBr + Br$	5×10^{12}	69

[N.B. , reaction (b) may be used as a method of producing ground state O-atoms to ensure the elimination of excited species,

eg. $O_2(^3\Sigma_u^+)$, $O_2(^1\Sigma_g^+)$ usually produced in electrical discharges (section 2.3)].

a greenish-yellow chemiluminescence appears in the flowing gas. The glow arises from the electronically excited NO_2 formed in the reaction;

$$O + NO + M = N^*O_2 + M$$

$$N^*O_2 = NO_2 + h\nu \quad \text{(green-yellow)}$$

The method is absolute, precise, sensitive and can be applied in simple apparatus.

E.S.R. provides a modern tool for the measurement of atomic concentrations. The intensity of the E.S.R. signal is directly proportional to the atomic concentration provided certain conditions are met and provides a good specific measurement. The reaction is not perturbed and there is virtually no interference from other species since magnetic resonance occurs only with species of unpaired electrons. However, although calibration is relatively simple, E.S.R. equipment is bulky and expensive and atomic concentrations generally have to be measured at a fixed point in a quartz tube. Measurement of temperature coefficients thus becomes difficult and elaborate design of flow systems is required. The technique can be used as an absolute or relative one, and is the most sensitive of all absolute methods. Atomic concentrations as low as 10^9 atom cm^{-3} have been measured.

Turning to relative methods, (resonance-fluorescence described below can also be used as a relative one), the technique used in the present work stems from the chemiluminescent reaction given immediately above. The intensity of the yellow-green air- 'afterglow' is given (section 2.4) by $I = I_o[O][NO]$.

Only a minute concentration of NO is necessary since the small amount of NO used to form excited NO_2 is immediately regenerated by the very rapid reaction:

$$O + NO_2 = NO + O_2$$

The concentration of NO thus remains accurately constant along the flow tube and the intensity of the glow at any time is exactly proportional to the concentration of oxygen atoms. This technique can be made up to an order of magnitude more sensitive than E.S.R. and can be applied successfully to the measurement of temperature coefficients and to the measurement of rates of reactions such as:

$$O + CO + M = CO_2 + M$$

which have hitherto not been attempted successfully in a flow system.

Flash photolysis is a static technique which utilizes an intense flash of light (Energy 100-2000 J, λ=200-500 nm) to produce rapid dissociation or excitation in a chemical system in a time less than the time scale of subsequent reactions involving the species produced. Reactions with half-lives down to 10^{-5} s can be studied ($<10^{-8}$s by laser flash-photolysis). Transient species may be produced under isothermal or adiabatic conditions and observed by absorption spectroscopy, mass spectro-

metry, E.S.R. or some other suitable technique. The adiabatic technique is particularly suited to the study of pyrolytic and explosive reactions; early work was done on anti-knock additives in petroleum by this method. The isothermal technique (in which the heat capacity of the system is increased by addition of an inert gas) is useful for observing excited reactive species, eg. in the study of intermediates in combustion processes or the thermal decomposition of O_3 and oxidation of methane. In the isothermal decomposition of O_3, flash photolysis showed that the mechanism necessitated a chain reaction propagated by vibrationally excited ground state O_2 molecules ($v>17$) and not electronically excited molecules. This fact was later re-examined by Clyne et al.[19] who reported no evidence of an energy chain but found that species such as O_2 ($^1\Sigma_g^+$) (section 1.2) decelerated O-atom decay. Flash-photolysis has recently been used as a tool in developing new techniques for the determination of rates of atomic/free radical reactions and these are discussed below. Excellent work on oxygen atoms has been done by Huie et al.[59] with a flash photolysis-resonance fluorescence technique (section 8). Atomic oxygen decay was monitored by following atomic oxygen resonance radiation. The fluorescence signal was recorded on a multi-channel analyser and multiple flashes (>100) were used to generate one kinetic decay curve, thus greatly reducing statistical errors. Over the pressure range and conditions used (50-5000 torr), the important advantage of this method (cf. present work) is that secondary and wall reactions can be entirely neglected. This method is the most reliable alternative to the discharge flow

method although only first-order atomic reactions can be studied at present, and apparatus is expensive and elaborate to set up.

The shock tube[62] provides a static technique for the study of (a) very fast processes and (b) dissociation energies, by a purely thermal method. A shock 'wave' provides a means of producing a very high temperature in a gas by very rapid adiabatic compression in times of the order 10^{-10} s at N.T.P. The shock transition (a) is so abrupt that it is regarded as a mathematical discontinuity and (b) propagates without change through the medium (ie. it remains sharp). The shock is supersonic since some collisional processes occur at the speed of sound. The reacting gas, after passage of the shock front, is observed by spectroscopic, densitometric and other methods with a resolution <10 ms. Several studies (section 1.2) have been made with this technique. Jones and Davidson studied the thermal decomposition of O_3 in argon gas and obtained k_{-1} and hence k_1 knowing $\Delta H_f^{\ominus}(O_3,g)$. However, elaborate and expensive equipment is once again necessary, with electronic devices for measuring shock velocity, monitoring atomic decay profiles and other problems.

In the 'stirred-flow reactor' method of Mulcahy et al.,[50] a large volume (~2 litre) spherical reactor at a pressure 1-8 torr was used and relative concentrations of oxygen atoms at the inlet and outlet parts were determined photometrically from the air afterglow intensities at these positions. A special 'double cavity' E.S.R. detection method was used while studying atomic oxygen-sulphur dioxide reactions but this proved less reliable than the photometric technique. Perfect gas mixing is assumed to occur in this type of reactor but this has

been criticised.[50] Several corrections are also necessary to allow for reactions occurring in the tubing between the measuring points and the reactor giving rise to large positive systematic errors (eg. rate constants are too high). Surface reactions, however, are not so important here as in the discharge-flow method.

When oxygen is irradiated at a high dose-rate by an electron pulse, the primary processes leading to O-atoms are rapid compared with the subsequent reactions of the atoms. Thus pulse-radiolysis provides a convenient method for studying these reactions. Pulse-radiolysis is defined as including all experiments in which a transient species produced by a pulse of ionizing radiation is directly observed by means of one of its properties, eg. optical absorption, E.S.R. etc. A pulsed electron accelerator can produce a high current, microsecond-pulse of electrons ($\sim$20 MeV). Detection methods are basically similar to those used in flash photolysis but a Fricke dosimeter is used to measure the absolute amount of energy deposited in a cell by the electron pulse. Bevan and Johnson[51] used the technique to determine $k_{1,O_2} = 1.9 \times 10^{14}$ cm^6 mol^{-2} s^{-1} ($T = 295 \pm 1$ K) a value which is in excellent agreement with the present value (2.1×10^{14} cm^6 mol^{-2} s^{-1}), and observed the presence of two intermediates in the reaction (1) which were assumed to be vibrationally excited O_3. However, again, pulse-radiolysis methods are restricted to first-order atomic reactions usually, since O_3 is measured spectrophotometrically. Pressures used range from 1-100 atmospheres but there seems to be large negative systematic errors in some cases, possibly due to the presence of excited species such as $O(^1S)$ or $O(^1D)$, and/or due to distortion

of absorption bands by vibrationally excited products.

Donovan et al.[60] produced oxygen atoms by flash photolysis of O_2 (λ>175 nm) and observed the decay via the resonance absorption transitions ($3^3S_1 \rightarrow 2^3P_J$) in the region of 130 nm using a vacuum ultraviolet monochromator (kinetic absorption spectroscopy). Similarly, Stuhl and Niki[61] generated O-atoms by pulsed-u.v. photolysis of NO, O_2, CO_2 and N_2O and monitored them by N^*O_2 or C^*O_2 chemiluminescent emission. Third order rate constants in the range 10^{15}-10^{19} cm^6 mol^{-2} s^{-1} could be determined with good accuracy ($\pm$10%) but with the limitations of other resonance methods.

The technique of resonance-fluorescence/flash photolysis has already been described above. However, in atomic resonance-absorption, the measurement of the absorption of resonance radiation emitted from an appropriate source is involved. Oxygen atoms were determined using this method by Slanger and Black.[52] O-atoms were produced by photodissociation of O_2 by 147 nm radiation from a xenon resonance lamp. Dissociation resulted in the formation of one $O(^3P)$ and one $O(^1D)$ atom, the latter being rapidly deactivated by O_2 to $O(^3P)$ in a time short compared with recombination half-lives. Resonance radiation (130 nm) was then scattered from the $O(^3P)$ atoms into a solar blind photomultiplier. Pulsing of the xenon lamp permitted repeated measurements to be made of the $O(^3P)$ decay rate, which could be obtained as a function of the various reactant concentrations, enabling rate constants to be determined. However, the fact that the resonance lines of atoms (O, H, N) lie in the vacuum ultraviolet makes the design and operation complicated

and elaborate. The method can follow relative concentrations of any specific species (that is fluorescent), can be used at high pressures (50-500 torr) when surface effects are entirely negligible, and is very sensitive (concentrations down to 10^9-10^{10} atoms cm^{-3} can be reached). At lower pressures, (0-100 torr) the main disadvantage is that the wall losses must be minimized, otherwise the fluorescence signal becomes inconveniently small.

Cvetanovic[53] has developed a modulation technique for studying atomic reactions. This technique for the sinusoidally modulated production of $Hg6(^3P_1)$ was adapted for modulated generation of $O(^3P)$ atoms in the mercury photosensitized decomposition of nitrous oxide, viz;

$$N_2O + Hg6(^3P_1) \longrightarrow N_2 + O(^3P) + Hg6(^1S_0)$$

The oxygen atoms were then monitored by the NO_2 afterglow fluorescence from the reaction of $O(^3P)$ with admixed NO. Decay of $O(^3P)$ with reactant resulted in a phase shift of the NO_2 fluorescence relative to the incident 253.7 nm mercury resonance radiation. The phase shifts were accurately determined and related in a simple manner to rate constants. Again, this new method has only been used for first-order reactions to date.

With the development of new techniques since 1964, the discrepancies in the measurement of k_1 are still considerably greater than the estimated experimental errors of 10-25% (see section 8 for table of post-1964 data), and these must be attributed to unknown sources of systematic error. Similarly, the absolute discrepancy at 200K of the rate constant ($M=Ar,CO_2$)

of reaction (1) as determined by the earlier discharge-flow and static systems[7,16c] is up to an order of magnitude. The temperature coefficient is important in understanding photochemical smog and stratospheric chemistry.

The present discharge-flow method was further developed to resolve these discrepancies firstly by determining whether significant changes in surface recombination rates occurred in the presence of various third bodies at 295 K; for the more active surfaces, O_2 reduces the surface efficiency by poisoning. Secondly, the temperature coefficient needs to be re-measured in the flow-system ($M=Ar, O_2, CO_2$) to give a value in satisfactory agreement with the best alternative method (resonance-fluorescence). No direct determination of the temperature coefficient for $M=O_2$ over a large range of temperature has previously be made, even though this is one of the abundant third bodies in the upper atmosphere.

Of the newer techniques, the flash photolysis-resonance fluorescence, flash photolysis-resonance absorption, pulse radiolysis and modulation systems have been used only for relative atomic concentration neasurements, although steps are being made to develop absolute fluorescence and absorption measurements.[63] Thus, the discharge-flow method is still the most general and accurate method of determining rate constants for reactions of any kinetic order in atomic concentration. For this reason a critical examination of absolute accuracy and reliability of the discharge-flow method (especially with regard to surface effects) is especially relevant and important. This thesis describes some new flow measurement techniques as

applied to reactions (1) and (5) and shows that rate measurements are at least as reliable as those of the more recent static methods. Errors in homogeneous rate constants due to surface reactions are shown to be negligible. The same flow technique can be applied to reactions of higher kinetic order.

1.5 Summary

The present work was undertaken in an attempt to develop an accurate, cheap, sensitive, reliable alternative method to the modern techniques discussed above. The determination of $k_{1,M}$ is important in the photochemistry of the stratosphere and in providing data for theoretical model tests. Furthermore, it is necessary to solve the present discrepancy in the determination of the temperature dependence of $k_{1,M}(M=Ar)$ as determined by earlier discharge-flow methods and static methods (where wall effects are negligible). This work will show that wall effects (which were not overcome in earlier flow-systems) are not a serious drawback of the flow method when allowances are made for their dependence on gas composition, and agreement with the best static methods can be expected over a wide temperature range and under very different conditions of pressure and time constant. This is significant for atomic reactions of higher kinetic order which are mainly determined by flow methods.

SECTION 2

The Experimental Apparatus

2.1 Introduction

The present work was aimed at developing the discharge-flow method of studying atomic (small free radical) reactions; and the apparatus and techniques described are completely general and can be used to study any type of atomic reaction with a few modifications. The advantages and disadvantages of this method have been discussed (Section 1).

This section contains a detailed account of the discharge-flow apparatus and techniques used, especially the details of the methods used to eliminate surface reactions and other 'background' reactions, since these are an important part of the development of this method.

The region in which actual chemical processes have been studied will be designated 'the Reaction System', and the region where dissociation of gases occurred will be defined as the 'Discharge System'. The use of vacuum lines, glass-blowing, details of gauges, electronic coupling and the like will not be included since these are discussed fully [1,2].

2.2 The Reaction System

Two types of reaction system of conventional design[3,4] were used in this work. Fig. 2.1 shows the essential parts of Reaction System A which was used in the determination of the rate of the reaction[19]

$$O + O_2 + M = O_3 + M$$

($T = 295K$, $M = O_2$, Ar, He, N_2, CO, CO_2)

FIGURE 2.1

Diagram of reaction system A

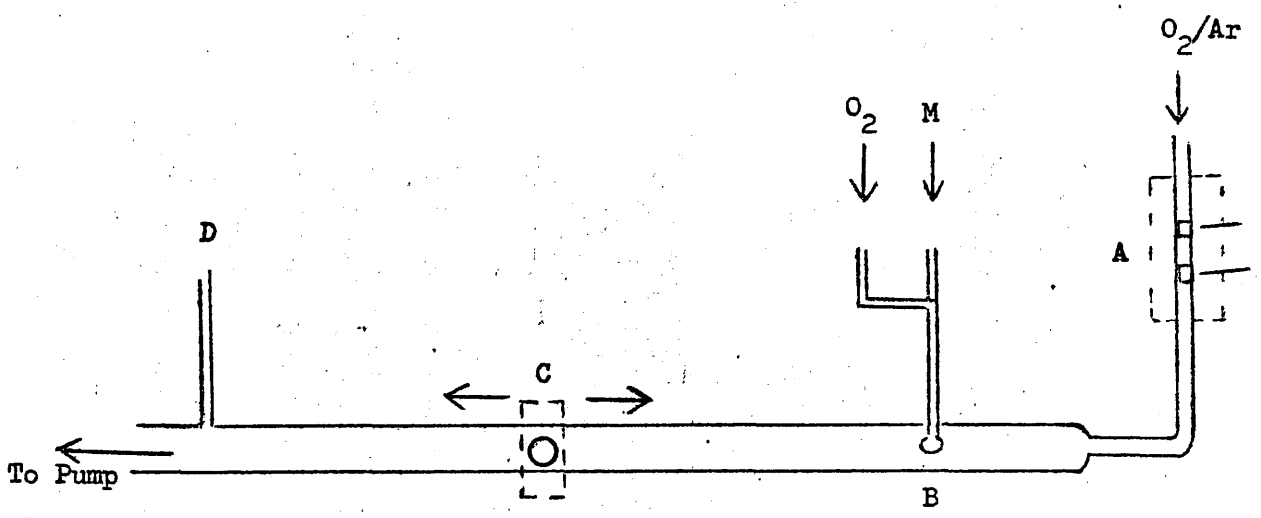

A = Wood's type discharge

B = Multiple-hole inlet jet

C = Moveable photomultiplier housing

D = Oil manometer

Figure 2.2

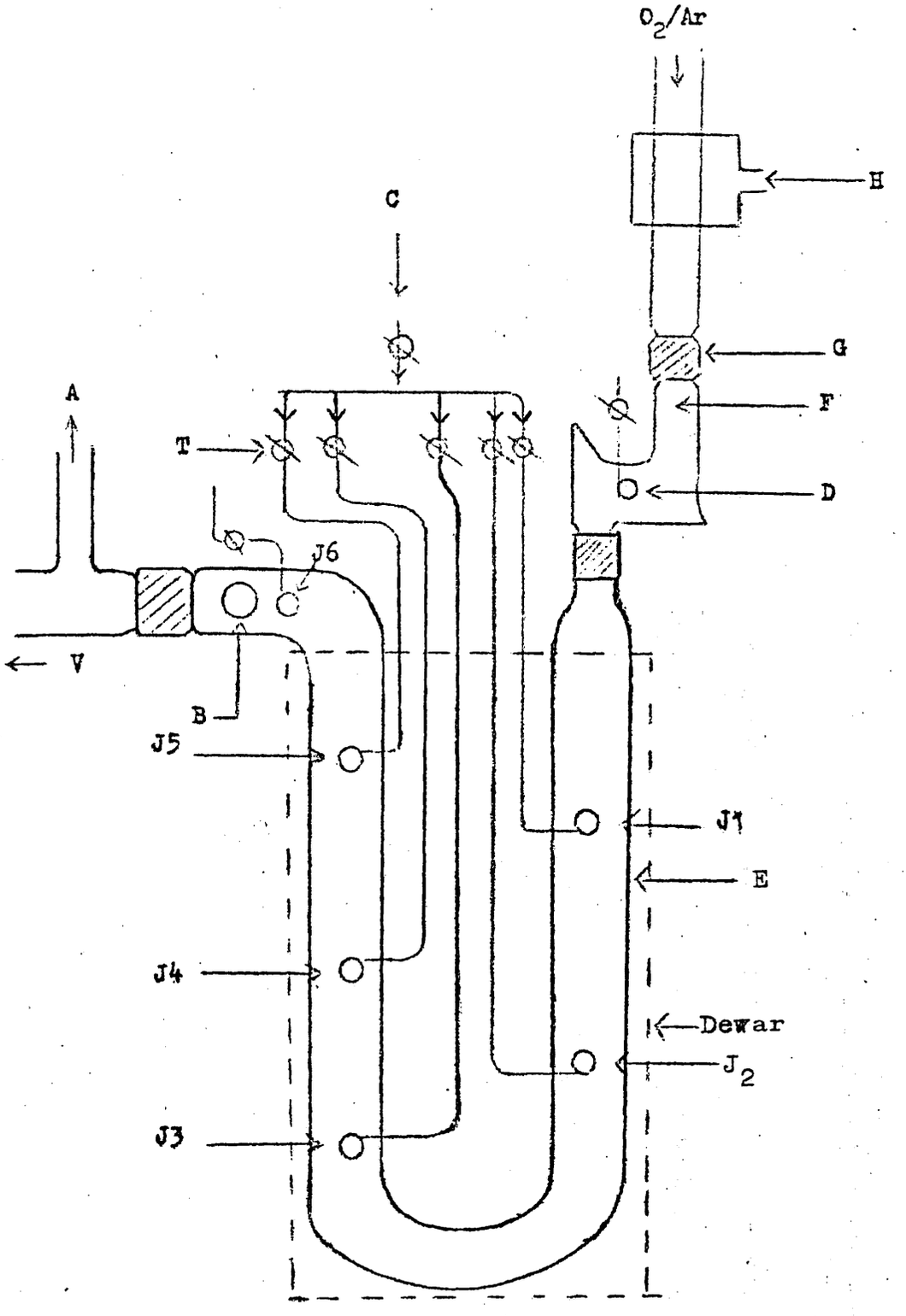

A = Oil manometer
B = Single observation point
C = To jets for O_2 addition
D = Jet for M addition
E = Pyrex flow tube
F = Wood's light horn
G = Greaseless screw joints
H = Microwave cavity
T = Greaseless taps
V = Vacuum pump

and fig 2.2, shows Reaction System B, used to determine the temperature coefficient of the reaction:[21]

$$O + O_2 + Ar = O_3 + Ar$$

(196 - 500K)

and the rates of the reaction:

$$O + SO_2 + M \longrightarrow SO_3 + M$$

($T = 295K$, $M = Ar$, SO_2)

The design of Reaction System B was such that it was possible to immerse it in a large Dewar (int. dia. = 10 cm, depth = 50 cm) connected to a 'LAUDA' thermostatted circulating system and a platinum resistance temperature controller for maintenance of steady temperatures to within $\pm$ 0.1K. System A was washed with an HF/Tepol (aq.) solution and system B with a 30% (w/w) phosphoric acid (aq.) solution, and the effects of this will be fully discussed (Section 2.7). Ease of connection and disconnection of both systems was provided by 'SOVIREL' high vacuum, greaseless, glass screw-joint seals which enabled the discharge, reaction and pumping systems to be dismantled independently. Reaction system A was constructed from 100 cm of Pyrex glass uniform-bore tubing ($r = 1.25 \pm 0.01$ cm) and had one jet, tapered to 1 mm diameter some 15 cm, downstream from the discharge for the addition of the reactant (either O_2 or SO_2) and third body M. In system B, the discharged gases and third body (M) passed through about 30 cm of Pyrex glass uniform-bore tubing ($r = 1.245 \pm 0.005$ cm), including a 'Wood's Horn' light trap, to preheat or precool the reactant gases before meeting the first of five 'pepperpot' type jets for the addition of

reactants. The jets were spaced at an accurately known distance apart of approximately 15 cm.

The quartz tube from the discharge system was 'pinched' in system B to minimize any back diffusion of M into the discharge.

It must be emphasised that the third body M was added after the discharge (unlike the system of Thrush et al[6]) so that species M capable of acting as a third body can be used (see Section 5 for the full implications of this) and high accuracy achieved by using large flow rates. Present flow rates ($0 - 600 \times 10^{-6}$ mol s^{-1}) of M could be increased by up to an order of magnitude for even better accuracy.

The average value of r in system B was measured by a 'volumetric' method. The flow tube was first filled with water to a level about 10 cm above the position of Jet 1 (see Fig. 2.2). The downstream end was then tightly corked. The level of water (h_1) in the right hand side tube was then measured with a travelling microscope (to $\pm$ 0.001 cm). 50 cm^3 of water was then added from a standard calibrated burette to this linear portion of the tube and the new level (h_2) of water in the tube was measured. Thus, knowing the length of tubing, L cm, ($h_2 - h_1$ cm) and the internal corresponding volume (50 cm^3), then the mean radius r cm of the tube was calculated from the simple equation

$$r = \sqrt{\frac{V}{L\pi}}$$

r was found to be 1.245 cm ($\pm$ 0.005).

The different designs of the jets had no influence on the rate measurements since the value of $k_{1,Ar}$ at 295K

determined in reaction system A was identical with that obtained in system B. This was also found by Clyne.[5]

The discharge gases (those gases passing through the discharge system) were principally high purity argon (50 - 100 x 10^{-6} mol s^{-1}), (for maximum impurities see sub-section 2.5) containing 500 p.p.m. O_2 and 5 p.p.m. N_2. Hydrogenous impurities were rigorously excluded (section 2.5) and tests by Clyne et al[6] indicated the absence of electronically excited species. If too high a flow of O_2 is added to the Ar (up to the order $\simeq$1%) then metastable electronically excited states such as $^1\Sigma_g^+$ regenerate oxygen atoms by reaction with ozone, formed in the reaction[6]

$$O_3 + O_2\ (^1\Sigma_g^+) = O(^3P) + 2O_2\ (^3\Sigma_g^-) \quad \Delta E = -12 \text{ kcal}$$

Similar processes can presumably also occur

$$O_3 + O_2\ (^1\Delta g) = O(^3P) + 2O_2$$

Hydrogenous impurities must also be eliminated since small amounts of hydrogen catalyze the removal of atomic oxygen.[7]

Reactant gas O_2 (35 x 10^{-6} mol s^{-1} when M $\neq O_2$) and large flows of the third body (0 - 600 x 10^{-6} mol s^{-1}) were also highly purified and M was added in large quantities for the reasons described above. Mean linear flow velocities ($\bar{V}$) were 100 - 600 cm s^{-1} and under these conditions concentrations of oxygen atoms (O^3P) always decayed by first order kinetics (preliminary discussion Section 5) in the presence and absence of O_2.

In system B it was also possible to introduce nitric oxide through jet 6 (Fig. 2.2) about 5 cm upstream of the quartz observation window. The intensity of the after-

glow (I) is related to the nitric oxide and oxygen atom concentrations by the relationship: (section 2.4 and Section 4)

$$I = I_o[O][NO]$$

where I_o is a constant, and since the method used in this work is a relative and not an absolute one (Section 1), the accuracy of the technique may be enhanced by working with higher intensities (since these give more stable readings than lower ones) or when working with lower concentrations of atoms (viz. at high pressures). In this work nitric oxide was purified by the standard technique of bulb to bulb distillation and then stored (5% in pure argon) at atmospheric pressure in a 5 litre glass bulb. However, the technique was not used since the trace of nitric oxide produced by the discharge system was sufficient to act as an 'indicator' molecule. The method may be more useful in the future study of faster reactions in this system

$$\text{e.g.} \quad O + SO + M \longrightarrow SO_2 + M$$

Gases were pumped through both flow-tubes by an 'Edwards' single stage (mechanical/oil) vacuum pump (type ES200) having a pumping capacity of 190 litre min^{-1} and an ultimate vacuum of 5×10^{-3} torr. A 10 litre metal bulb was interposed between the pump and the reaction system to minimize pressure fluctuations, and pressure in the system (typically 1 - 20 torr) was measured by a travelling microscope to within $\pm$ 0.001 cm oil on a silicone oil manometer. Pressures could be accurately adjusted by a large diaphragm valve (Edwards 1", CV grade) and this was important since in the method used in this work, linear

FIGURE 2.3 REAGENT HANDLING SCHEME FOR SYSTEMS A AND B.

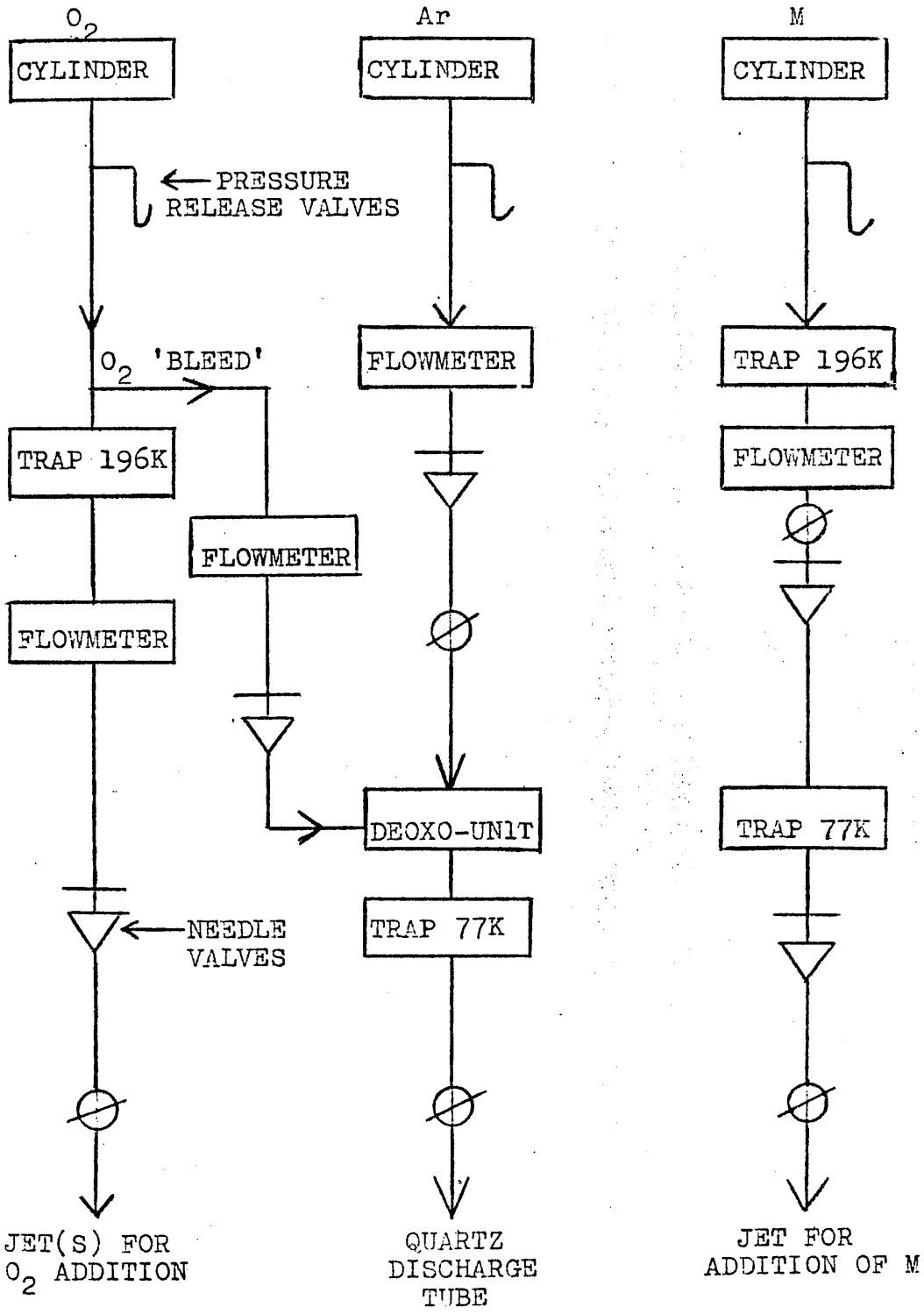

flow velocities had to be kept constant to within $\simeq 5\%$. The reason for this is fully discussed in Sections 4 and 5. A large Pyrex 'fast flow' liquid nitrogen trap was situated between the diaphragm valve and the reaction system to prevent the pump oil from corrosive gases in the flow stream.

Figure 2.3 shows a block diagram of the gas handling system for both reaction systems. Gas purification methods will be described later (section 2.5). All stopcocks were of 'Sovirel' 'Torion' mini- high vacuum type (4 mm bore, maximum vacuum 10^{-4} torr) and all gas flows were controlled by Edward's stainless steel, fine control, needle valves (type OS1D and LB1B) and measured by calibrated capillary flowmeters of various types (Section 2.6).

2.3 The Discharge System

Throughout this work three basic types of discharge were used, these being;

i) a 'Wood-Bonhoffer' tube, a high voltage (2000 volt) low frequency (50 cycle s^{-1}) A.C. type

ii) a Radio-Frequency Oscillator type (1 - 20 MHz)

and

iii) a Microwave 'cavity oscillator' type ($\simeq$ 3000 MHz)

500 - 1000 p.p.m. B.O.C. O_2 in an Ar carrier ($<$ 7 p.p.m. N_2) was dissociated in all three types and pumped along the reaction system for observation. Although argon was selected for the carrier gas in the determination of the temperature coefficient (Section 6) for ease of

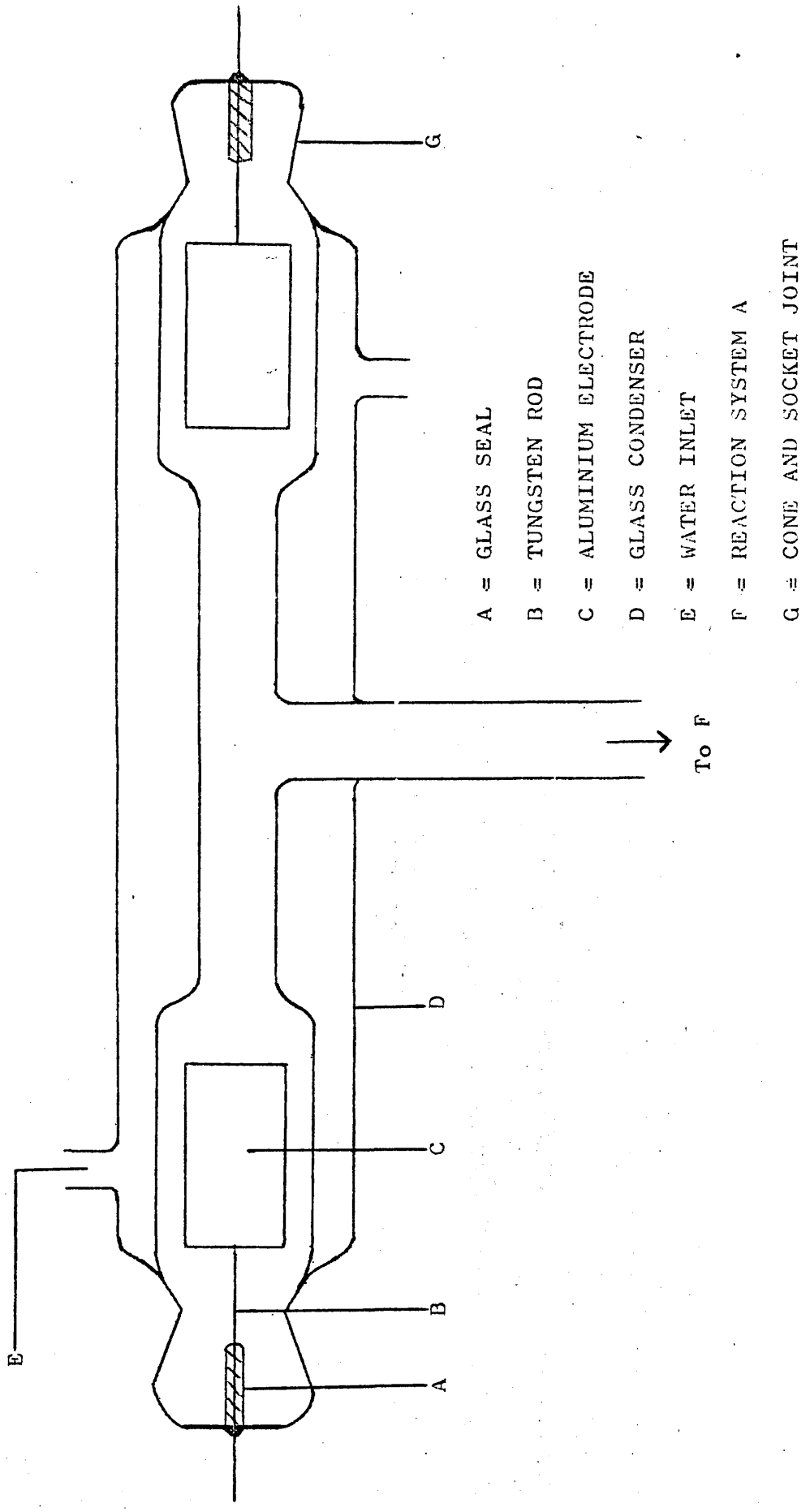
A = GLASS SEAL
B = TUNGSTEN ROD
C = ALUMINIUM ELECTRODE
D = GLASS CONDENSER
E = WATER INLET
F = REACTION SYSTEM A
G = CONE AND SOCKET JOINT
To F
A
B
C
D
E
G

Figure 2.4

comparison with other workers results, helium would have been a more suitable carrier gas since its thermal conductivity (33.6×10^5 cal cm^{-1} s^{-1} $degree^{-1}$ at 273K) is about ten times that of argon (3.9×10^5 cal cm^{-1} s^{-1} $degree^{-1}$ at 273K) thus ensuring that the discharged gases would have precooled or preheated to the temperature of the Dewar bath. O_2 had to be kept to below 0.1% to ensure the absence of excited O_2. Furthermore, the power in the discharge was always increased until no more dissociation of O_2 was observed, also ensuring no O_2^* was present. This was checked[6] by use of a 'Chance' OX1 filter (for characteristics, section 2.4) to isolate the Herzberg band of molecular oxygen around 360 nm. A trace of N_2 is necessary since atomic nitrogen ($N(^4S)$) is produced in the discharge and reacts with $O(^3P)$ atoms to produce the 'indicator' NO[8] molecule via the reaction (see section 2.4 for a discussion and full mechanism)

$$O + N + M \longrightarrow NO + M$$

Figure 2.4 shows the design of the first variety based on the well established Wood's tube[2,3]. A mains frequency high voltage (2000 volt) A.C. discharge was struck between two internal aluminium electrodes supported on tungsten wires accomodated by a cone and socket joint and the electrodes were connected to the output side of a large ballast transformer. The tube, 30 cm in length, consisting of 14 cm of 1.7 cm internal diameter Pyrex, and two cavities (internal diameter 3.3 cm) each 6 cm long, for the electrodes, was designed specially to avoid spluttering and was cooled by a water jacket to 273K. Although lower

temperatures were not used, this would probably improve the amount of dissociation. Atoms were taken from the centre of the tube via 8 mm internal diameter Pyrex tubing (figure 2.4) to minimise loss due to surface recombination, and due to the change in dimension of the tubing leaving the cavities, were accelerated out of the discharge. Spluttering from metal oxides formed at metal electrodes are known[12] to travel into flow tubes and catalyse recombination of atoms and thus the inside of the cavities and tube were frequently washed with HF/Tepol (aq.) solution to efficiently clean the glass surface and minimise surface recombination.

During kinetic experiments about 60 watt nominal power was used and oxygen atoms were easily generated in sufficiently high concentrations. The tube was thus used for almost all experiments in system A for 6 third bodies (295K), and no difficulties due to spluttering were encountered.

A radio frequency discharge was also used in some experiments (M = Ar) since this type is also well established[64]. The discharge gases entered a quartz, 8 mm internal diameter discharge tube, connected to reaction system A via graded glass seals and 'SOVIREL' Pyrex glass-screw joints. R.F. power from an ex-U.S. Navy R.F. generator operating at 7 MHz (maximum power $\simeq$65 watt) was coupled into the discharge tube capacitively via two strips of copper or aluminium foil wrapped externally round the tube, placed about 2 cm apart, and tuned by an inductance coil. A specially designed tube shield

surrounded the discharge and was earthed to minimise interference with the photomultiplier tube. This also provided a housing in which a stream of compressed air could be passed to cool the discharge. Some difficulty was experienced due to incomplete shielding and in some cases the photomultiplier recordings were adversly affected. Moreover, stability was no better than that for the Wood's tube. However, there could be no possibility of splutter-ing and the frequency could be adjusted between 4 and 7 MHz. Input power was always tuned for maximum coupling but it was not possible to estimate power imput.

A microwave 'Cavity oscillator' operating at 2.45 GHz was used in the determination of the temperature coefficient (see Section 6) and the rates of the reaction

$$O + SO_2 + M \longrightarrow SO_3 + M$$

This is the most common type of discharge currently in use. The same discharge tube (described above for the R.F. type) was used and cooled by a stream of compressed air, forced through the cavity and directed onto the dissociation area. However, an Electro-Medical Supplies Microwave Generator (Microtron 200, mark III) supplied up to 200 watt (maximum) power with optional modulation; this was coupled via a Resonant Cavity (type E.M.S. 210 L) into the discharge gases and was finely tuned such that the 'reflected' power meter on the Microtron registered a minimum value (typically less than 3 watt). Nominal incident power used ranged from 20 - 100 watt .

Dissociation of molecular gases at low pressures is a result of ion-molecule interactions in discharge plasmas

and some discussion has been reported previously.[93] It should be stated that by using an O_2/carrier gas mixture, it is possible to obtain complete dissociation even with very low impurity levels (unlike dissociation in pure O_2, N_2 or H_2) and thus by using a small enough concentration of O_2 the production of $\overset{*}{O}_2$ (see above) in any discharge system can be avoided.

Each of the three types described have various advantages and disadvantages.[11] The Wood's type described above dissociates a high percentage of the gas, operates up to fairly high pressures ($\simeq$10 cm Hg with this discharge design) and very high powers (500 watt or more if required) can be coupled in. Wood's tubes are now not often used unless carefully designed since they can lead to contamination of reaction systems by spluttering. R.F. and microwave power require a quartz tube for coupling since Pyrex absorbs significantly.[15] Furthermore, the discharge cannot be cooled with water, and a liquid such as paraffin, which does not absorb the power must be used. Hence cooling by liquids becomes inconvenient. R.F. oscillators produce a moderately large percentage dissociation and are electrodeless, but maximum usable pressures are low ($\simeq$ 1 - 3 cm Hg) unless specially designed discharge tubes and high power imputs are used. Finally, the microwave oscillator is electrodeless and gives a high percentage dissociation up to high pressures. However, due to the very high frequencies employed ($\simeq$ 3 GHz) it has been found in part (especially for N_2) that formation of electronically and vibrationally excited species occur in the discharge

products which are usually objectionable.

2.4 The Detection System and Housing

Relative measurements of atomic oxygen concentrations along the length of the reaction tube (atomic decay profiles) were made by observing the air-afterglow ($\overset{*}{NO}_2$) chemiluminescence. Absolute measurements, which can be made by chemical 'titration' with NO_2 were not required in the present work. The principle of using air-afterglow chemiluminescence detection has been well established, and was first used extensively by Kaufmann[7]. Later, Thrush et al[8] used the same method when studying the present gas system in a discharge-flow system. The chemiluminescence has the kinetics of the type described by reactions 2.1-2.4 below. The emitting species[8] in these reactions is formed in a combination process involving participation by a chaperon (M) and the slow rate determining reaction for removal of this excited species is the collisional quenching step involving M, described by reaction 2.3. In this combination reaction the steady-state population of any vibrational energy level, v, of the excited electronic state, $\overset{*}{NO}_2$, can be represented by the rates of the following processes:-

i) Stabilization and redissociation,

$$O + NO + M \underset{k_{-1v}}{\overset{k_{1v}}{\rightleftharpoons}} \overset{*}{NO}_{2(v)} + M \qquad 2.1$$

ii) Vibrational energy transfer,

$$\overset{*}{NO}_{2(v)} + M \underset{k_{v',\,v}}{\overset{k_{v,\,v'}}{\rightleftharpoons}} \overset{*}{NO}_{2(v')} + M \qquad 2.2$$

iii) Radiation,

$$NO^{*}_{2(v)} \xrightarrow{k_{2v}} NO_2 + h\nu \qquad 2.3$$

iv) Collisional electronic quenching,

$$NO^{*}_{2(v)} + M \xrightarrow{k_{3v}} NO_2 + M \qquad 2.4$$

The blue CO_2 emission formed in the O + CO reaction, which was also used in the work combined with the NO^{*}_2 emission for the work of M = CO at 295K, can be described in a similar manner (Section 5).

In this work the concentration of NO formed in the discharge system quickly reaches a steady state in the reaction system since reaction 2.3 above is followed by the very rapid reaction[19] (at 296K)

$$O + NO_2 = NO + O_2 \qquad 2.5.$$

($k_4 = 9.3 \times 10^{-12}$ cm^3 mol^{-1} s^{-1})[28]

and so remains accurately constant along the tube.

Kaufmann[7] has shown that the equation

$$I = I_o\,[O][NO]$$

is obeyed by the air-afterglow (NO^{*}_2) emission but did not observe a dependence of I_o on the nature of M. Clyne and Thrush[8] showed that I_o has a small temperature coefficient and depended on the nature of M. They report an approximate value for the overall absolute emission intensity $I_o = 4.7 \times 10^7$ cm^3 mol^{-1} s^{-1} for M = Ar, O_2, at 293K.

Since the NO concentration remained accurately constant down the length of the flow tube , then since $I \propto [O]$, then

$$\frac{I_o}{I} = \frac{[O]_o}{[O]}$$

(where I_o and $[O]o$ are the emission intensity and the oxygen atom concentration in the absence of reactant O_2 respectively). Thus with the nitric oxide present in the gas stream acting as an 'indicator' the decreasing light intensity along the flow tube directly measured the decay of $[O]$

$$\text{i.e. } \frac{-dI}{dX} = \frac{-d[O]}{dX}$$

under flow conditions described in Section 4. This presented a convenient and accurate measurement of the relative concentration of oxygen. The amount of NO required was very small to ensure that a negligible amount of oxygen recombined by reactions 2.1 - 2.5. In system B the method of adding NO at J6 (figure 2.2) near the photo-multiplier could be used if necessary for future work in this system

$$\text{e.g. } O + SO + M \longrightarrow SO_2 + M$$

This is a better method since intensities can be obtained as high as are required.

In reaction systems A and B observations of the after-glow were made at two positions, X1 and X2 cm from the discharge, of intensity $I_o 1$ and $I_o 2$ (no added O_2) and I1 and I2 (O_2 added) respectively (see Section 5). Thus, by measuring the <u>ratios</u> $I_o 1/I1$ and $I_o 2/I2$ at 2 positions an accurately known distance apart, any small absorption by glass, filters, reflection losses, changes in the state of the wall, stray light etc. was always <u>cancelled out</u>. This fact is particularly important in measuring the values of the wall recombination coefficients γ and γ^* in the

presence and absence of O_2 respectively. This will be further discussed in section 2.7 and Section 5. This technique also assists in minimising interfering effects due to a very small amount of chemiluminescence from reactions[20] such as

$$NO + O_3 = NO_2 + O_2 \qquad \Delta H = -40 \text{ kcal}$$

which occur in the gas stream, although under the conditions used in this work the influence of this reaction is negligible.

Observations of the NO_2^* emission were made using an R.C.A. 931A photomultiplier tube having a stated overall sensitivity of 50 Amps/Lumen and a wavelength of maximum response equal to 400 $\pm$ 50 nm. The tube was conveniently supported in a black, cylindrical, stainless steel housing which had a shutter and could accomodate filters and was attached to a second cylindrical, stainless steel housing lined with black felt (about 15 cm long) to ensure light-tight fitting. The NO_2 continuum was thus viewed normally. In system A the whole assembly could be slid along the length of the reaction tube (painted black where possible) while in system B the photomultiplier viewed the after-glow through a quartz glass window (diameter 26 mm) normally, and at a fixed position ($\simeq$ 15 cm) upstream of jet fire (figure 2.2).

The O + NO continuum extends from 400 - 900 nm and has a maximum near 650 nm. The emission was therefore isolated with a Kodak Wratten 61 filter which is transparent in the range 500 - 560 nm. While studying the

$$O + O_2 \ (M)$$

reaction for M = CO, no filter was used since the blue

emission from excited CO_2^*, formed from

$$O + CO\ (+ M)$$

of comparable intensity was used. Although both emissions were detected a signal was obtained proportional to $[O]$ since Clyne[8] and Thrush have shown that the relationship

$$I = I_o [O] [CO]$$

is also obeyed under the conditions stated in Section 5 of this work. Thus, using no filter was advantageous for the work on M = CO since the total emission intensity was enhanced by addition of CO (0 - 400 μ mole s^{-1}). However, if required, this emission (extending from 300 - 500 nm) could be separated by using a Chance OX1 filter which has a sensitivity range of 320 - 390 nm.

The phototube was incorporated in an Evans-Electro-Selenium "Photometer" stabilized power supply, including an amplifier and sensitivity range control, operating at a potential of 800 volts ($\pm$ 5%). This was screened from scattered light by painting the discharge, reaction tube and the laboratory windows with black matt emulsion. Under such conditions the dark current (typically 5×10^{-9} Amp) and effects of stray light were negligible compared to the measured signal (0 - 2×10^{-6} Amp) although small corrections for dark current were always made. Axial diffusion of light along the reaction tube was checked experimentally (since no Wood's Horn light trap was used in system A) by observing the intensity down the tube with no O_2 in the discharge, but with the discharge on. This reflected light level was found to be negligible and work was always carried out in a darkened windowed laboratory.

TABLE 2.1

Typical analyses of B.O.C. gases (i.e. maximum impurities in parts per million).

GAS	GRADE	O_2	H_2O	N_2	H_2	CO_2	HYDROGENOUS IMPURITIES
O_2	Commercial		6.0	15.0		2.0	20.0
Ar	Commercial	5.0		15.0			1.0
Ar	High Purity	4.0		15.0			1.0
N_2	White Spot	5.0	2.0		1.0	1.0	1.0
He	Standard (Grade A)	2.0	3.0	10.0	1.0	1.0	1.0
CO_2	C.P.	2.0	4.0	10.0	0.5		0.5
CO	C.P.	20.0	25.0	500.0	20.0	300.0	60.0
SO_2	Special		50.0				
NO	Technical			200.0			

The output current from the photomultiplier was recorded on an electronic digital voltmeter (type, Weir Instruments; series 600, 0 - 1900 volts with internal calibrator) which was resistance shunted (a variable resistance box) to record the output current in the 10^{-6} Amp region. Intensity measurements were only made when any zero drift had stopped.

These types of photomultiplier tubes have a linear response provided the output current does not exceed the maximum rating and that the shunt resistance used in this work does not cause high voltages to build up on the anode. A. Fontijn[9] et al. showed the extreme sensitivity of an E.M.I. 9558QA by measuring a nitric oxide concentration down to 4 parts per billion when monitoring $\overset{*}{NO}_2$ chemiluminescence. The dark current in this tube was 2×10^{-9} Amp , a factor of 2 better than the R.C.A. 931A tube used in this work. Also the noise level in the latter tube was typically 1.4×10^{-13} Lumen compared with 3×10^{-12} Lumen for the R.C.A. tube, and the overall sensitivity was 4 times better (200 Amp /Lumen). Thus, both types of tube are particularly suited to the study of chemiluminescence reactions emitting light of low levels.

2.5 The Purification of Gases

All gases used in this work were obtained exclusively from B.O.C. Special grade gases used were SO_2, CO_2 and CO, mineral gases were O_2, He and Ar, N_2 was 'white spot' commercial and Ar for the discharges was 'high purity'. Typical analyses of these gases are given in Table 2.1. The reaction systems had three gas lines (see Section

2.2, fig 2.3), one for the introduction of M, one for reactant O_2 and one for carrier gas/O_2 'bleed'. In the case of O_2 and M, the gases travelled from cylinders, through pressure regulating valves, flowmeters (cf 2.6), firstly to a 15 cm long Linde 5Å molecular sieve trap maintained at 196K and at a pressure just below 1 atmosphere. This trap effectively eliminated CH_4, all water vapour and non-volatile impurities. Any sieve powder was trapped by the use of porous sintered discs. CH_4 and atomic hydrogen[21] are known to catalyze the removal of ground state $O(^3P)$ atoms through the reactions

$$O + CH_4 = CH_3 + OH$$
$$O + OH = H + O_2$$
$$H + O_2 + M = HO_2 + M$$
$$O + HO_2 = OH + O_2$$

$O(^1D)$ excited atoms react with water[20] generating OH radicals which react very rapidly with $O(^3P)$ atoms giving H atoms,[21]

$$O(^1D) + H_2O = OH + OH$$
$$O + OH = H + O_2$$

but $O(^1D)$ was shown to be absent in this work (see above in section 2.2).

The gases then passed through a second type of trap, again containing (15 cm long) 'Linde' 5Å molecular sieves but maintained at 77K with liquid nitrogen and at pressures of the reaction system. Discharge Argon containing <500 p.p.m. O_2 also passed through a 'Deoxo' catalytic unit (Englehard Industries) to remove any H_2 present (down to < 1 p.p.m.) by conversion to H_2O which was subsequently

trapped. In the case of M = CO, a 15 cm long Linde 5A trap at 77K was used but at pressures of $\frac{1}{2}$ - $\frac{3}{4}$ atmosphere in an effort to ensure that no CH_4, H_2O or $Fe_2(CO)_9$ entered the reaction system. This proved to be efficient and very satisfactory as will be shown (Section 5).

Inert gases could also be passed through a B.O.C. Rare Gas Purifier, which removes all impurities down to a level of 0.1 p.p.m. Although it was not used in the present work this device will prove useful in the future study of reactions by the present method such as

$$O + CO + M = CO_2 + M$$

when it may be required to reduce the level of N_2 impurities to a level approaching zero in order to avoid interference to the CO_2^* emission (see sub-section 2.4) by the NO_2 afterglow.

Previous workers have had considerable difficulty in attempts to purify CO. Slanger and Black[52] found that their reaction cell had to be washed frequently with soap and water due to wall polymerization attributed to C_2O_3 polymers from excited CO in the flow stream, even though they trapped CO with liquid N_2 at low pressure. Arin and Warneck[65] used a long spiral trap maintained at 77K and pressure 25 torr to purify the gas and stated that molecular sieves as adsorbant (grade unknown) proved inefficient, suggesting that CH_4 and not $Fe(CO)_5$ was the contaminant. This seems likely since CO is prepared industrially from methyl formate. However, Stuhl and Niki[61] stored CO at 196K in vacuo and also used a low pressure glass trap at 77K (the initial fraction of the vapour phase was discarded before using

the specimen). They state that this precedure considerably lengthened $O(^3P)$ lifetimes, and report a value of $k_{1,CO}$ of 2.41×10^{14} cm^6 mol^{-2} s^{-1}, in excellent agreement with the value of 2.35×10^{14} cm^6 mol^{-2} s^{-1} reported here.

The molecular sieves in this work (Linde 5Å) were freshly generated at 473K for one hour before each kinetic run since failure to do this resulted in rate constants much higher (up to an order of magnitude, see sub-section 5.3) than the final values. The 77K trap was also maintained at a pressure of the order of $\frac{1}{2}$ an atmosphere unlike the methods from the literature described above (these were all kept at low pressure). Furthermore, the absence of metal carbonyls in this work was shown by mass spectral analysis although these compounds are expected to be removed by a 77K trap. Thus, CH_4 impurities are probably the main reason for discrepancies in the values of reported rate constants involving reactions of the gas.

2.6 Flowmeter Design and Calibration

Two types of flowmeter were used in this apparatus, and always used at atmospheric pressure except for the O_2 'bleed' (see sub-section 2.2). The first type, made by 'Glass Precision Engineering' was 'Meterate' rotameter or ball-type glass precision flowmeters with interchangeable glass, stainless steel or other 'floats' of various density. These have the advantage that they are direct reading (i.e. calibrated or flow rate calculable) and are resistant to attack by corrosive gases (hence were used to measure the flow rates of SO_2 in the range 0 - 70 x 10^{-6} mol s^{-1}).

The second type was the more common glass capillary tube/manometer variety used previously. Non-corrosive gases were allowed to pass through the capillary and the resulting pressure difference set up was measured on the attached silicone oil (MS550R) manometer. A 'Quickfit' B7 cone-joint joined the capillary to the flowmeter and was attached by a spring to facilitate removal or exchange. A stopcock provided a 'short' for gas flow across the manometer, and the pressure of the manometer could be measured by a travelling microscope (to $\pm$ 0.01 cm) but usually a short length of rule was sufficiently accurate. The gas flow was calibrated to within $\pm$ 0.25% by the timed flow through an 'Alexander Wright' wet type gas meter.

At very low flow rates ($< 35 \times 10^{-6}$ mol s^{-1}) for most gases such as N_2, O_2, CO_2 etc., Poiseiulle flow is a fair approximation, thus;

$$F = \frac{\pi r^4}{8\eta LRT} \cdot P\Delta p = K P\Delta p$$

at constant pressure (1 atmosphere in this work) where F = flow rate, r = radius of the capillary, η = gas viscosity, L = length of the capillary, Δp = pressure difference across the capillary.

The flow rate is therefore proportional to Δp.

Thus, in principle, the capillary could be calibrated by determining r; however, the approximation of Poiseuille is not satisfactory at higher flow rates and so capillaries were always calibrated by the gas meter. Another method of calibrating the capillaries which is especially useful for corrosive or water soluble gases, is to measure the rate of fall of pressure in a bulb for a known pressure

difference Δp across the capillary and given pressure p in the bulb. The gas meter was used throughout, however, (except for SO_2) since this was the most accurate.

2.7 The Surface

The strong influence exerted on chain reactions by the recombination of atoms and radicals at reaction tube walls, coupled with the fact that this phenomenon often sets a limit to investigations of the kinetics of elementary gas reactions has led to the need for reliable studies of heterogenous recombination. Many studies have been directed at atomic recombination. This subject has been well reviewed by Kaufman[26] who summarized the work done by Linnet, Greaves et al[24] who determined , the recombination coefficient (see definition below) on various surfaces e.g. Pyrex, Silica, metals, metal oxides, alkalis, Teflon and phosphoric acid. A summary of relevant values of γ recently obtained are shown in Table 8.4. This table shows the disturbing fact that γ varies by 10 - 100 in different laboratories. Mulcahy,[50] Greaves[24] and this work (see Section 5) have shown the heterogenous recombination to be first order on most surfaces including Pyrex, quartz etc. Kaufman[26] reports a value of $\gamma = 2 \times 10^{-5}$ on untreated Pyrex in good agreement with the value of $2 - 12 \times 10^{-5}$ obtained here (see Section 5).

A few suggestions for the first order surface recombination have been made. Langmuir, in deriving his adsorption isotherm provided strong evidence for first order recombination. The mechanism was later further

clarified by Schuler and Laidler[66] on the grounds of energy requirements alone.

γ is defined as the ratio of the number of gaseous atoms recombining to the number of gas phase atoms striking the wall, and is, therefore, the probability that a gas phase atom striking the surface will react to form a product molecule. In this work the expression

$$\gamma = \frac{2rk_w}{\bar{C}} \quad \text{(for a cylindrical tube)}$$

(where r = the radius of the tube, k_w = the wall recombination rate constant and $\bar{C}$ = the mean velocity of the gas) was used to determine γ, k_w being calculated by the expression given in Section 4.

Reaction system A in the present work was kept clean by washing with a 5% solution of HF in Tepol for one hour, repeatedly rinsing with distilled water and leaving to dry for 24 hours.

Values of γ ranged from 1 - 12 ($\times 10^{-5}$) and γ was also found to depend on whether O_2 was absent or present and this has not been reported previously, although the fact that γ^* and γ (in the absence and presence of O_2 respectively) may be different was first suggested by Benson.[10] The difference is probably due to a surface reaction such as

$$O + O_2 + \text{wall} = O_3 + \text{wall}$$

Thus, the use of the discharge flow method has been advanced to eliminate all surface errors, mainly due to the use of the kinetic equation described in Section 3.3 which does not assume $\gamma = \gamma^*$.

Reaction tube B was first rinsed with acetone to

remove grease, distilled water and finally by a 30% (w/w) aqueous solution of M-phosphoric acid, a well-known surface poison. Values of γ for this tube were of the order 1 - 3 ($\times 10^{-5}$) which are slightly lower than those obtained for HF rinsed Pyrex. No poison was used in the discharge since there was a possibility of contamination at the temperatures and conditions used. 'Drifilm' was found to increase the wall activity but in the presence of O_2 this activity was reduced. This agrees with reports that acidic groups on the wall surface are better than basic ones for the recombination of oxygen atoms.

The significant changes in surface recombination in the presence and absence of O_2 mentioned above may account for the discrepancies in the determination of the temperature coefficient of

$$O + O_2 + M = O_3 + M$$

between various flow methods and static systems, and a reexamination of the temperature coefficient in the light of the facts mentioned above will appear in Section 6.

SECTION 3

Kinetics and Derivation of Rate Equations

3.1 Introduction

Chemical kinetics is the study of the rate and mechanism of chemical change. It s function is firstly to determine the rates at which chemical reactions take place under different conditions, for example, concentration of reactants, temperature, pressure etc., and then to arrive at an understanding of the mechanistic steps. Generally, the rate of a reaction increases with increasing concentrations of reactants and also with increase of temperature. Atomic recombination reactions such as those described in this work afford an exception to the rule and usually have small negative temperature coefficients (or have an Arrhenius activation energy of $-(0 - 2)$ kcal. mol $^{-1}$. A brief discussion on the reason for this exception can be found in section 6.

For a non-reversible reaction at constant temperature;

$$aA + bB + \ldots\ldots\ldots \longrightarrow qQ + rR + \ldots$$

It is found in general

$$\frac{-d[A]}{dt} = \frac{-a}{b} \cdot \frac{d[B]}{dt} = \frac{a}{q} \cdot \frac{d[Q]}{dt} = \frac{a}{r} \cdot \frac{d[R]}{dt} = \ldots$$

where the terms $[A]$, $[B]$, etc. denote reactant concentrations in units such as mol cm^{-3}. Thus, rates of reaction depend on the overall stoichiometry of the reaction if it consists of a single step process. In general, for a multiple step process in which the first step is rate controlling, the reaction rate can be expressed in the form (for example, in the case of (3a)

$$\text{Rate} = k[A]^a[B]^b$$

where k is the rate constant for the reactants A,B,... and the terms a,b,... are defined as the orders of the reaction with respect to A,B,... and with the overall order of a + b + ... When the overall order is 1st, 2nd, and 3rd order, then the units of k are s^{-1}, $cm^3\ mol^{-1}$, and $cm^6\ mole^{-2}\ s^{-1}$ respectively. Sometimes the concentrations of all reactants but one remain effectively constant during a reaction. This may be because their initial concentrations are much greater than that of the reactant which changes. When the latter disappears according to a first-order law, it's behaviour may be conveniently discussed in terms of a PSEUDO first-order rate constant k , i.e. for a single step reaction,

$$A + B \xrightarrow{k} \text{Products}$$

then an expression $$\frac{-d[A]}{dt} = k[A][B]$$

can be replaced by $$\frac{-d[A]}{dt} \simeq k\psi[A]$$

but $k\psi$ is only constant for the particular value of B . Similarly, single-step reactions of the type A+B+C $\longrightarrow$ Products can be made pseudo-2nd order by arranging <u>one</u> component to be in large excess over the others, or be made pseudo-1st order by having <u>two</u> components in large excess.

The mechanism for the reaction of oxygen atoms with oxygen molecules occuring in the present flow system can be represented by the following scheme:

$$O + \text{wall} = \tfrac{1}{2}O_2 + \text{wall} \qquad (w)$$

$$O + O_2 + M = O_3 + M \qquad (1)$$

$$O + O_3 = 2O_2 \qquad (1.1)$$

$$O + NO + M = NO_2 + M \qquad (2)$$

$$O + NO_2 = NO + O_2 \qquad (2.1)$$

$$O + O + M = O_2 + M \qquad (3)$$

according to the results of previous investigations.[7,10] Since the removal of O-atoms by process 2.1 is much faster than by 2 under the conditions of this work, the rate constant for removal of O by NO is $2k_{2,M}$. On the other hand removal of O by 1.1 can be shown to be much slower than by 1 since steady-state O_3 levels are not achieved.

From reactions 1 and 1.1 above, applying the steady state approximation:

$$\frac{d[O_3]}{dt} = k_1[O][O_2][M] - k_{1.1}[O][O_3] = 0$$

whence the steady state concentration of ozone in given by:

$$[O_3]_{ss} = \frac{k_1}{k_{1.1}} \cdot [O_2][M]$$

Hence, using the above relationship, typical flow conditions in the present work when $F_{O_2} = 35\times10^{-6}$ mol s^{-1}, and when M = Ar, $F'_{Ar} = 315\times10^{-6}$ mol s^{-1} (at 295 K), and using $k_{1,Ar} = 1.5\times10^{14}$ cm^6 mol^{-2} s^{-1} (present work) and $k_{1.1} = 4\times10^{9}$ cm^3 mol^{-1} s^{-1} (ref. 17) then $[O_3]_{ss} = 0.4\times10^{-9}$ mol cm^{-3}.

It can be shown by applying the equation of Benson[54] that steady state O_3 levels are not reached for typical conditions in this work; for consecutive reactions,

$$\frac{B}{K} + 2\ln\left(1-\frac{B}{K}\right) = -\frac{A_o}{K}\left(1-\frac{A}{A_o}\right)$$

where $K=k_1/k_{1.1}$, A_o= concentration of oxygen atoms at beginning of reaction and B= concentration of intermediate (O_3). By plotting B as a function of A, B(O_3) will approach a limiting value of K only when A_o/K is very large compared to unity. If this condition does not hold, then the concentration of B will remain substantially smaller than K for the duration of the reaction.

Thus, for a typically maximum flow rate of M = 310×10^{-6} mol s^{-1} (M=Ar), F_{O_2} = 35×10^{-6} mol s^{-1} at 295 K in the present work,

$$A_o/K = A_o k_{1,a}/k_1 = 0.25$$

(values of A_o and method of calculation are given in Benson). Thus,[54] even for a full extent of reaction ($1-A/A_o=1.0$), the concentration of ozone(B) will only be 0.091 of its limiting value (1.0) i.e. its steady state level. Finally, the overall kinetics of O-atom decay can be made pseudo-first order providing that reaction (3) is a negligible sink for O-atoms, and the reactants O_2 and M are in large excess. (Section 3.2)

Several chemiluminescent methods are known for monitoring oxygen atom concentrations in atomic recombination reactions; these methods (Section 1.4) are absolute or relative ones. The 'titration method' (Section1.4 and 2.4) concerns the titration of O-atoms with NO_2 in a very rapid reaction (2a) (about 1 in 100 collisions brings about a reaction). The yellow-green chemiluminescence which appears arises from the formation of electronically-excited NO_2 in

a sequence of steps (Section 2.4). The intensity of the glow depends on the nature of M. As further NO_2 is added to the O-atoms, the intensity passes through a maximum and is extinguished when the flow rate of NO_2 equals that of the O-atoms.

The afterglow emission can be used to follow relative changes in O-atom concentrations by adding NO to the system. The overall emission intensity (I) is given by

$$I = I_o[O][NO]$$

(see below) where I_o is independent of total pressure above o.1 torr and $I_o = 4 \times 10^7$ cm^3 mol^{-1} s^{-1} (400-800 mn) for M=Ar, O_2 at 293 K as determined by Clyne.[8] Also, I_o was found to be slightly greater for $M=O_2$ and Ar than for He and was thus dependent on the nature of M according to the expression for I_o. For $M=O_2$ in the range 200-300 K I_o has a small negative temperature coefficient:

$$I_o = 3 \times 10^6 \exp(+1500 \pm 400)/RT$$

In this method, a minute concentration (10^{-12} mol cm^{-3}) of NO is needed and this can be added independently (Section 2.2) or the small amount formed in discharges can be used. Any NO consumed under these circumstances by reaction (2) is immediately regenerated by reaction (2.1). Thus the concentration of NO remains accurately constant and by relation (above) at any time of reaction, the glow intensity is directly proportional to $[O]$. NO can thus act as an 'indicator' molecule without significantly affecting the

kinetics of O-atom decay. Reactions such as:

$$NO + O_3 = NO_2 + O_2 \qquad \text{and}$$

$$2NO + O_2 = 2NO_2$$

can be shown to be too slow under the present conditions to significantly change NO concentrations.

This method can be extended to the study of other chemiluminescent reactions of the type

$$O + XO + M = XO_2 + M \qquad (X = C \text{ or } S)$$

However, the reaction in which X is C can alternatively be followed by observing the blue CO_2 emission since I_c in the relation

$$I_c = I_{o_c}[O][CO]$$

is independent of total pressure. This has been verified between 0.86 and 2.69 torr but depends on M. Clyne and Thrush[8] determined I_{o_c} over the range 198 to 284 K and found that it increased by a factor of 8 as a function of increasing temperature, and fitted the expression

$$I_{o_c} = 6\times10^6 \exp(-3700 \pm 500)/RT \quad cm^3\ mol^{-1}\ s^{-1}$$

by using this method, filters need not necessarily be used to eliminate any emission from the O + NO + M reaction since this is several hundred times faster than than the O + CO + M reaction.

3.2 Choice of Experimental Conditions

In studying the kinetics of a chemical reaction, it is usually possible to adjust the experimental conditions such

that the kinetics of recombination can be dominated by an individual term in the rate equation.

Thus, for the present study, the ideal conditions will be shown below to be:

$$\sum_M k_{1,M}[O_2][M] >> k_W + \sum_M 2k_{2,M}[NO][M] >> \sum_M 2k_{3,M}[O][NO]$$

since in this case, the homogeneous reaction (1) predominates and the overall recombination in the presence and absence of molecular O_2 is first order in oxygen atoms. In addition to this, the intensity of emission (I) must be at a sufficiently high level (Section 2.4) to obtain detection with good accuracy. This requires that $[O]$ and $[NO]$ should not be too small, of the order 10^{-10} and 10^{-12} mol cm^{-3} respectively. For all kinetic runs attempted (Sections 5,6,7), $[O]$ and $[NO]$ were sufficiently large and although 5% NO in Ar could be added in system B just upstream from the observation point to enhance the glow, this technique was not necessary.

NO can also be used as a catalyst to swamp any second order recombination besides acting as an 'indicator' molecule. Thus by ensuring that the condition:

$$\frac{\sum_M k_{2,M}[NO]}{\sum_M k_{3,M}[O]} >> 1$$

then any second order recombination must be negligible. Since[33] $k_{2,Ar} = 2.7 \times 10^{16}$ cm^6 mol^{-2} s^{-1}, and[30] $k_{3,Ar} = 6 \times 10^{14}$ cm^6 mol^{-2} s^{-1} at 298 K, then the condition is typically $\frac{[NO]}{[O]} = \frac{F_{NO}}{F_O} >> 0.022$. However, this 'swamping' effect by

NO was not used exclusively in the present work although F_{NO}/F_O was usually of the order 0.028-0.01.

In the present system, however, it is necessary that the condition:

$k_W + \sum_M 2k_{2,M}[NO][M] >> \sum_M 2k_{3,M}[O][M]$ should hold and since

$$k_W >> \sum_M 2k_{2,M}[NO][M]$$

therefore $$k_W >> \sum_M 2k_{3,M}[O][M]$$

To show that $k_W >> \sum_M 2k_{2,M}[NO][M]$

$F_M = 100\text{-}500\times10^{-6}$ mol s^{-1}

$F_{NO} = 14\times10^{-10}$ mol s^{-1}

F_{Ar}(discharge) $= 100\times10^{-6}$ mol s^{-1}

F_{O_2}(discharge) $= 5\times10^{-8}$ mol s^{-1}

$\bar{v}$ = 150-450 cm s^{-1} (taking a typical value of 250 cm s^{-1})

then

$$2k_{2,Ar}F_{NO}F_M/(\bar{v}\pi r^2)^2 = \frac{(5.4\times10^{16})(14\times10^{-10})(100\times10^{-6})}{((250)(\pi)(1.25)^2)^2} = 5.2\times10^{-3}$$

$(0.5\text{-}1.5\ s^{-1})$

Therefore k_W is always greater than the above term in this system.

Typically, k_w was in the range 0.5 to 1.5 s^{-1} at 298 K whereas $\sum_M 2k_{2,M}[NO][M]$ and $\sum_M 2k_{3,M}[O][M]$ ranged between 5×10^{-3} s^{-1}(minimum) and 2.5×10^{-2} s^{-1}(maximum) and between 4×10^{-3} s^{-1}(minimum) and 2×10^{-2} s^{-1}(maximum) respectively for flow velocities of 250 cm s^{-1} at 298 K and conditions used in Sections 5,6 and 7.

Thus, NO did not influence the kinetics significantly in the presence or absence of reactant O_2 but acted mainly as an 'indicator' molecule. Any influence that NO has on the kinetics of reaction in this system can be neglected, although kinetic equations will be developed including NO for the sake of completeness, and to show that the effects of $[NO]$, even when significant, do not impair the method.

However, the condition

$$\sum_M k_{1,M}[O_2][M] >> k_W + 2k_{2,M}[NO][M]$$

$$\text{or} \quad \frac{\sum_M k_{1,M}F_{O_2},F_M}{(\bar{v}\ r^2)^2} >> k_W + \frac{\sum_M 2k_{2,M}F_{NO}F_M}{(\bar{v}\pi r^2)^2}$$

was not always satisfied in earlier experimental work, particularly for M=He or Ar at 295 K and higher temperatures. k_W ranged between 1-3 s^{-1} while $\frac{\sum_M k_{1,M}F_{O_2}F_M}{(\bar{v}\pi r^2)^2}$ ranged between a minimum value of 1.4 s^{-1} and a maximum of 7.1 s^{-1} for a range of $k_{1,M}$ = (1.2 to 5.1)x10^{14} cm^6 mol^{-2} s^{-1}.

To show that

$$\sum_M k_{1,M}[O_2][M] >> k_W \text{ or } \frac{\sum_M k_{1,M}F_{O_2}F_M}{(\bar{v}\pi r^2)^2} >> k_W$$

k_W = 1-2 s^{-1}

$k_{1,M}$ 1-5x10^{14} cm^6 mol^{-2} s^{-1}

F_{O_2} = 35x10^{-6} mol s^{-1}

Then $$\frac{(1x10^{14})(35x10^{-6})(500x10^{-6})}{[(250)(\pi)(1.25)^2]^2} = 1.4\ s^{-1}$$

However, this condition was upheld reasonably well for the remaining third bodies. Thus, from this point of view, the microwave discharge provides an opportunity for future improvement since it is capable of operating up to total pressures of 1 atmosphere, and therefore F_{O_2} and F_M can be increased for higher accuracy (Section 2.3) and $\bar{v}$ reduced.

However, k_W was reduced to a low value, 0.1-1 s^{-1} (Sections 2.7 and 2.8) by surface poisoning with metaphosphoric acid in system B, and the ratio of homogeneous/heterogeneous recombination was then much more favourable (10-50 fold). Finally, the conditions used in this work can be summarized as:

$$\sum_M k_{1,M}[O_2][M] >> k_W + \sum_M 2k_{2,M}[NO][M] >> \sum_M 2k_{3,M}[O][M]$$

with values ranging between 1-50 >> 0.1-3.0 >> 10^{-2}-10^{-3} s^{-1}.

3.3 The Determination of Rate Constants

The rate constant of a chemical reaction is most easily obtained from experimental data using the rate equation in the integrated form. The equation cannot always be directly integrated, or the integrated equation is too complex for ready use. It then becomes necessary to use graphical or approximate numerical methods of integration.

A graphical method was used to solve a differential rate equation by Larkin[49] in his study of the recombination of hydrogen atoms

$$H + H + M = H_2 + M$$

As this wall recombination was first-order in H, the rate equation contained two terms, one first-order and the other second-order in H. A rate expression of this kind cannot be readily integrated but in the present system, all significant terms are first-order in O and thus the rate expression can be readily integrated. An integrated rate equation was used by Hartley and Thrush,[55] in determining the rate constant for the related reaction:

$$H + NO + M = HNO + M$$

Their complete reaction scheme (including wall recombination) is analogous to the reaction:

$$O + O_2 + M = O_3 + M$$

and leads to terms which are all first-order in H. Although their treatment is similar to that used in this work, it is more difficult to apply and does not enable wall recombination rate constants to be obtained.

The rate equation for the reaction scheme given in Section 3.1 is

$$\frac{-d[O]}{dt} = k_W[O] + \sum_M 2k_{2,M}[NO][O][M] + \sum_M k_{1,M}[O][O_2][M]$$

i.e. assuming negligible second-order recombination for O-atoms (Section 3.2)

Integration gives

$$\frac{\bar{v}}{x} \ln \frac{[O]_o}{[O]} = k_W + \sum_M 2k_{2,M}[NO][M] + \sum_M k_{1,M}[O_2][M]$$

where $[O]_o$ is the concentration at t=0 and $[O]$ at t=t;

$\bar{v} = \frac{x}{t}$ x is a reaction distance corresponding to a reaction

time t from some arbitrary point at which t=0. Since $I=I_o[O][NO]$ and $[NO]$ = constant, then $[O] \propto I$. Also $[X] = \frac{F_X}{V}$ where $V=\bar{v}\pi r^2$ is the volume swept out in 1 s and F_X is the flow rate of the species X in mol s^{-1}. Then:

$$\frac{V^3}{V_R} \ln\left[\frac{I_o}{I}\right] = k_W V^2 + \sum_M 2k_{2,M} F_{NO} F_M + \sum_M k_{1,M} F_{O_2} F_M$$

where $V_R = \Delta x \pi r^2$ = reaction volume (corresponding to a reaction time t). In this form, the equation is very suitable for computation purposes [illegible]. Only the reaction volume need be noted and not reaction distance. The reaction volume can be measured accurately by a volumetric method (Section 2.3)

It is useful to distinguish between $M=O_2$ and $M=M'$ where $M' \neq O_2$. This gives the equation:

$$\frac{V^3}{V_R} \ln\left[\frac{I_o}{I}\right] = k_W V^2 + \sum_{M'} 2k_{2,M'} F_{NO} F_{M'} + 2k_{2,O_2} F_{NO} F_{O_2} + \sum_{M'} k_{1,M'} F_{O_2} F_{M'} + k_{1,O_2} F_{O_2}^2 \quad \ldots 3.1$$

In the most general situation $F_{M'}$, F_{O_2} and V may be varied independently and simultaneously. If one set of conditions is represented by $F_{M'}$, F_{O_2} and V, and another set by $F^*_{M'}$, $F^*_{O_2}$ and V^*, then the first-order decay for each set of conditions can be represented diagramatically (Fig. 3.1). Writing equation 3.1 for each set of conditions and subtracting one from the other, gives:

Figures 3.1 and 3.2

Diagramatic representation of first-order decay for conditions described by equation 3.1.

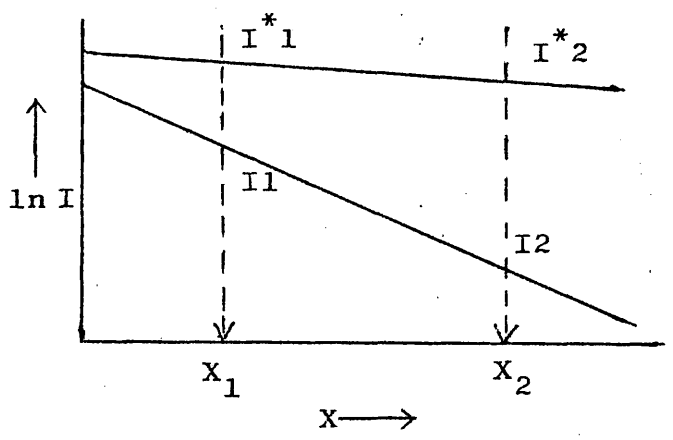

System A - Single observation point method

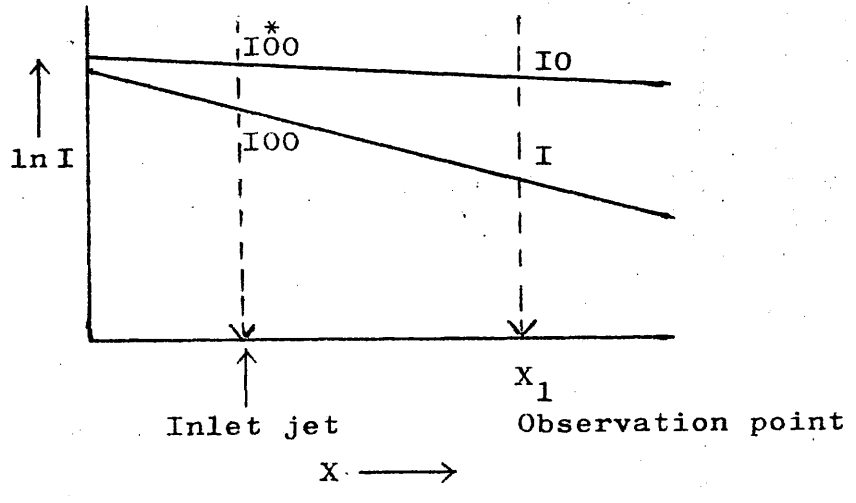

$$\frac{V^3}{V_R}\ln\left[\frac{I1}{I2}\right] - \frac{(V^*)^3}{V_R}\ln\left[\frac{I^*1}{I^*2}\right] = \left[k_W V^2 - k_W^*(V^*)^2\right] + \sum_{M'} 2k_{2,M'}F_{NO}\Delta F_{M'}$$

$$+ 2k_{2,O_2}F_{NO}\Delta F_{O_2} + \sum_{M'} k_{1,M'}\Delta(F_{O_2},F_{M'}) + k_{1,O_2}\Delta F_{O_2}^2 \quad \ldots\ 3.2$$

where $\Delta F_{M'} = F_{M'} - F_{M'}^*$, $\Delta F_{O_2} = F_{O_2} - F_{O_2}^*$, $\Delta(F_{O_2},F_M) = F_{O_2}F_{M'} - F_{O_2}^*F_{M'}^*$,

$$\Delta F_{O_2}^2 = F_{O_2}^2 - (F_{O_2}^*)^2 = (F_{O_2} + F_{O_2}^*)(\Delta F_{O_2}).$$

The term k_W^* indicates that, in general, k_W may be dependent on the set of conditions chosen. In this work, it was assumed (as indicated by previous work[47]) and as later verified experimentally, that k_W may be different in the presence and absence of O_2, possibly due to a wall reaction such as:

$$O + O_2 + \text{wall} = O_3 + \text{wall}$$

or a surface adsorption process which covers the active sites on the wall, but was not dependent on F_{O_2}. This phenomenon was examined and found to be significant but relatively small (Section 5.3). A simplification of equation 3.2 was always made (apart from in a few preliminary experiments) during this work by maintaining V and V^* as an accurate and equal quantity by adjusting the main controlling needle valve. For a given set of conditions, a determination of $k_{1,M}$ involved the maintenance of a relationship between the two sets of conditions $(V^*, F_{O_2}^*, F_{M'}^*)$ and $(V, F_{O_2}, F_{M'})$. The first set will be termed the 'reference' conditions, whilst the latter set were continually changed to enable $k_{1,M}$ to be evaluated.

Determination of k_1 for $M=O_2$

When $V=V^*$, $F^*_{O_2}=0$, $F^*_{M'}=F_{M'}$, then equation 3.2 can be written as

$$\frac{V^3}{V_{R}.F_{O_2}} \ln\left[\frac{I1}{I2}\frac{I^*2}{I^*1}\right] = \frac{V^2}{F_{O_2}}(k_W-k^*_W) + 2k_{2,O_2}F_{NO} + \sum_{M'} k_{1,M'}F_{M'} + k_{1,O_2}F_{O_2} \quad \ldots.3.3$$

where k_W indicates reaction (W) in the presence of O_2, and M', the carrier gas, always argon. Thus, k_{1,O_2} can be obtained from a plot of $\frac{V^3}{V_{R}.F_{O_2}} \ln\left[\frac{I1}{I2}\frac{I^*2}{I^*1}\right]$ against F_{O_2}.

When $\frac{V^2}{F_{O_2}}$, F_{NO} and $F_{M'}$ are maintained constant, $k_W - k^*_W$ can be determined from the intercept (Computer programme) and thus k_W can be calculated (k^*_W was also measured during each run from the 'reference' conditions). The wall recombination coefficients, γ^* and γ were calculated from

$$\gamma = \frac{2rk_W}{\bar{c}} \qquad \text{or} \qquad \gamma^* = \frac{2rk^*_W}{\bar{c}}$$

where r is the radius of the reaction tube, and $\bar{c}$ the mean atomic speed.

In practice, the term $\frac{V^2}{F_{O_2}}(k_W-k^*_W)$ was very small since F_{O_2} was large (Section 5.3) and it was not necessary to maintain V^2/F_{O_2} constant. However, this requirement can be removed altogether by arranging the conditions as $V^*=V$, $F^*_{O_2} \neq 0$, F_{O_2}, $F^*_{M'}=F_{M'}$, then equation 3.2 becomes

$$\frac{V^3}{V_R.\Delta F_{O_2}} \ln\left[\frac{I^*2}{I^*1}\frac{I1}{I2}\right] = 2k_{2,O_2}F_{NO} + \sum_{M'} k_{1,M'}F_{M'} + k_{1,O_2}(F_{O_2}+F^*_{O_2}) \quad \ldots 3.4$$

since k_W^* should be independent of F_{O_2}. In this case, to determine k_{1,O_2} the term $\frac{V^3}{V_R \cdot \Delta F_{O_2}} \ln\left[\frac{I1}{I2}\frac{I^*2}{I^*1}\right]$ is plotted against $(F_{O_2} + F^*_{O_2})$. This procedure is considerably more tedious.

Determination of $k_{1,M}$ for $M = M' \neq O_2$

When $V^*=V$, $F^*_{O_2}=0$ and $F^*_{M'}=F_{M'}$, then equation 3.2 becomes the same as equation 3.3 i.e.

$$\frac{V^3}{V_R F_{O_2}} \ln\left[\frac{I1}{I2}\frac{I^*2}{I^*1}\right] = \frac{V^2}{F_{O_2}}(k_W - k_W^*) + 2k_{2,O_2}F_{NO} + \sum_{M'} k_{1,M'}F_{M'} + k_{1,O_2}F_{O_2}$$

The term $\sum_{M'} k_{1,M'}F_{M'}$ can be expanded to $k_{1,M'_1}F_{M'_1} + k_{1,M'_2}F_{M'_2}$ where M'_1 is argon carrier gas and M'_2 the third body under consideration. Thus if V, F_{NO}, F_{O_2} and $F_{M'_1}$ are maintained constant, then k_1 for $M=M'_2$ can be obtained from a plot of $\frac{V^3}{V_R F_{O_2}} \ln\left[\frac{I1}{I2}\frac{I^*2}{I^*1}\right]$ against $F_{M'_2}$.

Once more, elimination of the wall recombination term is possible by choosing the conditions $V^*=V$, $F^*_{O_2} \neq 0$, F_{O_2}, $F^*_{M'_1} = F_{M'}$, which leads to equation 3.4, but the procedure then becomes tedious, no more sensitive, and any information on wall recombination is lost. However, intensity measurements can be made with increased rapidity since the wall always contains adsorbed O_2 and the decay profile reaches a steady

state very rapidly.

In preliminary experiments, k_{1,O_2} and $k_{1,M'}$ were determined by the single observation point method, and later by the double observation point method for accurate measurements, both in the sliding detector/single inlet-jet system A described below.

System A-Single Observation Point Method

A diagramatic representation of this method is given in Fig. 3.2. The intensities here have been re-assigned for clarity in distinguishing between the methods from the general diagram (Fig. 3.1) thus:

$$I^*1 \equiv I^*00, \quad I1 \equiv I00, \quad I^*2 \equiv I0, \quad I2 \equiv I.$$

It is assumed in this method that $I^*00 = I00$ and this is true providing the addition of M' (or reactant O_2) causes no serious flow perturbations. However, a direct determination of $I^*00/I00$ showed that this was not strictly justified and consequently, this method was lacking in accuracy (Section 5.2). The principle advantage of the method is it s rapidity.

System A/Double-observation Point Method

This method is represented diagramatically in Fig. 3.3. This notation is used for clarification when reference is made to this method. The method is exact, (unlike the single observation point method).

Summary for System A

Equation 3.3 requires that $V=V^*$ and V be kept constant during a run, and therefore total flow rates and pressures

Figures 3.3 and 3.4

System A - double observation point method

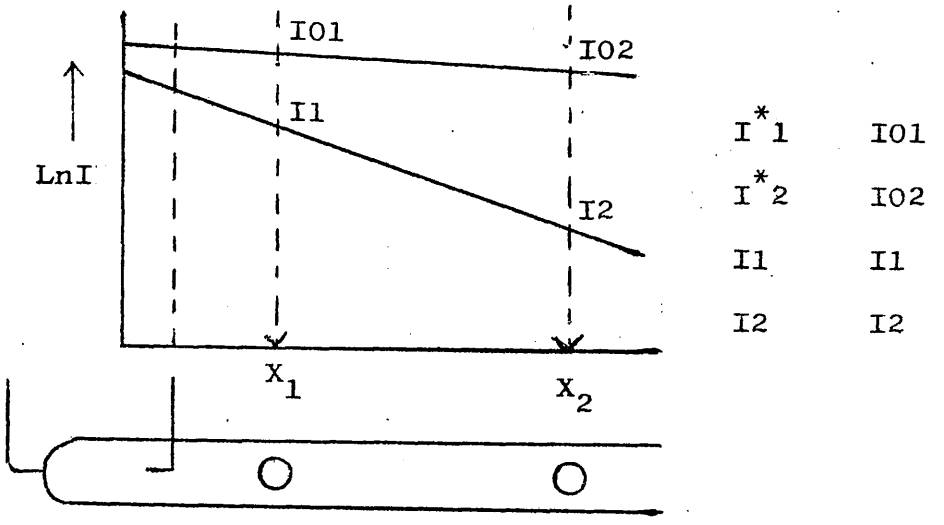

System B - Multiple inlet jet/Fixed detector method

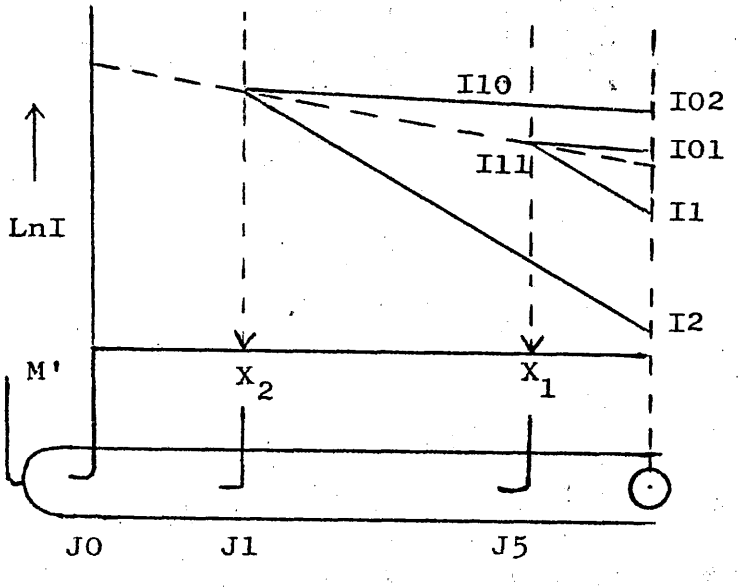

had to be calculated before a run. Furthermore, in general, the total pressure needed adjusting twice for one experimental point (once for each set of conditions) i.e. $(F^*_{O_2}, F^*_{M'})$ and $(F_{O_2}, F_{M'})$. The measurement of each set of conditions makes up one data point on a typical plot. For $M \neq O_2$, the two conditions $(F^*_{O_2}, F^*_{M'})$ and $(F_{O_2}, F_{M'})$ differed only in as much that a small additional flow of O_2 was added to a large excess of M' (Section 5.3) and in this case, $V \doteq V^*$ without adjusting the flow controlling valve since the overall change in gas flow velocity was negligible.

Another method of reducing the number of adjustments to the flow valve involves maintaining $(F^*_{O_2} + F^*_{M'})$ and $(F_{O_2} + F_{M'})$ constant by increasing $F^*_{M'}$ by the amount ΔF_{O_2}. However, this method is almost as tedious and not used in system A but was utilized in system B.

System B-Multiple Inlet Jet/Fixed Detector Method

In analysing this system, it was found that equation 3.2 can be applied only when $V=V^*$ as a result of the single observation point, and is therefore less versatile in this respect. Fig. 3.4 is the diagram for the kinetics of O-atom decay in this system. Here, O_2 is added through the inlet jets J1 and J5, M' through a separate jet (JO).

In constructing the diagram, it is assumed that the total pressure along the reaction tube is always constant although it will be shown that the accuracy of the method is not impaired by very small pressure fluctuations caused by

flow pertubations at the inlet jets. This situation is now analagous to system A with the double observation point method. Here, I01 and I02 are the intensities for sets of conditions ($F^*_{M'}$, $F^*_{O_2}$) added at x1 and x2 respectively. I1 and I2 are intensities for sets of conditions ($F_{M'}$, F_{O_2}) added at x1 and x2 respectively, and for each set of conditions, the total pressure must be maintained constant so that:

$$\frac{I1}{I2} = \frac{I11}{I12} \qquad \text{and} \qquad \frac{I01}{I02} = \frac{I11}{I10}$$

Therefore, the ratio required which is $\frac{I10}{I12}$ is equal to $\frac{I1}{I2} \cdot \frac{I02}{I01}$ since $V=V^*$, thus $(F^*_{M'} + F^*_{O_2}) = (F_{M'} + F_{O_2})$, (Fig. 3.4). The general equation (II) can now be applied with the new assignments

$$I^*1 = I01, \qquad I1 = I1$$
$$I^*2 = I02, \qquad I2 = I2$$

Determination of k_1 for $M=O_2$ or $M' \neq O_2$

Choosing the relationships $V^*=V$, $F^*_{O_2}=0$, $F^*_{M'}=F_{M'}+F_{O_2}$ and using equation 3.2 leads essentially to equation 3.3 as before with the exception that the term $2k_{2,O_2}F_{NO}$ is effectively cancelled, since $k_{2,O_2} \simeq k_{2,Ar}$. This arises since F^*_M is increased from $F_{M'}$ in equation 3.3 to $F_{M'}+F_{O_2}$, (the term $2k_{2,O_2}F_{NO}$ is negligible).

Once more, wall recombination can be eliminated by choosing $V^*=V$, $F^*_{O_2} \neq 0$ or F_{O_2}, $F^*_{M'} = F_{M'} + \Delta F_{O_2}$ which leads to equation 3.4 except that the term $2k_{2,O_2}F_{NO}$ is replaced by $-k_{1,M'}F^*_{O_2}$ (the latter can be made negligible and is a

constant). In this work, equation 3.3 was used for M' $\neq O_2$ (Section 5.3)

At temperatures below 300 K (Section 6) $\frac{I02}{I01} \simeq 1$ and it was possible to keep $F^*_{M'} = F_{M'}$. This arises since $\ln\left[\frac{I02}{I01}\right] = \frac{V_R}{V} \cdot \frac{F_{O_2}}{F_{M'}} \cdot k_W$ (when the terms in F_{NO} are neglected) and for M' $\neq O_2$, $F_{M'} >> F_{O_2}$ and k_W is small below 300 K, and $V >> V_R$. Above 400 K, this corrections is called the 'blank correction' and is not negligible (i.e. <5%). It should be noted, that as $(F^*_{M'} + F^*_{O_2}) = (F_{M'} + F_{O_2})$ then flow rates are identical and thus any flow perturbations at the inlet jets cancel: this is very significant when flow rates added through the inlet jets are larger or comparable to total flow rates and extends the use of system B to measurements for $M=O_2$, although this was not carried out in this work (see Section 7 on SO_2).

The general equation for the determination of k_W in system B can be shown to be:

$$\frac{V}{V_R} \cdot \frac{F^*_{Ar}}{\Delta F_{Ar}} \ln\left[\frac{I02}{I01}\right] = k_W + \frac{2k_{2,NO} F_{NO} F_{Ar}}{V^2} \left[\frac{F_{Ar} + F^*_{Ar}}{F^*_{Ar}}\right] \quad \ldots \quad 3.5$$

Where F^*_{Ar} = Flow rate of Ar through the discharge

F_{Ar} = Total flow rate of Ar.

$\Delta F_{Ar} = F_{Ar} - F^*_{Ar}$, flow rate of Ar through inlet jet.

k_W is thus obtained by plotting the left hand side of this equation against $\frac{F_{Ar}}{V^2}\left[\frac{F_{Ar} + F^*_{Ar}}{F^*_{Ar}}\right]$

Summary for systems A and B

The use of equation 3.3 for both systems A and B with

$M=O_2$ and $M\neq O_2$ gives rate constants in which wall recombination is subtracted out providing that V^2/F_{O_2} is kept constant, and cancels out perturbations around the inlet jets. From kinetic runs, k_W^*, k_W (and hence γ^* and γ) can be obtained. The quantities k_W^* and k_W are strictly mean values if they vary along the reaction tube (although experiments showed k_W was constant, and the same reaction zone is used during each rate constant determination) but in spite of this equation 3.3 remains valid even when the terms in F_{NO} are not negligible. However the terms are included for the sake of mathematical exactness, in principle, when NO concentrations are significant. Systems A and B are exactly equivalent in the mathematical sense, but system B is more convenient for measurement of temperature coefficients, since intensity measurements are always ratios, then effects due to wall adsorption, filter absorption, variation of the quantity I_o with third body etc. cancel out. These systems therefore allow mathematically sound rate constants to be determined since no approximations are made in the rate equations.

Appendix

M = O_2, Ar, He, N_2, CO, CO_2, SO_2.

F_M = Flow rate of gas M in mol s^{-1}

T = Temperature in °K.

P = Gas pressure in mmHg

r = Internal radius of flow tube in cm.

$\bar{v}$ = Mean linear gas flow velocity in cm s^{-1}.

V = Reaction volume swept out of flow tube in cm^3 s^{-1}.

M = Concentration of gas M in mol

The computer program 'Eureka' used to evaluate experimental data from sections 5-7 to produce rate constants is listed below.

```
      PROGRAM EUREKA     74/74   OPT=2                    FTN 4.6+428        24

 1              PROGRAM EUREKA (INPUT,OUTPUT)
                DIMENSION X(10),Y(10),VBAR(10),XX(10),YY(10)
                REAL I01,I1,I02,I2
                READ 101,L
 5        1     FORMAT(I2)
                DO 12 LL=1,L
          101   FORMAT(I2)
                READ 1,N
                READ 2,T,D
10        2     FORMAT(2F5.1)

          C     T IN DEGREES K, D IS DISTANCE IN CMS.

                PRINT 11
15              PRINT  123
                PRINT 22,T,D
          123   FORMAT(4X,'T',4X,'D')
          22    FORMAT(1X,2F5.1)
          11    FORMAT(1H1,///////)
20              PRINT 4
                DO 100 J=1,N

          C     F IS FLOW RATE IN CC/MIN., P IN CM. OF OIL ,I IS ARBITRARY.

25              READ 3,F1,F2,F3,I01,I1,I02,I2,P
          3     FORMAT(7F5.1,F6.3)
          4     FORMAT(3X,' F1',3X,'F2',6X,'F3',8X,'I01',7X,'I1',5X,  'I02',
                16X,'I2',9X,'P')
          33    FORMAT(1X,3(F5.1,3X),4(F5.1,4X),F6.3)
30              PRINT 33,F1,F2,F3,I01,I1,I02,I2,P
                R=82.06
                AREA=3.142*(1.245**2)

          C     C = LOG RATIOS OF INTENSITIES....
35
                C=ALOG((I02/I01)*(I1/I2))

          C     VBAR IS MEAN LINEAR FLOW VELOCITY
          C     0.688E-6 IS CONVERSION FACTOR FOR CC/MIN TO MOL/SEC.
40
                VBAR(J)=((F1+F2)*(0.688*1.E-6)*(82.06)*(76*T))/((P*0.078)*(AREA))
                Y(J)=((VBAR(J)**3)*(AREA**2)*C)/(D*F1*(0.688*1.E-6))
          100   X(J)=F3*0.688*1.E-6
          7     FORMAT(//,* VALUES OF Y= *10E12.4,//)
45        8     FORMAT(//,* VALUES OF X==*10E12.4,//)
                PRINT 7,(Y(J),J=1,N)
                PRINT 8,(X(J),J=1,N)
          9     FORMAT(//,* VALUES OF VBAR=*10E12.4,//)
                PRINT 9,  (VBAR(J),J=1,N)
50              CALL ALPHA(N,X,Y)
                CALL GRAPH(N,X,Y)

                CALL ALPHA(N,X,Y)
                CALL GRAPH(N,X,Y)
55        12    CONTINUE
                STOP
                END
```

```
   SUBROUTINE ALPHA      74/74   OPT=2

 1                SUBROUTINE ALPHA(N,X,Y)
                  DIMENSION X(20),Y(20)
                  SUMX=SUMY=SUMX2=SUMY2=SUMXY=SUMXX=0.0
                  DO 1 J=1,N
 5                SUMX=SUMX+X(J)
                  SUMY=SUMY+Y(J)
                1 SUMXX=SUMXX+X(J)*X(J)
                  XBAR=SUMX/N
                  YBAR=SUMY/N
10                XXBAR=SUMXX/N
                  DO 2 J=1,N
                  XX=XBAR-X(J)
                  YY=YBAR-Y(J)
                  SUMX2=SUMX2+XX*XX
15                SUMY2=SUMY2+YY*YY
                2 SUMXY=SUMXY-XX*YY
                  SLOPE=SUMXY/SUMX2
                  TOP=ABS(SUMX*SUMXY-SUMX2*SUMY2)
                8  ROOT=SQRT(TOP/(N-2))
20                 SD=ROOT/SUMX2
                   YINT=YBAR-SLOPE*XBAR
                  SDI=SD*SQRT(XXBAR)
                3 FORMAT(//,* SLOPE=*E12.4,//)
                4 FORMAT(//,* STANDARD DEVIATION=*E12.4,//)
25              5 FORMAT(//,*INTERCEPT=*E12.4,//)
                6 FORMAT(//,10X,'DATA FOR 0+02+M')
                  PRINT 3,SLOPE
                  PRINT 4,SD
                  PRINT 5,YINT
30                PRINT 4,SDI
                  PRINT 6
                  RETURN
                  END
```

```
SUBROUTINE GRAPH      74/74   OPT=2                    FTN 4.6+428

 1                    SUBROUTINE GRAPH (N,X,Y)
                      REAL X(100),Y(100),AX(101),AY(51),MINX,MINY,MAXX,MAXY
                      INTEGER IX(100),IY(100),D(101),DOT,SPACE,STAR,PLUS
                      DATA DOT,SPACE,STAR,PLUS/1H.,1H ,1HX,1H+/
 5          30        FORMAT(1H1)
                      PRINT30
                      MINX=X(1)
                      MAXX=X(N)
                C     SORTING OF X AND Y INTO DESCENDING ORDER
10              C
                      L=N-1
                1     K=0
                      DO 2 J=1,L
                      IF(Y(J+1).LT.Y(J)) GO TO 2
15                    TOP=Y(J+1)
                      Y(J+1)=Y(J)
                      Y(J)=TOP
                      T3P=X(J+1)
                      X(J+1)=X(J)
20                    X(J)=TOP
                      K=1
                2     CONTINUE
                C     SCALING PROCESS
                      IF(K.EQ.1) GO TO 1
25                    MINY=Y(N)
                      MAXY=Y(1)
                C     SCALING PROCESS....
                      SCALEX=100.0/(MAXX-MINX)
                      SCALEY=50.0/(MAXY-MINY)
30                    DO 3 I=1,101,10
                3     AX(I)=(((I-1)/SCALEX)+MINX)
                      DO 4 I=1,51,5
                4     AY(I)=(((I-1)/SCALEY)+MINY)
                C     CONVERSION TO INTEGERS
35                    DO 5 I=1,N
                      X(I)=(X(I)-MINX)*SCALEX
                      IX(I)=INT(X(I))
                      Y(I)=(Y(I)-MINY)*SCALEY
                5     IY(I)=INT(Y(I))
40              C     OUTPUT PRINT SCALE
                6     FORMAT(9X,5(11X,E9.3))
                7     FORMAT(8X,E9.3,5(11X,E9.3))
                      PRINT 6,(AX(I),I=11,91,20)
                      PRINT 7,(AX(I),I=1,101,20)
45              C     GRAPH PLOTTING LOGIC .....
                      DO 9 I=2,100
                8     D(I)=DOT
                      DO 9 I=1,101,10
                9     D(I)=PLUS
50              10    FORMAT(12X,103A1)
                      PRINT 10,SPACE,D,SPACE
                      K=M=50
                      L=1
                11    DO 12 I=1,101
55              12    D(I)=SPACE
                13    IF(IY(L).NE.K) GO TO 14
                      IXL=IX(L)+1
                      D(IXL)=STAR
                      L=L+1
60                    GO TO 13
                14    IF(K.EQ.M)GO TO 15
                      PRINT 10,DOT,D,DOT
                      K=K-1
                      GO TO 11
65              15    J=K+1
                      PRINT 16,AY(J),PLUS,D,PLUS,AY(J)
                16    FORMAT(2X,E9.3,X,103A1,E9.3)
                      IF(K.EQ.0)GO TO 17
                      K=K-1
70                    M=M-5
                      GO TO 11
                17    DO 18 I=2,100
                18    D(I)=DOT
                      DO 19 I=1,101,10
75              19    D(I)=PLUS
                C     OUTPUT PRINT SCALE
                      PRINT 10,SPACE,D,SPACE
                      PRINT 7,(AX(I),I=1,101,20)
                      PRINT 6,(AX(I),I=11,91,20)
80                    RETURN
                      END
```

SECTION 4

The Limitations of the Flow System and Estimation of Errors

4.1 Introduction

Many investigations of atomic recombination reactions have been made by flow methods, where radicals enter a flow tube of constant cross sectional area in the main bulk of gas. Stable molecules enter through a diffuser jet. The exact mathematical description of gas flows in such tubes becomes extremely complicated if effects of wall reactions, viscous flow and axial and radial diffusion are considered. Krongells[27] made a numerical analysis of the flow patterns in the case of second order volume recombination and first-order wall recombination by neglecting viscous pressure drop and axial diffusion. Kaufman[26] assessed the limiting conditions for oxygen atoms for which diffusion effects and viscous flow can be neglected in a homogenous pseudo first-order reaction (Section 4.2). The reliability of experimental values of rate constants can also be assessed by estimating the total error associated with them, (Section 4.3).

4.2 Limitations

When experimental gas flows are very fast, the pressure drop along the flow tube may not be negligible. For simple Poiseuille flow:

$$p_2^2 - p_1^2 = \frac{16FL\eta RT}{r^4\pi}$$

where p/mm Hg is the pressure, F the flow rate of gas, L the length of the reaction tube, r the tube radius and η the gas

coefficient of viscosity. For small pressure drops, the fractional change in p due to viscous flow is given by:

$$\frac{\Delta p}{p} = \frac{8\bar{v}L\eta}{r^2 p}$$

where $\bar{v}$ is the mean linear flow velocity. The pressure drop during experiments only becomes serious (1%>) in argon-oxygen mixtures when, (for L=50 cm, η =22.1x10^{-5} poise for Ar, r=1.25 cm and p=1.5 torr) $\bar{v} > 10^3$ cm^3 s^{-1} at 295 K. The relative error, Δ p/p increases with decrease in pressure.

It therefore appears[26] that slow flow rates are desirable, because of their negligible pressure drop and rapid radial diffusion, but this may create large axial concentration gradients and increase back diffusion. If radial concentration gradient is neglected and first order decay of O-atoms assumed, then the steady state concentration of oxygen atoms is given by:

$$\bar{v}.\frac{d[O]}{dx} + k_1[O] - \frac{Dd^2[O]}{dx^2} = 0 \quad .... \quad 4.1$$

where D is a diffusion coefficient of O-atoms into the gas. The homogeneous recombination will be assumed to proceed by a first order process ($k_1[O]$).

However, if the diffusion term is small, the first order rate constant, k_1, is given by:

$$k_1 = k_1^*(1 + \frac{k^* D}{\bar{v}^2})$$

where k^* is the observed, uncorrected rate constant given by

$$k^* \quad \frac{-\bar{v}d.\ln[O]}{dx} = \frac{-d.\ln[O]}{dt}$$

Thus, the condition for negligible back diffusion is therefore $Dk_1/\bar{v}^2 << 1$. For a pressure of 1 torr, $D \simeq 270$ cm^2 s^{-1}, k_1 = 1-5 s^{-1} due to wall recombination in a glass tube with r = 1 cm, the above inequality shows that for a typical flow velocity of 100 cm s^{-1}, the error in k is between 2% and 10%. Thus D increases with increase of pressure for volume recombination. The assumption of no radial concentration gradients is valid only if diffusion is sufficiently fast to swamp the gradients caused by wall recombination and viscous flow. Kaufman[26] has made an approximate estimation of radial concentration gradients assuming a parabolic velocity distribution. Once again assuming a first order volume recombination, the stationary state equation for this is given by:

$$v_o\left(1-\frac{r^2}{r_o^2}\right)\frac{d[O]}{dx} + k_1[O] - D\left(\frac{d^2[O]}{dx^2} + \frac{d^2[O]}{dr^2} + \frac{1}{r}\cdot\frac{d[O]}{dr}\right) = 0 \qquad \ldots\ldots \quad 4.2$$

where r_o is the radius of the reaction tube and $\bar{v}_o$ the flow velocity at r=0. For the boundary conditions $\frac{d[O]}{dr} = 0$ and $\frac{d[O]}{dr} = \frac{-k_w r [O]_w}{2D}$ at r=0 (where $[O]_w$ is the atomic concentration at the wall), the solutions of the above partial differential equation are of the form

$$[O] = [O]\, r\, e^{-\mu x} \qquad \ldots\ldots \quad 4.3$$

where $\mu = \frac{(k_1 + k_w)}{\bar{v}} \left[1 - \frac{2(k_1 + k_w)D}{\bar{v}^2}\right]$

if D is small and $[O]_w \simeq [\bar{O}]$ where $[\bar{O}]$ is the average atomic concentration.

Integration of 4.2 leads to an approximate radial concentration gradient given by

$$\frac{[O]_o - [O]_w}{\bar{O}} \simeq \frac{r_o^2}{4D}\left(\frac{\mu v_o}{4} + k_w\right) \simeq \frac{r_o^2}{8D}(k_1 + 3k_w)$$

Taking a typical low pressure=1.5 torr, $D = 200\ cm^2\ s^{-1}$ and r_o=1.25 it is seen that the differences in concentration between the centre of the tube and wall will not be > 1% for $k_w \simeq$ 1-5 s^{-1}. At higher pressures, and in large tubes, this effect can become large.

4.3 Estimation of Error

Errors encountered in the determination of a physical quantity fall into two categories, systematic and random errors. The first category, random errors, are those whose magnitude can vary in a random manner. The second category are systematic errors and are considered to be those errors which remain constant in sign and magnitude. The reproducibility or precision of an experimental measurement depends on the random errors involved whereas accuracy depends on systematic errors.

In general if a quantity y is a function of n variables, $x_1, x_2, \ldots x_n$, i.e. $y=f(x_1,x_2,\ldots.x_n)$ so that

$$dy = \left(\frac{dy}{dx_1}\right)_{x_2,x_3..} .dx_1 + \left(\frac{dy}{dx_2}\right)_{x_1,x_3,..} .dx_2 \quad \ldots\ 4.4$$

small errors in y are given by

$$dy = \left(\frac{dy}{dx_1}\right)_{x_2,x_3,..} .dx_1 + \left(\frac{dy}{dx_2}\right)_{x_1,x_3,..} .dx_2$$

In the case of systematic errors, there is a relation between $\frac{dx_1}{x_1}$, $\frac{dx_2}{x_2}$....etc., and so the total systematic error is given by the arithmetic sum of terms in 4.4. For random errors, $x_1, x_2, \ldots$ are all independent so y becomes algebraically less than the sum of the separate terms, and is given by [16]

$$dy^2 = \left(\frac{dy}{dx_1}\right)^2_{x_2,x_3,..} .dx_1^2 + \left(\frac{dy}{dx_2}\right)^2_{x_1,x_3,..} .dx_2^2$$

$$\text{or} \quad \left(\frac{dy}{y}\right)^2 = \sum_{i=1}^{n} \left(\frac{d\ln f}{d\ln x_i}\right)^2 \left(\frac{dx_i}{x_i}\right)^2 \qquad .... \quad 4.5$$

where dy is the expected relative error in y.

In the present work, the total error in the rate constants obtained was assessed by estimating all the random and systematic errors associated with each of the measurements and applying equation 4.4 and 4.5. These errors in individual measurements are given below.

(a) Reaction distance:

The distance between the two observation points in reaction system A was measured with a standard metre rule to within 0.5 mm. The distance between the jets in reaction system B was measured by a travelling mecroscope also to within 0.5 mm. The total error associated with the measurement of reaction distances was estimated to be

$$\frac{dx}{x} = \frac{0.05}{x} \qquad (x \text{ in cm.})$$

(b) Pressure:

The total expected error in the pressure readings was

estimated to be

$$\frac{dp}{p} = \frac{0.05}{p} \quad (p \text{ in cm Hg})$$

(c) Flow Rates:

The systematic error in the capillary flow meter and gas meter measurement was estimated to be

$$\frac{dF}{F} = \frac{0.05}{F} \quad (F \text{ is in mol } s^{-1})$$

(d) Temperature:

The temperature of the reaction tube was maintained to within $\pm 0.5^{o}C$ by a thermostated bath, by acetone-solid CO_2 mixtures or by liquid nitrogen. Estimated total error :

$$\frac{dT}{T} \text{ were } < 1x10^{-3}$$

(e) Radius of the Reaction Tubes:

The volume of a measured length of tube was determined by a burette and the radius was estimated to within 1%.

Further systematic errors arise from secondary recombination reactions or from the effects of diffusion and viscous flow. The former type of errors were avoided as far as was possible by suitably adjusting the experimental conditions (Section 3.2) while the latter contributed a total error of not more than 10% to the measured rate constants (Section 4.2).

The total error in the measured rate constants can be assessed by calculating the error associated with $k_{1,M}$ for recombination according to the plots of:

$$\frac{V^3}{V_R F_{O_2}} \cdot \ln\left[\frac{I1}{I2}\ \frac{I^*2}{I^*1}\right] \text{ against } F_M \text{ for } k_{1,M}$$

(Section 3.3) where $k_{1,M}$ is the slope of the line. The total expected error in the measurement of the term on the left hand side is (for F_M), (applying equation 4.5)

$$3\left(\frac{d\bar{v}}{\bar{v}}\right)^2 + 2\left(\frac{dr}{r}\right)^2 - 2\left(\frac{dF_{O_2}}{F_{O_2}}\right)^2 - 2\left(\frac{dr}{r}\right)^2$$

$$= 3\,(1\times10^{-3}) + 2(1\times10^{-4}) - 2\,(4\times10^{-4}) - 2\,(1\times10^{-4})$$

$$\text{therefore} \quad \frac{dY}{Y} \simeq 2\times10^{-3} = 0.2\%$$

and $$\frac{dX}{X} = \left(\frac{dF_M}{F_M}\right)^2 = \left(\frac{1}{500}\right)^2 = 4\times10^{-3}$$

Therefore total expected error in the slope is $\sim$ 5%. Therefore the maximum error expected is < 10%, allowing for systemic errors $\frac{dr}{r}$ and $\frac{dF}{F}$.

The maximum total error in the rate constant measurements (both random and systematic errors) is therefore probably < 20% and the precision of measurements is of the order of 10% or less. Determinations of $k_{1,M}$ are made as indicated in Section 5. The error limits of $k_{1,M}$ given in Sections 5, 6 and 7 refer to the error in measuring the slopes of the graphical plots described in these sections.

SECTION 5

The Experimental Determination of the Rate of the Homogeneous Reaction: $O+O_2+M=O_3+M$

5.1 Introduction

This section contains a description of the determination of the rate of the homogeneous combination of oxygen atoms with oxygen molecules at 295 K. A report of the determination of the temperature coefficient over the range 196-500 K is given in Section 7. Rate coefficients of reaction (1) were measured for six different third bodies, viz, M=O_2, Ar, He, N_2, CO and CO_2 and for each third body, sufficient determinations were made to establish the reproducibility of the value of $k_{1,M}$; until <u>at least</u> three values in agreement (5-15%) were obtained.

Although this reaction has been the subject of many studies in recent years, (Table 8.1) only a few workers have reported values of the rate constant for three or more third bodies. Thus Kaufman,[7] using a thermal decomposition-flow method studied nine third bodies, including M=CO_2, SF_6, H_2O, O_2, provided a comparison of third body efficiencies, but he found that $k_{1,M}$ had a larger probable error for the least efficient M, i.e. $\pm$10-15% for the most efficient and $\pm$15-25% for the least efficient. As in the present work, Kaufman's values showed the expected qualitative dependence on the nature of M, increasing with molecular complexity although here, the standard deviation is better, having values generally between $\pm$5-15%, and in many cases close to 5%. (cf. results for M=N_2, CO, CO_2). Mulcahy and Williams[50] using a stirred-

flow method studied 4 third-bodies, the standard deviation being ±10% for Ar to ±13% for CO_2 and ±4% for $M=O_2$ and He. Huie et al.[59] using the flash-photolysis resonance-fluorescence technique studied 3 third bodies with standard deviations of ±5-11%. Stuhl and Niki,[61] using a flash photolysis-chemiluminescence method and Meaburn et al.[76] using pulse radiolysis are the only workers, other than this work, to report values for M=CO, the value here of 2.4×10^{14} cm^6 mol^{-2} s^{-1} where the standard deviation is ±5% has the smallest error margin (Stuhl and Niki = ±9% and Meaburn = 10%). Thus this work is only the second report of a range as large as 6 third bodies for the reaction and the standard deviations are as good, and in some cases better, than those reported by other workers.

However, the important point is that the estimated absolute accuracy of 10-15% (Section 4) for the reported rate constants, in most cases shows a significant improvement on those estimated for the literature values (Table 8.1). A comparison of the inherent absolute accuracy of this discharge-flow method with the accuracy of alternative methods is given in Section 8.

Under the conditions described in Sections 2 and 3.2, no significant contribution from the reaction (. 3) or other homogeneous reactions occured. Rate constants were computed from the kinetic equations (Section 3.3) and the computer program.

The main aim of work described in this section was to re-examine and develop the discharge-flow method for determining the rate constants of fundamental atomic recombination

reactions at 295 K by means of several steps, viz:

(1) by seeking the conditions for the complete elimination of errors in the homogeneous rate constant $k_{1,M}$ which arise from heterogeneous surface recombination. This has not previously been achieved satisfactorily and has been a serious disadvantage of the method;

(2) by seeking the improvement of the precision (standard deviation) and absolute accuracy of the rate measurements over those currently reported in the literature, which are generally not better than 10-25% and 25-50% respectively;

(3) by developing a rapid and systematic method for the determination of atomic decay profiles to enable sufficient experimental points in a kinetic rate determination to be made in a reasonable time (1-2 hours) using relatively quickly constructed and inexpensive apparatus.

The first aim was achieved by maximizing the ratio of homogeneous to wall recombination (see Section 3.2) and also by allowing for differences in k_w and k_w^* (equation 3.3) and hence in γ and γ^* the wall recombination coefficients in the presence and absence of O_2 respectively. In fact, these <u>are</u> generally different and ignoring such differences can lead to significant errors in the determination of the homogeneous rate constant. This fact is shown here for the first time although Benson[12] suggested that γ and γ^* may be different as early as 1965.

The second aim was achieved by (i) measuring the parameters in equation 3.3, i.e. temperature, pressure, distance, flow

rate etc. (Section 2) as accurately as can be achieved with current instruments and (ii) by adding a large excess of third body M to ascertain that homogeneous recombination occured predominantly by M.

Finally, the third aim was effected by showing in preliminary experiments (Section 5.2) that atomic oxygen decay profiles were always first-order in the absence and presence of O_2 over the range of conditions used in rate constant measurements (Section 3.2). Hence, in the actual determination of rate constants, first-order decay of O could always be assumed and decay profiles were established by making relative measurements of $[O]$ at two points only along the reaction tube. This reduced the time required to measure a rate constant to approximately half an hour compared to 3-4 hours by conventional methods. Furthermore, the apparatus can be constructed in a few weeks at a minimal cost (£250).

In this section some of the many advantages of the discharge-flow method will be mentioned, and a full discussion of the results can be found in Section 8. The experimental apparatus used is described in Section 2.

5.2 Preliminary Experimental Work

The first part of the preliminary work was to determine whether or not the mean linear flow velocity $\bar{v}$ remained reasonably constant for a given setting of the main flow controlling valve (Section 2.2) for various mixtures of gases.

In the case of Ar/O_2 mixtures, it may be expected that $\bar{v}$ would be slightly greater in O_2 rich mixtures since the coefficient of viscosity (η) of Ar (221×10^{-6} poise at 296 K) is greater than that of O_2 (206×10^{-6} poise at 293 K) assuming Poiseuille flow along the reaction tube ($\bar{v} \propto 1/\eta$). This was determined in the following manner. Experimental flows of Ar and O_2 (350×10^{-6} mol s^{-1} each) were set up and admitted together through the inlet jet to reaction system A and the pressure was then fixed at a precise value between 4 and 5 cm measured on the oil manometer. The argon flow was then reduced by increments of 70×10^{-6} mol s^{-1} and the corresponding changes in pressure recorded until the argon flow rate was zero. The flow rate of oxygen was then reduced in a similar manner, again noting the pressure changes. The results are shown in Figure 5.1. The mean linear flow velicity, calculated from the equation given in Section 3.3 over the range of flow rates used, were found to be 10% higher for pure O_2 than for Ar in agreement with the Poiseuille flow equation (Section 2.6). $\bar{v}$ had intermediate values for various gaseous Ar and O_2 mixtures. Thus, generally whenever the composition of the flow stream was changed during kinetic runs, it was necessary to maintain $\bar{v}$ constant (to within $\sim$3%) by carefully adjusting the main flow controlling valve.

The second series of preliminary experiments carried out was to show that atomic decay profiles are first-order in O in the absence and presence of O_2 over the full range of flow conditions used in subsequent rate constant determinations.

Figure 5.1

Graph showing variation of mean linear flow velocity with various gas mixtures.

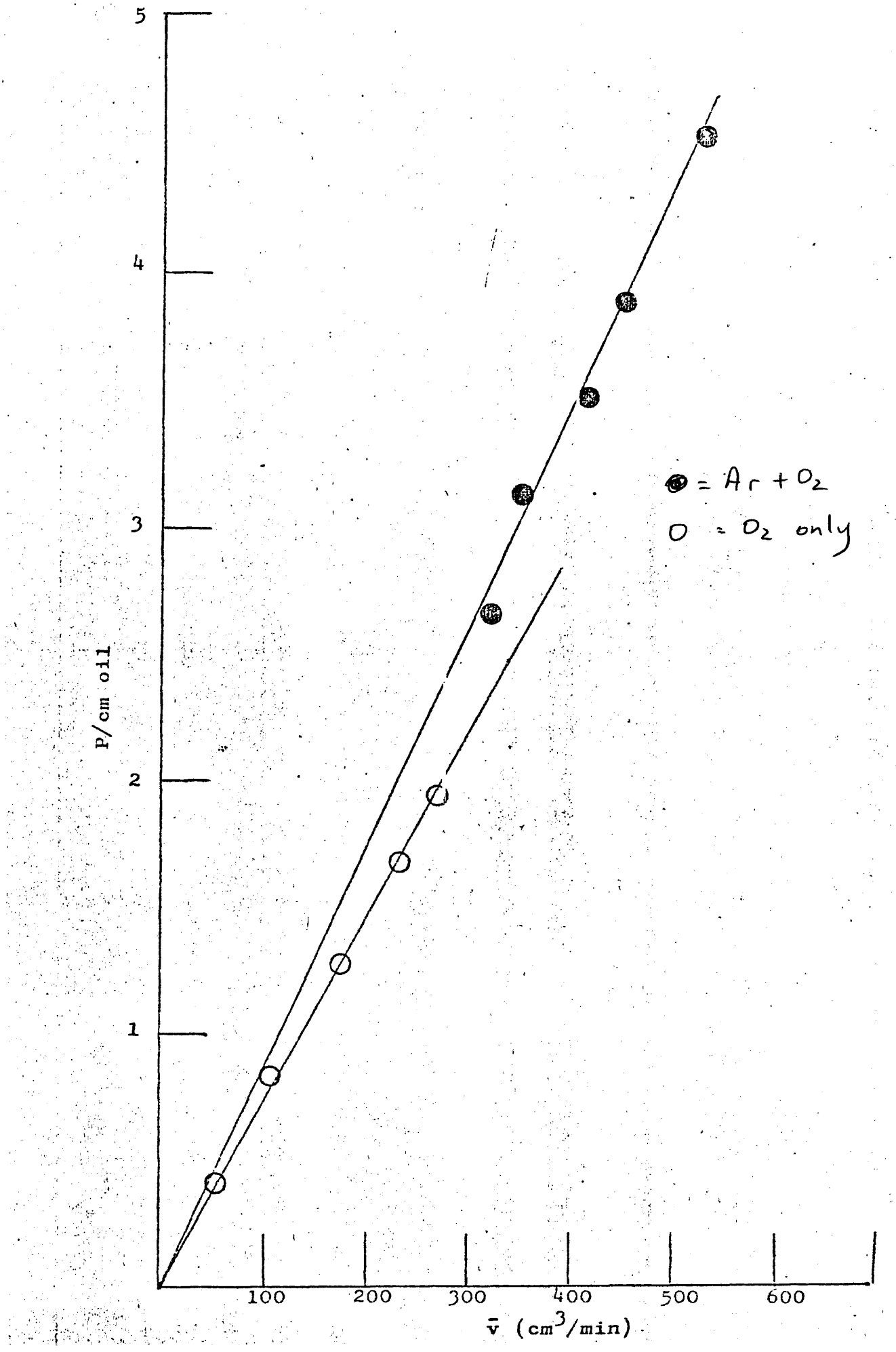

As discussed (Section 3.2), atomic recombination occured predominantly by reaction (1) in the presence of O_2 and predominantly by wall recombination in the absence of O_2. Thus, the 'indicator' molecule NO had no significant influence on the kinetics of recombination. Since it has been established[47] that wall recombination occurs by first-order kinetics in O, then providing the wall recombination coefficient is constant along the reaction tube, decays of O along the reaction tube should always be first order in the absence or presence of O_2. Also, impurities such as a hydrogenous molecules and electronically excited species were removed or shown to be absent (Section 2.3), these therefore had no influence on the decay kinetics. Thus, the relative decay of O-atoms along the length of the tube in reaction system A was recorded by measuring I (intensity of light) as a function of x cm (distance) downstream of the inlet jet over the full range of conditions used in subsequent rate constant determinations. This procedure ignores any changes in the light transmittance of pyrex glass along the tube but these are insignificant in this system. This was shown by examining the linearity of decay plots under conditions of negligible decay. Furthermore, in the determination of rate constants by either the single or double observation methods, this effect was absent under conditions given in Section 3.2 and in kinetic equations 3.1-3.3. Therefore, decays of O-atoms were recorded by manually sliding the photomultiplier down the tube and measuring the intensity at intervals of about 10 cm and plotting $\log_e$ I against x cm. Table 5.1 contains the data for

Figure 5.2

Typical atomic decay profiles showing first order decay of oxygen atoms in the absence (A) and presence (B) of O_2.

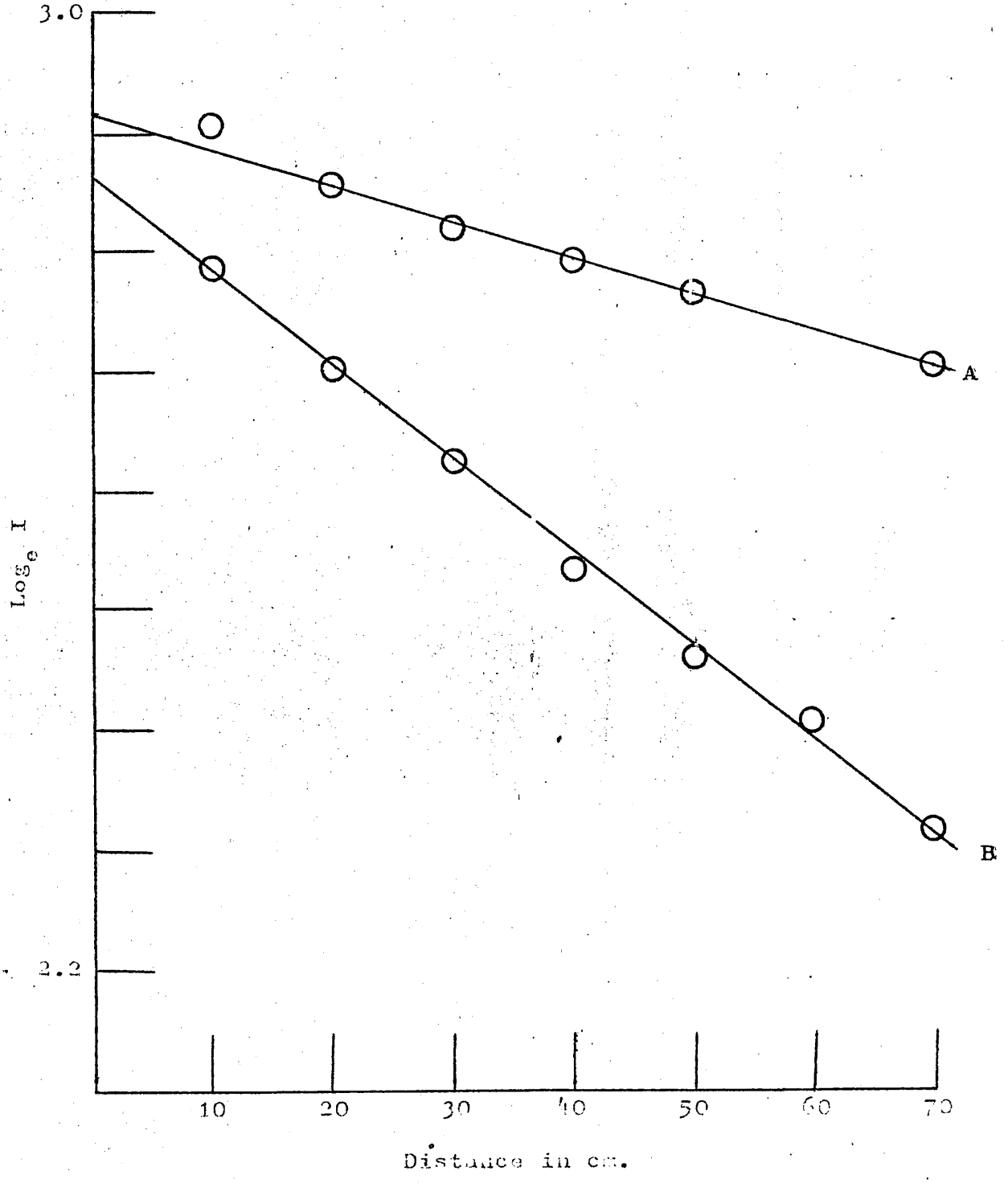

Figure 5.3

Typical atomic decay profiles showing first order decay of oxygen atoms in the absence (A) and presence (B) of O_2.

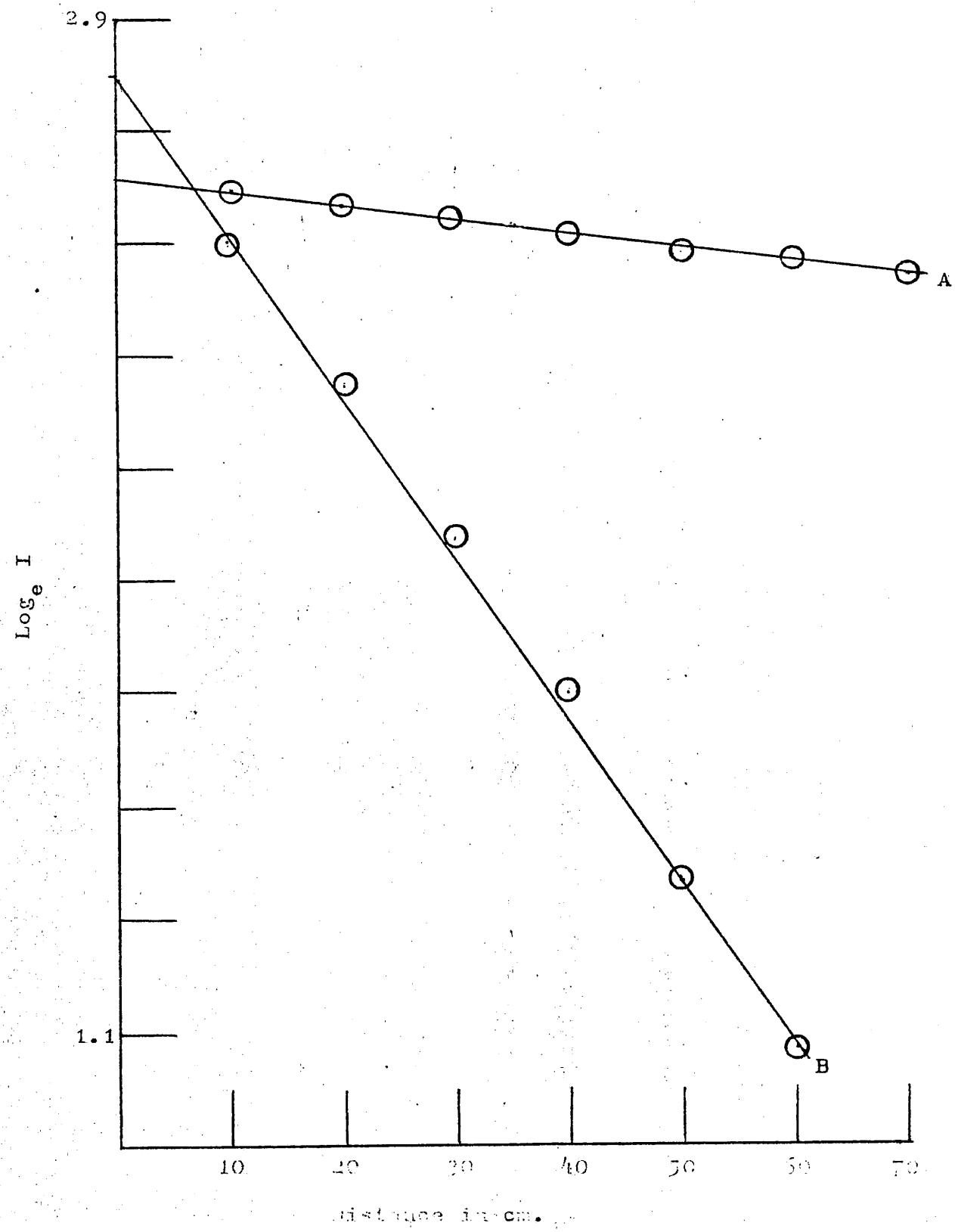

Fig. 5.2 showing typical atomic decay profiles for O in the absence of O_2 (A) and presence of O_2 (B). The two plots are both accurately linear over several half-lives, corresponding to the lower total pressure end of experimental conditions. Similarly, Fig. 5.3 shows a typical atomic decay profile for atomic oxygen in the absence (A) and presence (B) of O_2. These two latter plots which correspond to the higher pressure end of experimental conditions are again linear over several half-lives proving accurate first-order kinetics.

Table 5.1

Experimental data to construct typical atomic decay profiles showing first order decay of oxygen in the presence and absence of oxygen.

$P = 1.94$ mm Hg. $T = 295$ K. $\bar{v} = 460$ cm s^{-1}.

$F_{Ar} = 260 \times 10^{-6}$ mol s^{-1}. $F_{O_2} = 90 \times 10^{-6}$ mol s^{-1}.

A (absence of O_2)			B (presence of O_2)		
$\log_e I$	x cm	I	I	$\log_e I$	x cm
2.907	10.0	18.28	16.22	2.787	10.0
2.857	20.0	17.42	14.93	2.705	20.0
2.822	30.0	16.79	13.80	2.625	30.0
2.795	40.0	16.37	12.91	2.558	40.0
2.767	50.0	15.92	11.69	2.460	50.0
2.708	70.0	15.00	10.14	2.317	70.0

N.B. The symbols F_{Ar}, F_{O_2}, x, P, T are described in 'glossary' of symbols (Section 3).

The value of γ and γ^* were not determined from the decay profiles but were obtained fron equation 3.3 or 3.4 during rate constant determinations described in Section 5.3. In reaction system B, atomic decay profiles were also examined in the presence and absence of O_2 over the range of conditions to be subsequently used (at 295 K). Profiles were examined by observing the change in afterglow intensity as a function of distance by adding 35×10^{-6} mol s^{-1} O_2 through the 5 mixing jets (Section 2.2, Fig. 2.4), individually to the gas stream containing between 150 and 550×10^{-6} mol s^{-1} Ar, and recording each afterglow intensity at the fixed observation window. The data of Table 5.2 plotted in Fig. 5.4 shows typical atomic decay profiles in the presence of O_2 for the range of conditions used during the work. Accurate linear first-order kinetics in O were obeyed in all cases.

Table 5.2

Experimental data to construct a typical atomic decay profile in the presence of O_2

T = 295 K $\quad\quad$ $\bar{v}$ = 250 cm s^{-1}

10^6 F/mol s^{-1}	Intensity readings at					P/mm Hg
	J1	J2	J3	J4	J5	
144.5	156.7	162.1	168.5	172.8	178.1	2.66
192.6	142.0	149.5	157.8	163.5	170.7	3.94
240.8	121.0	129.8	139.3	146.1	154.2	4.93
288.9	093.9	103.9	116.1	124.9	134.3	5.97
361.2	063.5	071.7	082.4	089.1	097.5	7.41

Figure 5.4

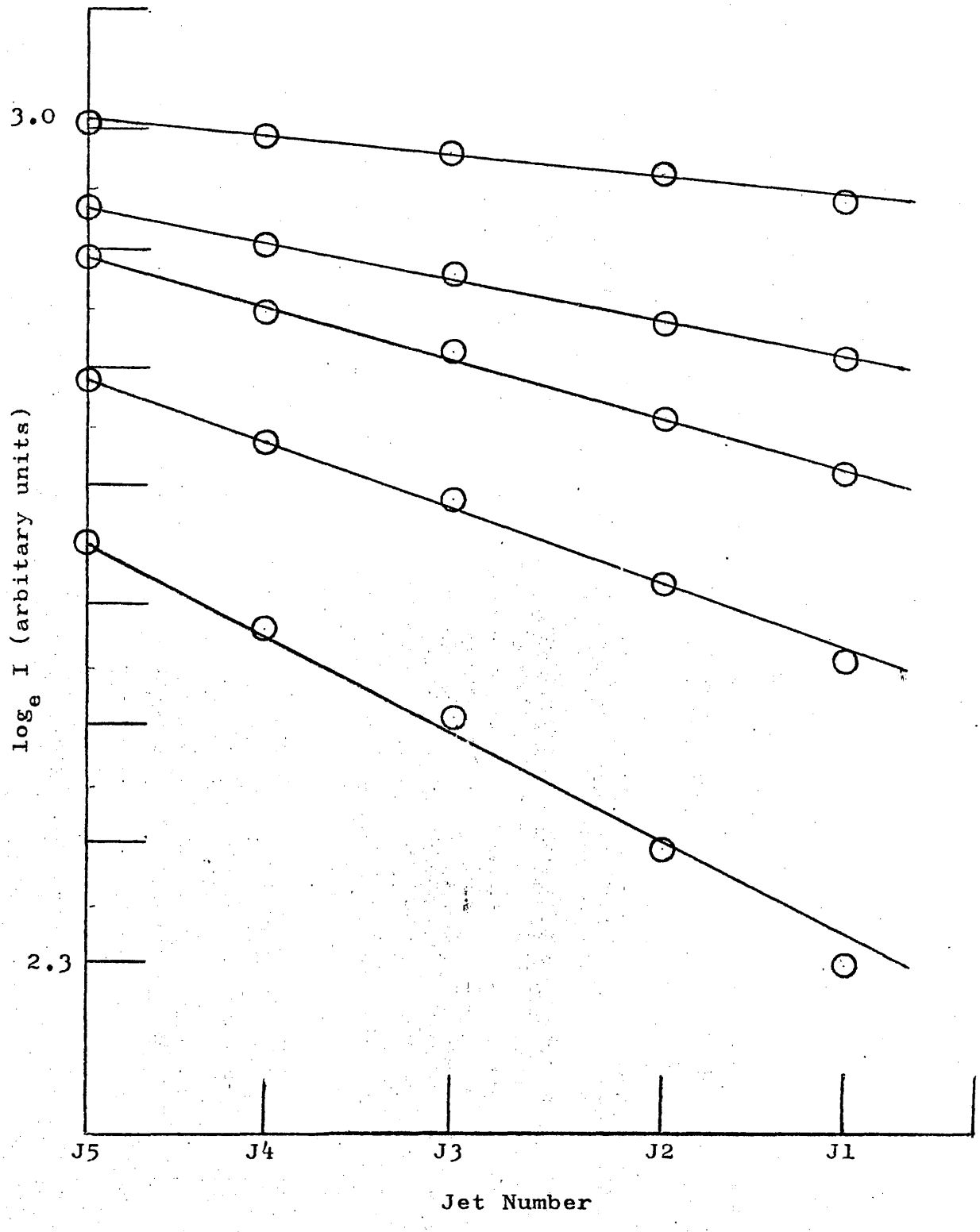

Typical atomic decay profiles showing first order decay of oxygen atoms in the presence of added O_2

These decay profiles in system B apply, with further preliminary experiments, to the determination of the temperature coefficient of reaction (1) for M=Ar, O_2, CO_2 and these further experiments will be described in Section 6.2. The wall in system B was poisoned with a layer of metaphosphoric acid (Section 2.7) to reduce wall recombination. In the first instance, decay profiles in the absence of O_2 were measured in exactly the same way as in system A, i.e. by measuring the afterglow intensities at various positions downstream of the discharge. Values of γ^* (in absence of O_2) were determined to be $\sim 3 \times 10^{-5}$ at 295 K in good agreement with the value of 2×10^{-5} quoted by Kaufman for phosphoric acid. In system B, as in system A, $(\gamma - \gamma^*)$ was determined during actual rate constant measurements from the equation 3.3. Also, in system B, γ^* could be determined during experimental runs in cases where 'blank' measurements (Section 6.2) were made by equation 3.5. Under the conditions used in this work, it is a reasonable assumption that atomic decay profiles are first-order in O in the presence and absence of O_2 (in the absence of hydrogenous and electronically excited species) since the kinetics have been well established elsewhere as first-order in O in a reaction tube of uniform catalytic activity. Thus the preliminary experiments proved mainly that the system was operating satisfactorily, the atom source was stable and that the light detection system was sufficiently stable and sensitive.

Having established that oxygen atoms decayed by first-order kinetics, initial attempts were made to measure the rate coefficient of reaction (1) in system A. Equation 3.3, (for $F^*_{O_2} = 0$, $F^*_{M'} = F_{M'}$) was used to compute rate constants firstly for $M=O_2$ by the single observation point method (Section 3.3). However, this method assumes that addition of O_2 through the inlet jet (Fig. 2.1) causes no change in I00, the light intensity <u>at</u> the inlet jet, due to any flow perurbations, over the experimental range of conditions. To test this assumption, the photomultiplier was attached 2 cm upstream from the inlet jet and the Ar carrier and pressure were first set to experimental conditions (viz, $F_{Ar} = 350\times10^{-6}$ mol s^{-1}, P = 2-4 torr). Increasing rates of O_2 up to 350×10^{-6} mol s^{-1} were then introduced through the jet and the change, if any, of intensity was noted. Typical results given in Table 5.3 show that the intensity did change significantly on addition of O_2 presenting evidence of some flow perturbation and/or back diffusion.

<u>Table 5.3</u>

<u>Change of I00 at jet on addition of oxygen</u>

T = 295 K $\quad \bar{v}$ = 400 cm s^{-1}

$F_{Ar}/cm^3\ min^{-1}$	$F_{O_2}/cm^3\ min^{-1}$	P/mm Hg	I00	I01
350	102.0	2.63	56.0	77.0
350	196.0	3.07	35.7	45.1
350	265.0	3.68	54.0	84.0

The only advantage of the single observation point method is it's convenience and rapidity, a rate constant can be measured in approximately 10 minutes. Even although I00 changed and the term V^2/F_{O_2} (Section 3.3) was not kept constant (the necessity of maintaining V^2/F_{O_2} constant to allow for changes in the wall recombination coefficient on addition of O_2 was not realised at this time), several kinetic runs were attempted using one observation point and the equation 3.3 to determine $k_{1,M}$ for $M=O_2$. The purified O_2 was admitted through the inlet jet and the ratio's $I0/I$ at a point 50 cm from the inlet jet were recorded for each individual concentration of O_2 used, i.e. $0-500\times10^{-6}$ mol s^{-1}. All experimental parameters eg. $\Sigma F,P,T$, x, were recorded. Altogether, about 8 runs were made with this method, of which 2 were retained for $M=O_2$ and 2 for M=Ar. The other 4 were rejected since they were obtained using a primitive initial design of Wood's tube (not the special design described in Section 2.3) in the case of $M=O_2$ and were affected by 'sputtering', and in the case of M=Ar, suffered from electrical interference between the R.F. unit and the digital voltmeter. Each kinetic run contained between 2 and 10 points, and a typical set of data for one run ($M=O_2$) is given in Table 5.4 which contains the data for the plot in Fig. 5.5. Although this method lacked precision (standard deviations of rate constants were about $\pm$25%), the value for k_{1,O_2} quoted in Table 5.4 is only about 10-20% above the value obtained by the final kinetic method adopted. This was possibly due to differences in γ^* and γ partly cancelling errors due to changes in I00. It was also

Figure 5.5

Single observation point method

Plot to determine k_{1,O_2} from data in Table 5.4.

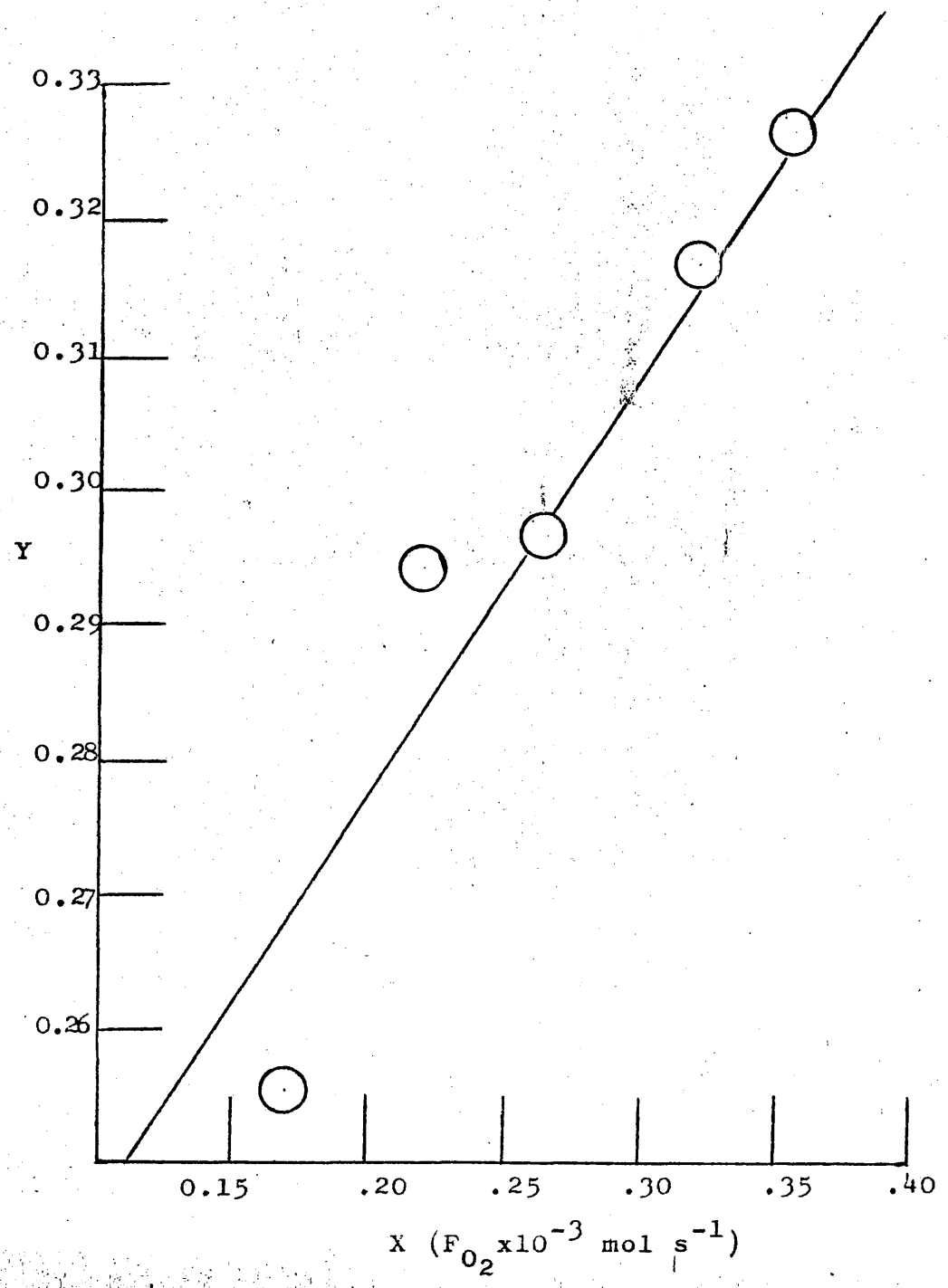

Experimental data for determination of k_{1,O_2} according to Fig. 5.6 and the single observation point method.

X = 57.5 cm, T = 295 K, $k_{1,O_2} = 2.41 \pm 0.40 \times 10^{14}$ cm^6 mol^{-2} s^{-1}

F_1/μ mol s^{-1}	F_2/μ mol s^{-1}	F_3/μ mol s^{-1}	IO	I	P/cm Hg	$\bar{v}$/cm s^{-1}
170.4	62.2	170.4	234.0	136.0	2.178	505
221.8	62.2	221.8	246.0	117.0	2.583	520
252.7	62.2	252.7	243.0	106.0	2.838	526
321.5	62.2	321.5	243.0	082.0	3.418	532
356.9	62.2	356.9	237.0	076.0	3.623	548

Table 5.4

found that in later runs, the standard deviation of the slope (calculated by the subroutine 'ALPHA' (. P87) i.e. the value for $k_{1,M}$, depended on the conditions being optimum (Section 3.2), whereas this did not affect the accuracy of the slopes.

The single observation point method is not the best one since the quantity I00 changed after addition of reactant and V^2/F_{O_2} was not constant throughout a run. Therefore, in an effort to improve the precision and overall accuracy of the technique, as a result of the theoretical arguement (Section 3.3) equations 3.3 and 3.4 were used to compute rate constants. Observations of the afterglow were made at <u>two</u> fixed points along the flow tube A, 50 cm apart; the first observation point was 30 cm downstream from the inlet jet (Section 2.2). Fig. 3.3 describes the experimental decay situation for this method which is unaffected by I00 changing on addition of O_2, whereas Fig. 3.1 shows the situation is affected; this is further borne out in Fig. 5.2 and 5.3 where the decay plots do not extrapolate back to the value of $\log_e$I00 under pressures used subsequently. For each point in a kinetic run, the ratio (I01/I1) was first determined at X1 and (I02/I2) at X2 by sliding the photomultiplier along the tube in that order. This was found to be preferable to the practice of measuring I01 and I02 together since the former method is quicker, more convenient and ensures that the ratios cancel out any geometrical factors in intensity measurements at X1 and X2. Intensities were only recorded when the reading on the output monitor was steady. Experimental variables were also recorded for each point and

accurately measured. Large flow rates of M (up to 500×10^{-6} mol s^{-1} for $M=O_2$) were studied, the flow of Ar 'carrier' in the discharge was maintained at a fixed steady rate of about $50\text{-}70 \times 10^{-6}$ mol s^{-1} to promote discharge and O-atom stability and more important, V^2/F_{O_2} was maintained at a constant value throughout each kinetic run by careful adjustment of the main controlling valve. Allowance was made for the background light (eg. from the discharge) and the photomultiplier dark current (Section 2.5) during rate measurements, although they were always less than 5% of light intensity measurements. Axial reflection of light was negligible (Section 2.4). The dark current was checked periodically since this 'drifted' about a mean reading although the drift was negligible. These final attempts to improve the accuracy and precision of the discharge-flow method proved to be most effective and the results of the determination of $k_{1,M}$ for $M=O_2$, Ar, He, N_2, CO and CO_2 and the corresponding values for γ and γ^* for these third-bodies are reported in Section 5.3.

5.3 Determination of the rate of the homogeneous reaction

$$O + O_2 + M = O_3 + M$$

at 295 K.

This section contains a report of the experimentally determined rate constants obtained in this work, which were produced by means of the kinetic equations previously described and the computer program (Eureka - p87). Values of $k_{1,M}$, $\gamma - \gamma^*$ are tabulated (Table 5.5) a full discussion of these

values is given in Section 8. Reaction system A was used for all determinations of $k_{1,M}$ at 295 K. Although 25 runs were carried out the results of only 20 were finally retained. The 5 rejected had standard deviations greater than 30% and and linear plots were not always obtained (eg. for M=CO in initial runs) due to the effect of impurities (Section 2.5). The results of the 20 runs generally had an overall accuracy of $\pm$ 5-15%. No difficulties were encountered with background light or metal sputtering, although reaction tube A was frequently cleaned with an HF/Tepol solution followed by rinsing with water.

The first third body to be studied using the double observation point/sliding detector method was O_2. The special 'Wood's' type discharge (Section 2.3) was switched on and the ground state O-atoms in the Ar carrier were allowed to travel along the flow-tube in the absence of reactant O_2 at a pressure of 2 Torr, to come to a steady state with the surface of the wall. After this surface 'conditioning' process, a minimum of about 30×10^{-6} mol s^{-1} O_2 acting as reactant <u>and</u> third body was added through the inlet jet. The total pressure (P) was recorded and the ratio I01/I1 was measured as described above. I02/I2 was also measured in the same manner. The flow of O_2 was then further increased to a maximum of 500×10^{-6} mol s^{-1}, and the procedure repeated until a run of 5 to 10 points was obtained. However, as in this case, when reactant and M are the same, the surface term $\frac{V^2}{F_{O2}} (k_W - k_W^*)$ can be neglected. A typical set of experimental data for $M=O_2$ is given in Fig. 5.6. The graphs are obtained

from equation 3.3. Values of $k_{1,M}$, γ and γ^* given in Table 5.5 with standard deviations of $k_{1,M}$ and the corresponding 'run number' eg. ($R20_2$). $\gamma - \gamma^*$ was calculated as described in Section 3.3. The linearity of the plots indicate that $(k_W - k_W^*)$ is negligible. The final mean value for k_{1,O_2} agrees well with values determined by the most reliable alternative techniques and a full comparative discussion will be given in Section 8.

Rate constants were then determined for M=Ar and values for $k_{1,Ar}$ (Table 5.5A). A typical set of experimental data using a radio-frequency discharge is plotted in Fig. 5.7. It was necessary to include a small correction for background, mainly electrical interference; in other runs, corrections were insignificant. The value $k_{1,Ar} = 1.46 \pm 0.09 \times 10^{14}$ cm^6 mol^{-2} s^{-1} was determined in system B in order to compare the errors in the two systems. The fact that the values of $k_{1,Ar}$ obtained in systems A and B are reproducible using equation 3.3 indicates that the two systems are accurate and exactly equivalent. Run R1Ar was made using a microwave discharge and R2Ar using the Wood's tube. All remaining runs for the determination of $k_{1,M}$ were carried out with 100×10^{-6} mol s^{-1} Ar passing through the discharge. The flow velocity for M=Ar was maintained at 250 cm s^{-1}. The mean rate constant of $1.49 \pm 0.18 \times 10^{14}$ cm^6 mol^{-2} s^{-1} for M=Ar has a precision of 12% which is better than the range reported by Kaufman[47] ($\pm$15 to 25%) and as good as that of Huie's[59] (10%). The agreement with the results of other workers is good and this rate constant is reasonably well established.

Data for M=He is plotted in Fig. 5.8. The mean value of $k_{1,He}$ was $1.34\pm0.22\times10^{14}$ cm^6 mol^{-2} s^{-1}, $\bar{v}$ was maintained at 200 cm s^{-1} and F_{O_2} 35×10^{-6} mol s^{-1}. The He flow rate was varied between 0 and 275×10^{-6} mol s^{-1}. The rate constant for nitrogen studied i.e. k_{1,N_2} appears to be absolutely established since it can be stated with 95% confidence (Table 8.3) that the value of k_{1,N_2} is $2.10\pm0.28\times10^{14}$ cm^6 mol^{-2} s^{-1} from the combined values reported here and those of other workers (Table 8.1), this confidence limit also includes the value of 2.52×10^{14} cm^6 mol^{-2} s^{-1} (Slanger and Black[52]) which is probably too high due to inadequate allowance for wall recombination. Fig. 5.9 gives a typical set of data (Run no. $R3N_2$), the mean value of k_{1,N_2}, $2.01\pm0.19\times10^{14}$ cm^6 mol^{-2} s^{-1} is in excellent agreement with the values reported by Kaufman and Huie. Flow velocities in these runs were 200 cm s^{-1} and N_2 was added at a maximum of 240×10^{-6} mol s^{-1}.

Only two other determinations of $k_{1,CO}$ have been reported (Table 8.1). The value of $2.41\pm0.6\times10^{14}$ cm^6 mol^{-2} s^{-1} ($\pm25\%$) obtained [61] (Section 8) using a flash photolysis-chemiluminescent technique is in excellent agreement with the mean value of $2.35\pm0.12\times10^{14}$ cm^6 mol^{-2} s^{-1} ($\pm5\%$) obtained here. Workers studying this gas have found considerable difficulty in purifying it (Section 2.6), but reproducible results in the present work were obtained using the trapping apparatus (Fig. 2.3). The molecular sieve traps were freshly regenerated at 473 K and then used at 196 K and 77 K in the order shown in the block diagram. In addition, the 77 K trap was maintained at a pressure between $\frac{1}{2}$ and 1 atmosphere to

trap impurities such as CH_4 while permitting the free passage of CO. This was achieved by careful setting of the needle valves. A sample of a Matheson (B.O.C.) CO was examined by a mass spectrometer for the presence of impurities. Iron carbonyl was found to be absent and other impurities present are given in Table 2.5. Three runs were carried out which gave accurate ($\pm$5%) and reproducible values for $k_{1,CO}$. A typical set of experimental results is plotted in Fig. 5.10. $\bar{V}$ was maintained at 260 cm s^{-1}. More independent determinations of the rate of this reaction are clearly needed. There is critical need for accurate rate data for the reaction since it has been ascertained that the reactions of O with O_2 and CO are important in the atmospheres of Mars and Venus. For similar reasons, the rate of reaction (1) for $M=CO_2$ also needs to be well established. About 6 determinations of k_{1,CO_2} have been made but the values are still in some disagreement, ranging from 3.56×10^{14} cm^6 mol^{-2} s^{-1} by Meaburn[76] to 9.7×10^{14} cm^6 mol^{-2} s^{-1} by Mulcahy et al[50] although the latter value is probably high due to incomplete mixing in their reactor and substantial corrections were applied to flow equations. However, the mean value of $5.33\pm0.51\times10^{14}$ cm^6 mol^{-2} s^{-1} obtained here is in good agreement with other workers.[47,51,76] A typical set of results are plotted on Fig. 5.11. Flow velocities in these runs were maintained at 300 cm s^{-1} and maximum flow rates of CO_2 were 380×10^{-6} mol s^{-1}. In an early experiment, a plot of the data of one run was curved and this was attributed to back diffusion of CO_2 to the microwave discharge used (in early work with the microwave discharge

it was placed too close to the inlet jet) and use of too high discharge power $<$120 watts. This results in production of O (^{1}D) atoms by the reaction:[52]

$$CO_2 \xrightarrow{h\nu} CO + O(^1D)$$

which interfere with the kinetics of the system. However, when the discharge was moved farther away from the jet and a minimal power ($<$20 watts) used, plots then became linear.

5.4 Wall recombination

The value of $\gamma \doteq 3 \times 10^{-5}$ on pyrex coated with phosphoric acid is in good agreement with Kaufman's value on the same surface. A brief review, however, has already been given (Section 2.7) and a full discussion will be given later (Section 8). The measured values of γ are reliable since they do not depend on diffusion. The linearity of the plots obtained for $k_{1,M}$ also provide experimental evidence that k_W is independent of the flow of M. Furthermore, in most cases, it can be seen that values of γ and γ^* are significantly different, although the difference here did not cause errors in the determination of $k_{1,M}$ (discussion, Section 8). The fact that O_2 changes the surface recombination coefficient has not been previously reported and may well be responsible for the discrepancy between temperature coefficients as determined by flow methods and in a static system (where surface recombination is negligible). A determination of the temperature coefficient for M=O_2, Ar, CO_2 can be found in

Section 6. 'Blank' determinations were made in Section 6 according to equation 3.5 and results of this will be fully discussed in Section 8.

Table 5.5 (A)

Mean values of $k_{1,M}$, γ and γ^* for reaction

$$O + O_2 + M = O_3 + M$$

Run No.	T/K	$k_{1,M}/10^{14}$ $cm^6\ mol^{-2}\ s^{-1}$	$\gamma^*(x10^5)$	$\gamma - \gamma^*$
R1 He		1.40 ± 0.26	10.6	2.2
R2 He		1.46 ± 0.31	10.0	4.0
R3 He		1.16 ± 0.08	8.8	2.3
Mean value with combined S.D.	295	1.34 ± 0.22	9.8 ± 1.0	2.8 ± 0.7
*R1 Ar		1.46 ± 0.09		
R2 Ar		1.47 ± 0.34	7.5	2.5
R3 Ar		1.53 ± 0.11	9.5	-0.8
Mean value with combined S.D.	295	1.49 ± 0.18	8.5 ± 1.0	1.6 ± 0.9
R1 N_2		2.05 ± 0.14	9.6	-3.3
R2 N_2		1.80 ± 0.13	8.8	-3.9
R3 N_2		2.14 ± 0.18	13.5	-3.0
R4 N_2		2.06 ± 0.19	10.0	
Mean value with combined S.D.	295	2.01 ± 0.15	10.5 ± 2.0	-3.4 ± 0.5

* Measured in system B.

Table 5.5 (B)

Mean values of $k_{1,M}$, γ and γ^* for reaction:

$$O + O_2 + M = O_3 + M$$

Run No.	T/K	$k_{1,M}/10^{14}$ $cm^6\ mol^{-2}\ s^{-1}$	$\gamma^*(x10^5)$	$\gamma - \gamma^*$
R1 O_2		2.27 ± 0.09	6.9	-0.6
R2 O_2		2.03 ± 0.18	9.5	-0.5
R3 O_2		2.07 ± 0.24	9.0	-0.9
Mean value with combined S.D.	295	2.12 ± 0.17	8.4 ±	-0.7 ±
R1 CO		2.40 ± 0.13	2.64	5.6
R2 CO		2.37 ± 0.12	2.74	4.0
R3 CO		2.29 ± 0.11	4.52	3.4
Mean value with combined S.D.	295	2.35 ± 0.12	3.3 ± 0.3	4.3 ± 0.3
R1 CO_2		5.08 ± 0.44	1.3	1.6
R2 CO_2		5.01 ± 0.79		
R3 CO_2		5.91 ± 0.30		
Mean value with combined S.D.	295	5.33 ± 0.51		

Figs. 5.5 to 5.11

Graphs of $\frac{V^3}{V\ F_{O_2}}\ \ln \frac{I1}{I2}\frac{I^*2}{I^*1}$ are represented by Y and are plotted against F_M represented by X in the reaction:

$$O + O_2 + M = O_3 + M$$

In the tabulated data at the head of each graph:

T is the temperature, K.

D is the reaction distance, cm.

F_1 is the flow rate of reactant O_2, mol s^{-1}.

F_2 is the flow rate of M plus flow rate of Ar from the discharge, mol s^{-1}.

F_3 is the flow rate of M, mol s^{-1}.

IO1	I^*1
I1	I1
IO2	I^*2
I2	I2

P is the reaction pressure, cm oil.

V Bar is the mean linear flow velocity; cm s^{-1}.

Fig. 5.6, $M=O_2$

Fig. 5.7, M=Ar

Fig. 5.8, M=He

Fig. 5.9, $M=N_2$

Fig. 5.10, M= CO

Fig. 5.11, $M=CO_2$

Figure 5.6

R102

T D
295.0 52.0

F1	F2	F3	I01	I1	I02	I2	P
41.9	76.0	41.9	271.5	237.0	219.0	189.0	.947
322.5	76.0	322.5	270.0	143.0	216.0	88.0	2.873
448.6	76.0	448.6	264.0	120.5	213.0	67.0	3.339
528.1	76.0	528.1	276.0	107.5	220.5	56.0	3.697
626.2	76.0	626.2	267.0	81.5	222.0	38.0	4.233

VALUES OF Y= .1290E+11 .5292E+11 .7894E+11 .8665E+11 .1034E+12

VALUES OF X== .2883E-04 .2219E-03 .3086E-03 .3633E-03 .4308E-03

VALUES OF GAMMA = .685731E-04 .791669E-04 .864429E-04 .940274E-04 .784783E-0

VALUES OF VBAR= .4148E+03 .4612E+03 .5235E+03 .5445E+03 .5527E+03

SLOPE = .2266E+15

STANDARD DEVIATION = .8842E+13

Y-INTERCEPT = .5624E+10 CORRELATION COEFF.= .997724

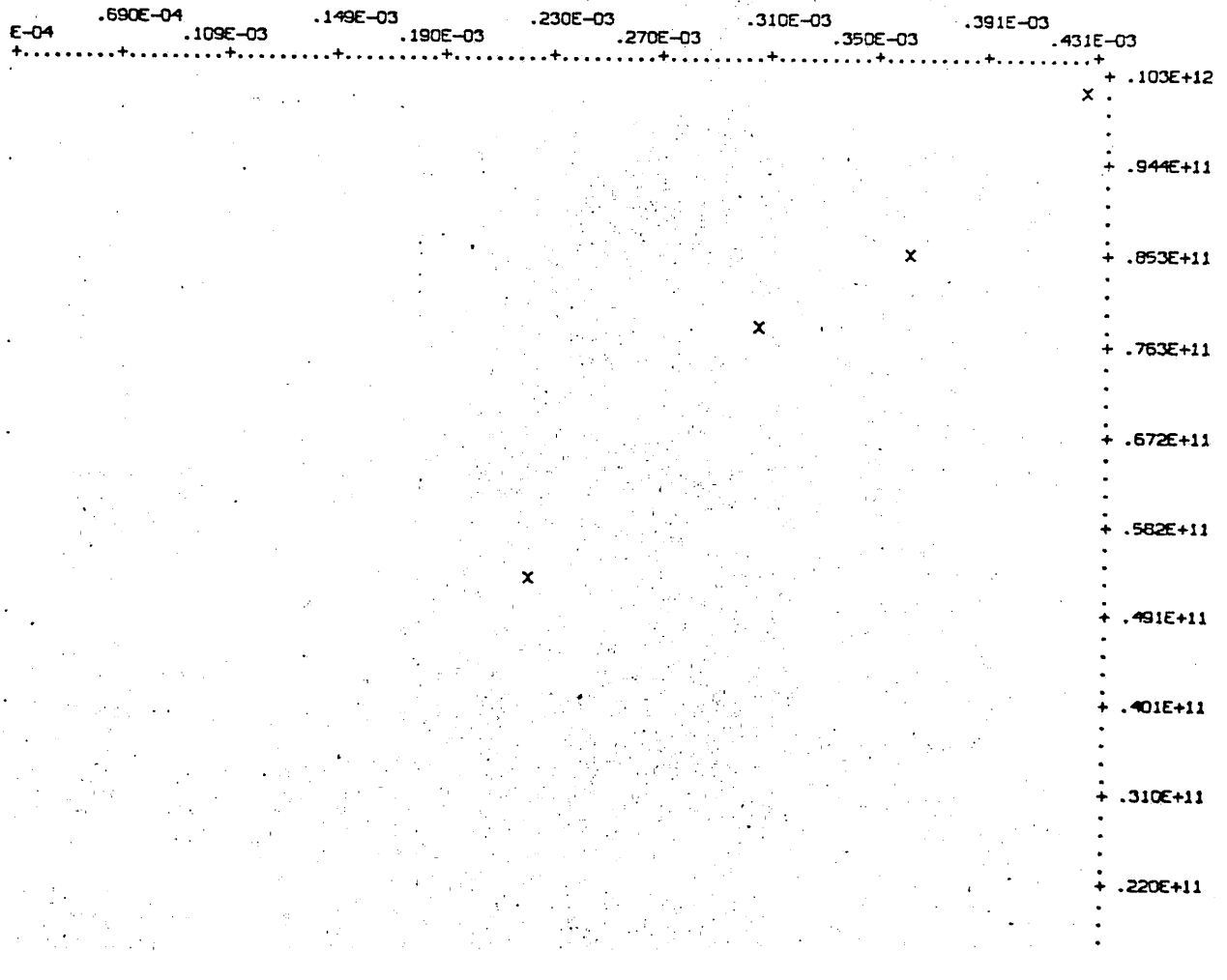

Figure 5.7

R3AR

T	D
296.0	52.0

F1	F2	F3	I01	I1	I02	I2	P
50.0	150.0	0.0	46.2	34.9	25.2	16.4	3.290
50.0	250.0	100.0	36.1	25.9	22.1	12.6	4.792
50.0	300.0	150.0	29.2	21.1	18.4	9.7	5.710
50.0	350.0	200.0	24.1	17.2	15.2	7.9	6.375
50.0	450.0	300.0	16.2	11.1	10.5	4.8	8.048

VALUES OF Y= .1659E+11 .2795E+11 .3599E+11 .3882E+11 .4809E+11

VALUES OF X== 0. .6880E-04 .1032E-03 .1376E-03 .2064E-03

VALUES OF GAMMA = .947647E-04 .790090E-04 .728023E-04 .743780E-04 .692867E-04

VALUES OF VBAR= .2032E+03 .2093E+03 .2049E+03 .2098E+03 .2077E+03

SLOPE = .1531E+15

STANDARD DEVIATION = .1123E+14

Y-INTERCEPT = .1768E+11 CORRELATION COEFF.= .992030

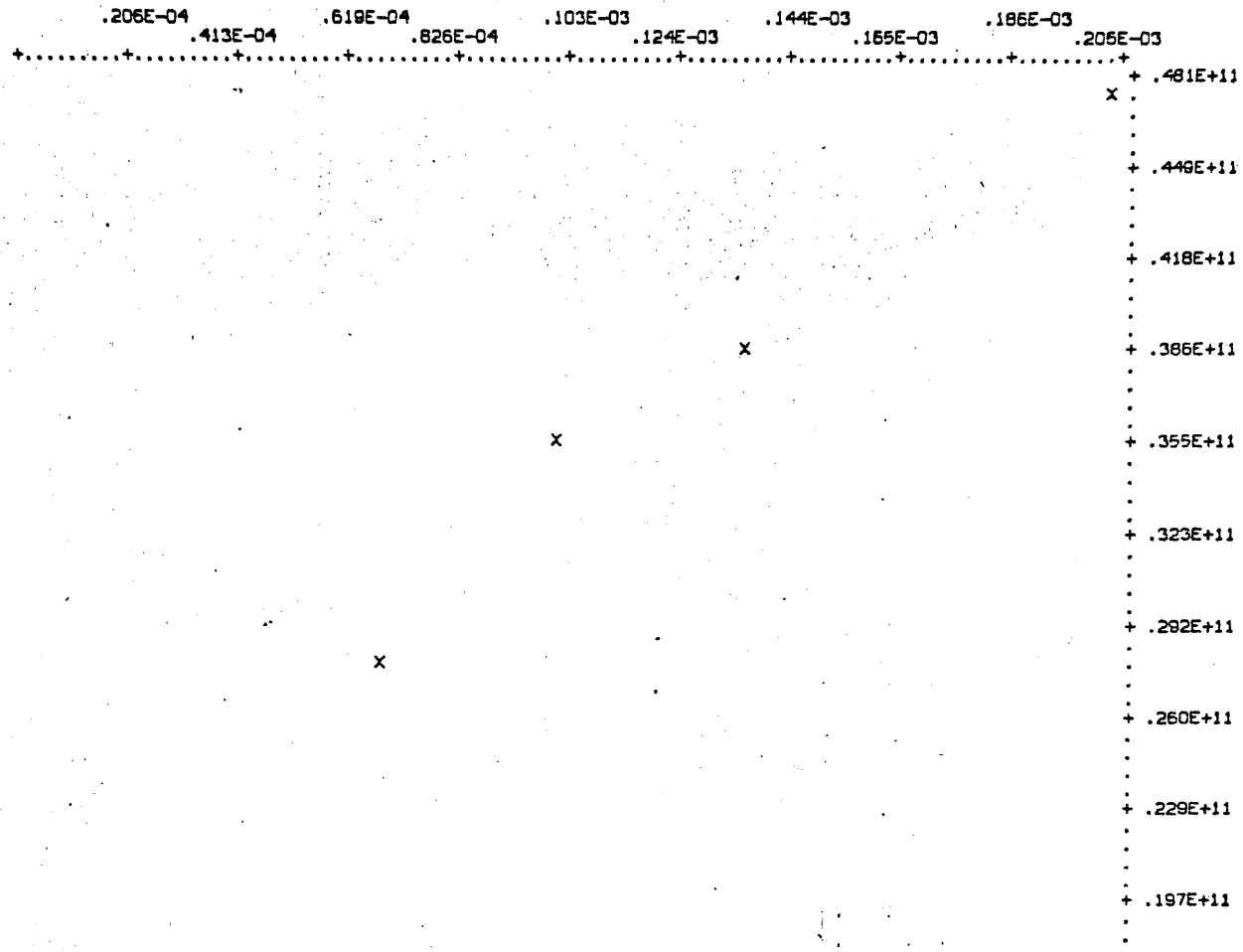

Figure 5.7

R3AR

T	D
296.0	52.0

F1	F2	F3	I01	I1	I02	I2	P
50.0	150.0	0.0	46.2	34.9	25.2	16.4	3.290
50.0	250.0	100.0	36.1	25.9	22.1	12.6	4.792
50.0	300.0	150.0	29.2	21.1	18.4	9.7	5.710
50.0	350.0	200.0	24.1	17.2	15.2	7.9	6.375
50.0	450.0	300.0	16.2	11.1	10.5	4.8	8.048

VALUES OF Y= .1659E+11 .2795E+11 .3599E+11 .3882E+11 .4809E+11

VALUES OF X== 0. .6880E-04 .1032E-03 .1376E-03 .2064E-03

VALUES OF GAMMA = .947647E-04 .790090E-04 .728023E-04 .743780E-04 .692867E-04

VALUES OF VBAR= .2032E+03 .2093E+03 .2049E+03 .2098E+03 .2077E+03

SLOPE = .1531E+15

STANDARD DEVIATION = .1123E+14

Y-INTERCEPT = .1768E+11 CORRELATION COEFF.= .992030

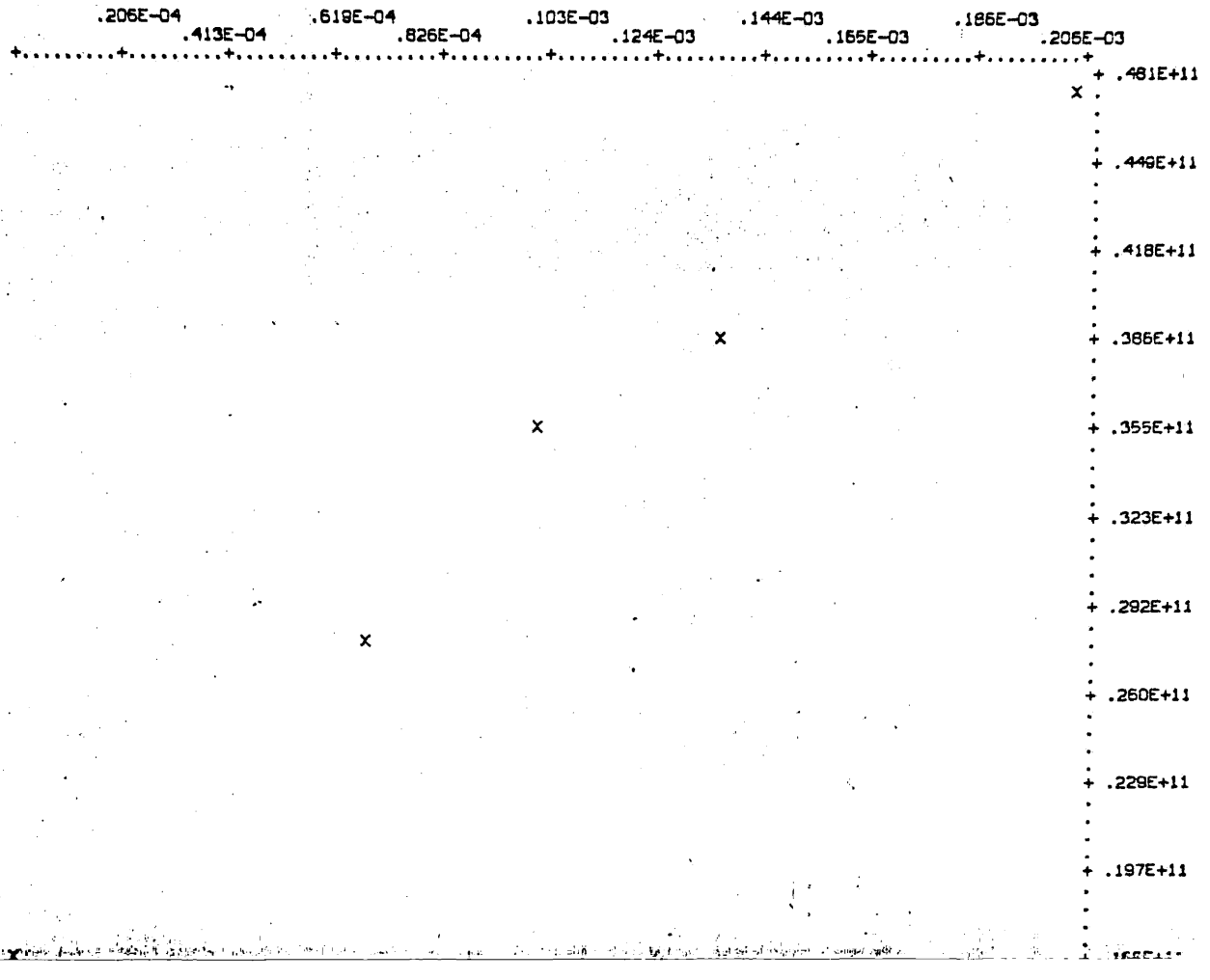

Figure 5.8

R3HE

T	D						
295.0	52.0						
F1	F2	F3	I01	I1	I02	I2	P
50.0	150.0	0.0	173.4	110.4	99.9	45.3	3.206
50.0	250.0	100.0	97.1	56.9	56.9	21.4	4.944
50.0	300.0	150.0	80.1	47.6	47.0	17.3	5.660
50.0	350.0	200.0	64.5	38.3	37.4	13.6	6.435
50.0	450.0	300.0	44.5	25.5	26.3	8.8	8.073
50.0	550.0	400.0	31.1	16.7	18.2	5.1	9.770

VALUES OF Y= .4042E+11 .4860E+11 .5556E+11 .5778E+11 .6270E+11 .7389E+11

VALUES OF Y== 0. .6880E-04 .1032E-03 .1376E-03 .2064E-03 .2752E-03

VALUES OF GAMMA = .881720E-04 .831226E-04 .844999E-04 .868313E-04 .834887E-04 .843375E-04

VALUES OF VBAR= .2079E+03 .2022E+03 .2060E+03 .2071E+03 .2064E+03 .2046E+03

SLOPE = .1161E+15

STANDARD DEVIATION = .8387E+13

Y-INTERCEPT = .4119E+11 CORRELATION COEFF.= .989720

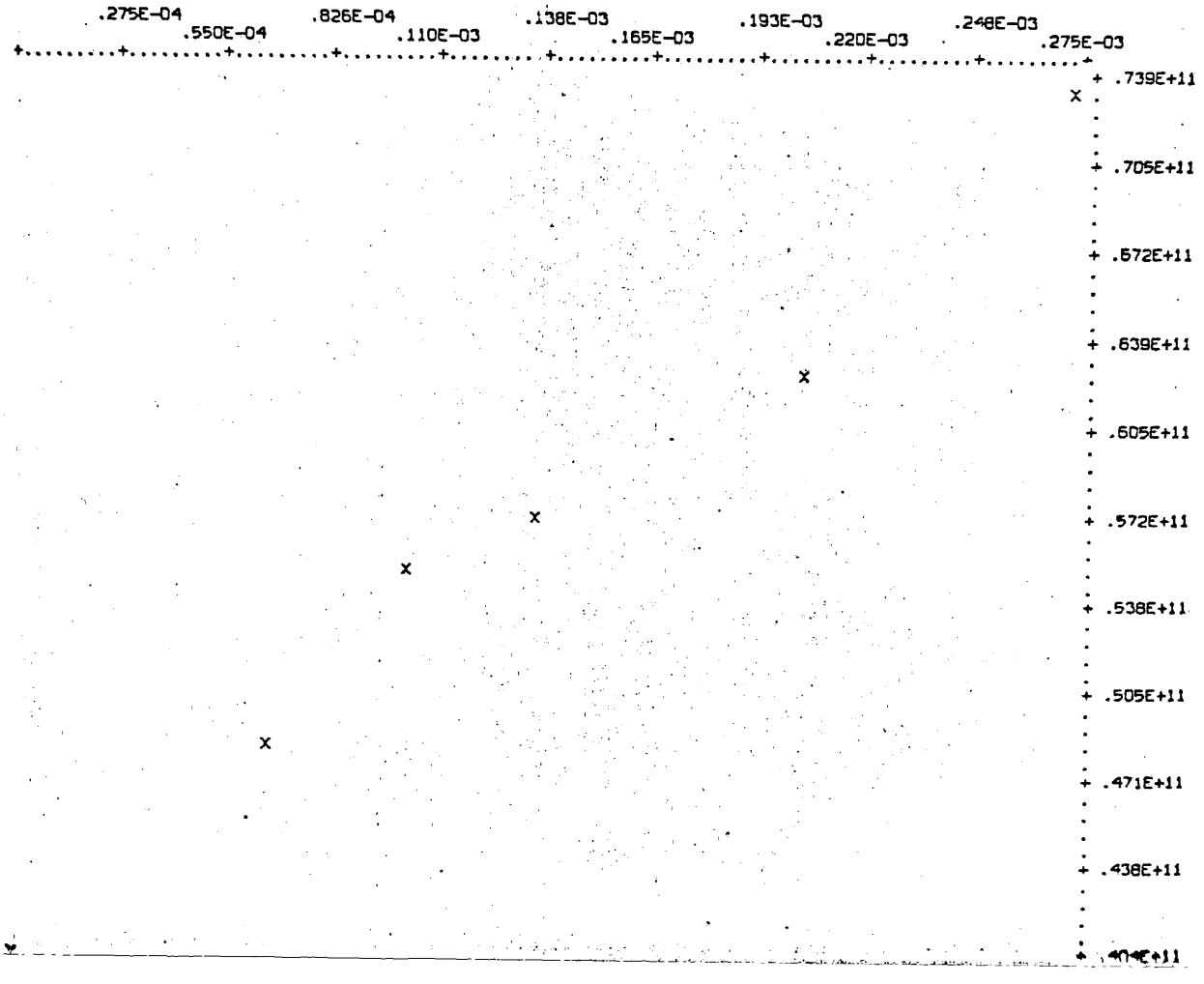

Figure 5.9

R3N2

T	D
295.0	52.0

F1	F2	F3	I01	I1	I02	I2	P
50.0	250.0	100.0	90.0	64.8	38.5	24.5	4.842
50.0	350.0	200.0	64.3	44.0	27.6	14.5	6.392
50.0	400.0	250.0	49.4	32.9	20.8	10.4	7.274
50.0	450.0	300.0	37.5	24.5	16.9	7.6	8.036
50.0	500.0	350.0	29.1	18.5	12.3	5.0	8.869

VALUES OF Y= .1441E+11 .3177E+11 .3329E+11 .4413E+11 .5232E+11

VALUES OF X== .6880E-04 .1376E-03 .1720E-03 .2064E-03 .2408E-03

VALUES OF GAMMA = .134851E-03 .135655E-03 .137160E-03 .127109E-03 .136878E-03

VALUES OF VBAR= .2064E+03 .2085E+03 .2061E+03 .2073E+03 .2066E+03

SLOPE = .2140E+15

STANDARD DEVIATION = .1869E+14

Y-INTERCEPT = -.1531E+09 CORRELATION COEFF.= .988753

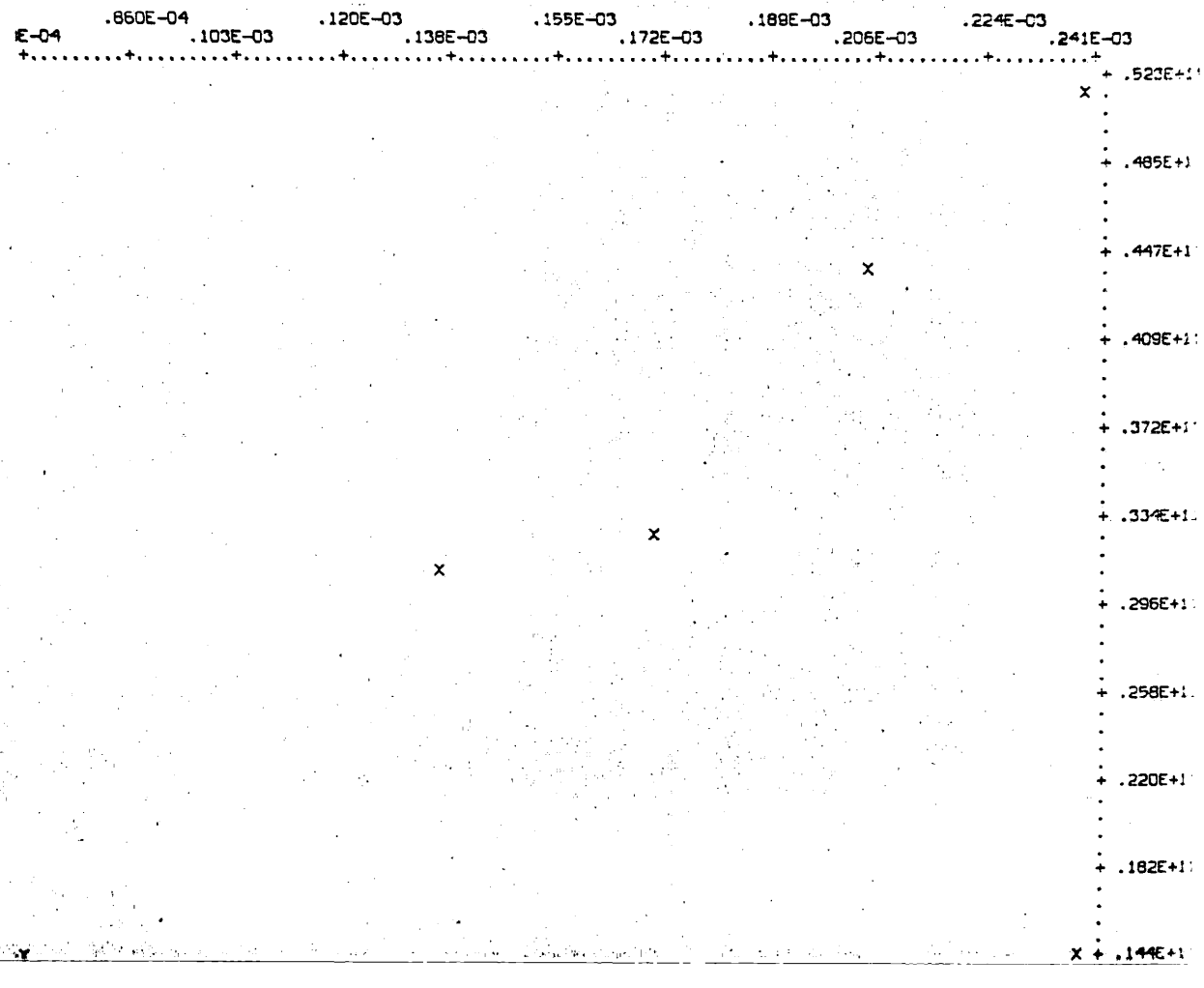

Figure 5.10

R1C0

T	D						
295.0	52.0						
F1	F2	F3	I01	I1	I02	I2	P
50.0	150.0	0.0	84.9	53.3	75.1	33.0	2.382
50.0	250.0	100.0	64.7	42.5	57.5	23.0	3.840
50.0	300.0	150.0	73.4	47.9	62.1	24.3	4.445
50.0	350.0	200.0	74.0	49.3	55.2	26.2	4.966
50.0	450.0	300.0	76.8	48.2	66.1	22.6	6.329
50.0	550.0	400.0	75.3	42.1	59.8	16.9	7.640
50.0	650.0	500.0	61.8	33.2	51.2	12.8	8.823

VALUES OF Y= .1036E+12 .1160E+12 .1225E+12 .1296E+12 .1469E+12 .1621E+12 .1874E+12

VALUES OF X== 0. .6880E-04 .1032E-03 .1376E-03 .2064E-03 .2752E-03 .3440E-03

VALUES OF GAMMA = .263962E-04 .236242E-04 .337402E-04 .261384E-04 .303611E-04 .463931E-04 .382640E-04

VALUES OF VBAR= .2798E+03 .2603E+03 .2624E+03 .2684E+03 .2632E+03 .2617E+03 .2644E+03

SLOPE = .2400E+15

STANDARD DEVIATION = .1298E+14

Y-INTERCEPT = .9938E+11 CORRELATION COEFF.= .992765

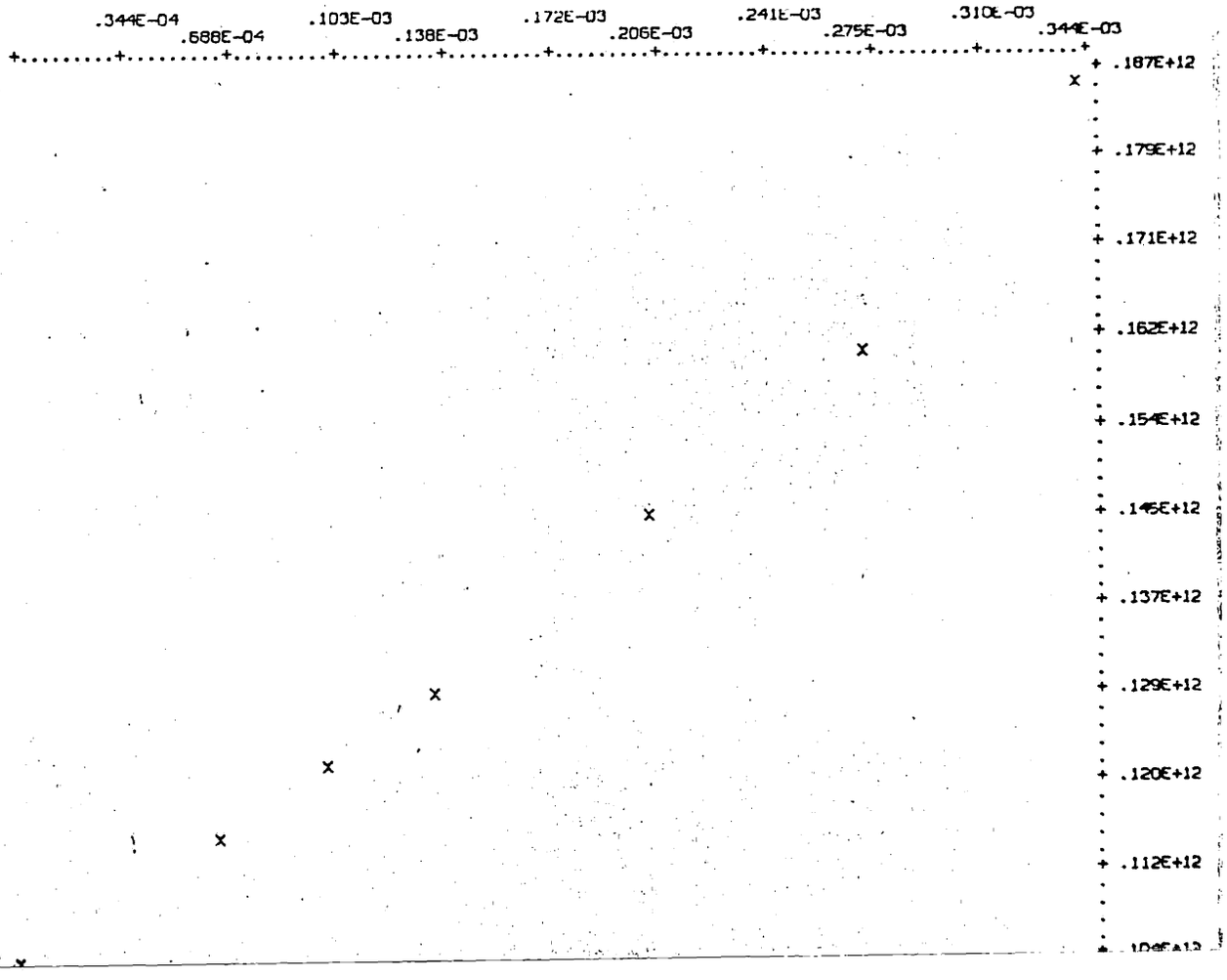

Figure 5.11

R1C02

T D
295.0 52.0

F1	F2	F3	I01	I1	I02	I2	P
50.0	150.0	0.0	76.9	64.3	72.6	53.7	2.177
50.0	350.0	200.0	153.9	115.9	136.0	75.3	4.322
50.0	500.0	350.0	122.8	81.6	105.6	43.9	5.922
50.0	600.0	450.0	102.5	52.0	88.5	32.5	7.053
50.0	700.0	550.0	81.8	48.6	69.5	22.1	8.090

VALUES OF Y= .4663E+11 .1196E+12 .1880E+12 .1916E+12 .2443E+12

VALUES OF X== 0. .1376E-03 .2408E-03 .3096E-03 .3784E-03

VALUES OF GAMMA = .135494E-04 .293316E-04 .336777E-04 .346910E-04 .387205E-04

VALUES OF VBAR= .3061E+03 .3084E+03 .3095E+03 .3071E+03 .3089E+03

SLOPE = .5081E+15

STANDARD DEVIATION = .4368E+14

Y-INTERCEPT = .4967E+11 CORRELATION COEFF.= .989093

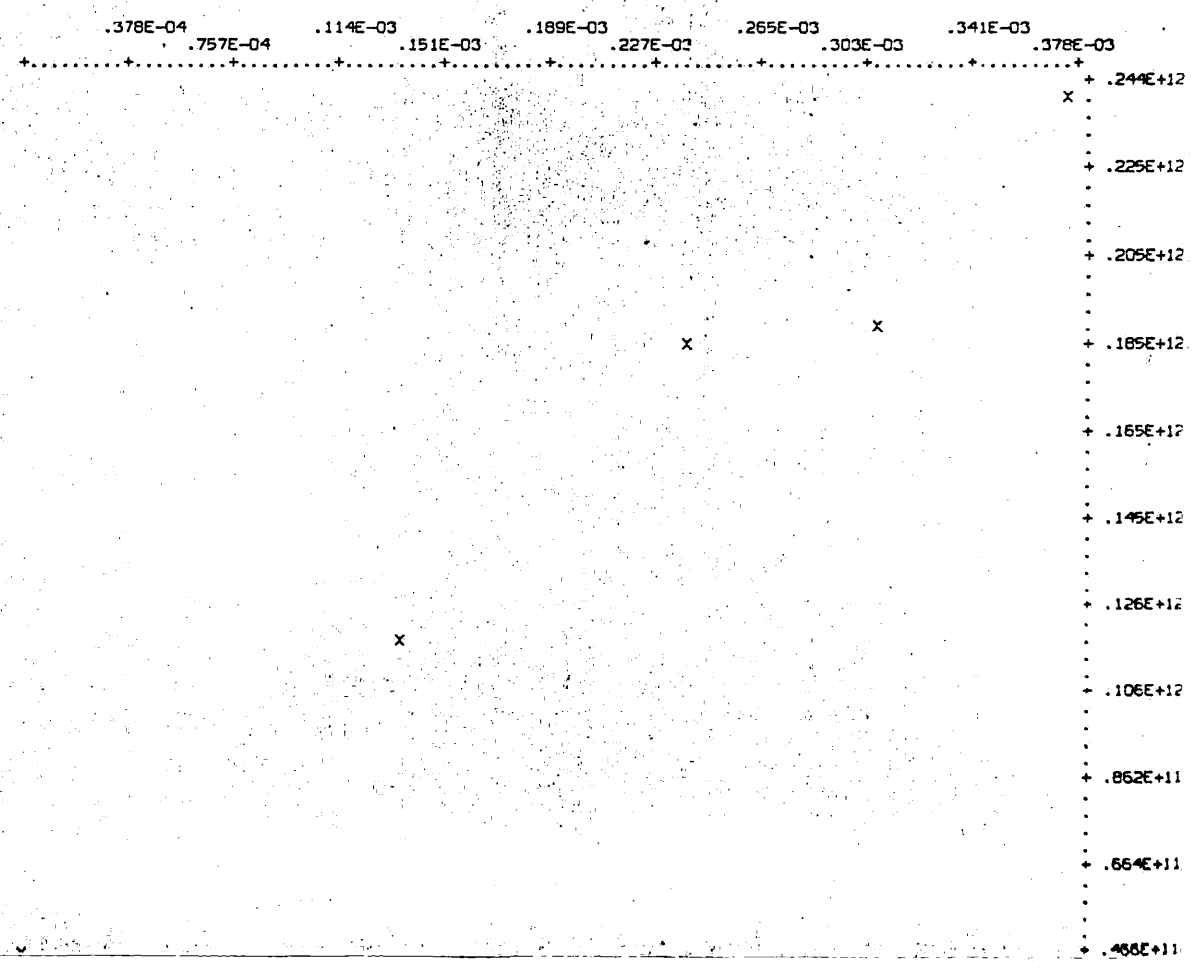

SECTION 6

The Experimental Determination of the Temperature Coefficient of reaction:

$$O + O_2 + M \longrightarrow O_3 + M$$

6.1 Introduction

Another important aspect of this work is the determination of the temperature coefficient of the reaction:

$$O + O_2 + M = O_3 + M$$

for M=Ar, O_2 and CO_2 over the range 196-500 K. This was carried out in reaction system B. The temperature coefficients for M=Ar and CO_2 between 213-386 K have been reported by Mulcahy[35] but the temperature coefficient for $M=O_2$ has not been measured directly. The advantage of the modified technique used here is that temperature coefficients for $M=O_2$ can be easily measured. For each temperature at which rate measurements were taken, i.e. four temperatures, 2-5 determinations of the rate constant $k_{1,M}$ were made and were retained only if they agreed and were reproducible (standard deviations $< \pm$ 10%). Rate constants were computed via the final kinetic equation 3.3 used in the determination of rate constants at 295 K (Section 5).

In recent years, several workers[1,4,50,56,59] have studied the temperature coefficient for M=Ar over various temperature ranges with several different techniques, there are still considerable discrepancies in the results of this determination. The temperature coefficient must be known accurately since the reaction is currently of considerable interest with reference to the calculation of stratospheric ozone levels and the role of certain HO_x and NO_x catalysts, assuming the

temperature coefficients for M=N_2 and O_2 are similar. Thus in general;

(a) there is a need for agreement between the temperature coefficient of reaction (1) as calculated theoretically[79] by computer methods based on classical R.R.K.M. theory and as determined by experiment;

(b) the reaction is of practical importance since it is the predominant ozone forming reaction in the stratosphere, and

(c) it is important in understanding photochemical air pollution.

Thus, Huie et al[59] using the static method of resonance fluorescence where wall recombination is negligible, studied the reaction over the range 200-346 K for M=Ar and obtained a negative activation energy E=-1.01 $\pm$ 0.05 kcal mol^{-1}. This value conflicts with that of -1.80 $\pm$ 0.4 kcal mol^{-1} (M=Ar) obtained by Clyne et al[56] over the range 188-373 K using a discharge-flow method. Mulcahy,[50] using a stirred flow-chemiluminescent method over the range 213-386 K obtained an activation energy of -1.68 $\pm$ 0.1 kcal mol^{-1} for M=Ar and -1.45 $\pm$ 0.14 kcal mol^{-1} for M=CO_2 while a value of -2.1 $\pm$ 0.4 kcal mol^{-1} (M=Ar) can be calculated from O_3 decomposition studies[12] at 300-400 K by manometric methods and at 800-1000 K by the shock-tube method.[14] The value of -0.90 $\pm$ 0.15 kcal mol^{-1} (M=Ar) for the activation energy obtained in the present work agrees well with the value of Huie[59] and corresponds to a temperature dependence of n=1.5 $\pm$ 0.15 (Section 8) when k is expressed in the form:

$$k = AT^n$$

where A and n are constants.

Thus it was the goal of this work firstly, to extend the best conditions (Sections 3.2 and 5.2), using the fixed detector multiple inlet jet method to a determination of the temperature coefficient over a larger range of temperatures than has been reported previously in a single work and, secondly, to examine the existing discrepancy in the temperature dependence as determined by the static method of Huie and the flow methods of Clyne et al. and Mulcahy and Williams. 'Blank' corrections were made for runs at temperatures above 300 K when they become significant. Preliminary experiments, similar to those carried out at 295 K were carried out (Section 6.2).

6.2 Preliminary Experiments

Preliminary experiments were carried out in reaction system B before attempting to determine the temperature coefficient of the reaction. A test was made at 295 K to determine whether it would be necessary to apply the 'blank' corrections (see below) to allow for flow perturbations (and small changes in V) caused by the addition of reactant to reaction system B at 295 K over the flow rates and pressures to be used consequently. These corrections are necessary at temperatures > 300 K when wall recombination efficiencies may be high. This test was carried out in the following manner. The photomultiplier was fixed in its housing at a position 11.5 cm upstream of Jet 1 and the microwave discharge

(Ar flow = 100×10^{-6} mol s^{-1}) was switched on. A fixed, steady flow of 'blank' Ar (172×10^{-6} mol s^{-1}), five times greater than the O_2 flow rate used in the actual experimental kinetic runs, was then admitted through J1. The mean flow velocity was then set at 200 cm s^{-1} and the light intensity at the photomultiplier position was noted (symbol I1 in Table 6.1). The flow of Ar was then switched off and the intensity (I'1) again noted, The Ar was then readmitted at J5 and the intensities at the photomultiplier were again noted in the presence (I5) and absence (I'5) of added Ar. This process was repeated over the range of flow velocities to be used in the temperature coefficient determination (viz. 150-300 cm s^{-1}) and results are given in Table 6.1. These show that the effects of flow perturbations are very small at 295 K or below.

Table 6.1

Data for initial 'Blank' test.

F_{Ar} (Discharge) = 100×10^{-6} mol s^{-1}

F_{O_2} (Discharge) = 500 p.p.m.

F_{Ar} (Inlet jet) = 172×10^{-6} mol s^{-1}

T = 295 K

I'1	I1	I'5	I5	$\bar{v}$ cm s^{-1}	P torr
015.8	013.8	015.6	014.0	200	5.07
054.9	054.8	054.9	054.9	250	3.94
016.5	017.3	016.7	017.4	300	3.39

For all runs in system B, blank corrections according to the surface equation 3.5 were made. (Not applicable to system A). The blank readings are given in data in Figs. 6.1-6.9. These corrections for flow perturbations lowered values of $k_{1,M}$ (400-500 K) by 5-25% and the results of this are also in Section 6.3. It is important to realise the anlogy made by the use here of 'blank' gas as a reference gas to the use of water as a reference in standard solution kinetics when using spectroscopic techniques (Section 8). Atomic oxygen decay profiles were constructed in system B to show accurate first-order kinetics in O; these have already been given (Section 5.2). It is sufficient to remember that such decays were always accurately first-order over the full range of experimental conditions at 295 K, and were assumed to be so at other temperatures.

The allowances for the wall recombination depend on the gas phase composition, and the 'blank' corrections used in this work were not made in the previous flow experiments by other workers. In addition, in previous flow methods, the temperature dependence was determined for a constant (or approximately constant) mole fraction of O_2 in the presence of a third body M. These conditions may be the reasons for the discrepancies in the temperature-dependence compared with the static method (Section 8). The wall recombination efficiency, γ, could not be determined from experimental measurements of $k_{1,M}$ (unless 'blank' corrections were made) only the term $\gamma - \gamma^*$ was determined at 295 K. γ^* was determined

in a separate experiment at 295 K (M=Ar), (Section 2.7) and this showed that the efficiency was much reduced ($\simeq 3 \times 10^{-5}$) by phosphoric acid. At temperatures other than 295 K, $\gamma - \gamma^*$ was determined from blank measurements and results of this are briefly discussed in Section 6.4.

6.3 The Experimental Determination of the Temperature Coefficient.

This section contains the results of kinetic runs for reaction (1) (for M=Ar, O_2, CO_2) carried out at 196, 295, 385 and 500 K, at least two duplicate runs which agreed accurately were retained for each temperature. All data was evaluated in exactly the same way as was described for work at 295 K (Section 5.3), i.e. using the kinetic equation 3,3.

The first work in system B was carried out at 295 K, the single value obtained for $k_{1,Ar}=1.46\pm0.09$ ($\pm 6\%$)$\times 10^{14}$ cm^6 mol^{-2} s^{-1} (Table 5.5). Values of $k_{1,Ar}$ obtained in reaction system A are identical with this value and no further runs at 295 K were attempted. Three runs, of which two were conducted under satisfactory conditions were then carried out at 196 K using the temperature controller (Section 2.2) which is capable of holding the required temperature to within $\pm$ 0.1 K. Reactant O_2 was added at Jets J2 and J5 and also for runs at all other temperatures. The discharge gases passed through about 30 cm of pre-thermostatted glass tubing to ensure that they came to the temperature of the thermostatted bath. This was shown to be true by studying decay

Figure 6.1

```
    T    D
136.0 63.8
   F1    F2      F3       I01       I1       I02       I2         P
 50.0   150.0     0.0   100.0      77.3     100.0      53.1      2.051
 50.0   250.0   100.0   100.0      68.2     100.0      37.1      3.132
 50.0   350.0   150.0   100.0      60.6     100.0      27.2      3.832
 50.0   350.0   300.0   100.0      55.8     100.0      21.7      4.341
 50.0   450.0   300.0   100.0      48.1     100.0      15.4      5.432
 50.0   550.0   400.0   100.0      40.0     100.0      11.0      6.525

VALUES OF Y=    .4083E+11   .6274E+11   .7158E+11   .8665E+11   .1042E+12   .1177E+12

VALUES OF X=  0.            .6880E-04   .1032E-03   .1376E-03   .2064E-03   .2752E-03

VALUES OF VBAR=   .2159E+03   .2121E+03   .2022E+03   .2040E+03   .2038E+03   .2036E+03

SLOPE =    .2843E+15


STANDARD DEVIATION =    .1515E+14


Y-INTERCEPT =    .4312E+11
```

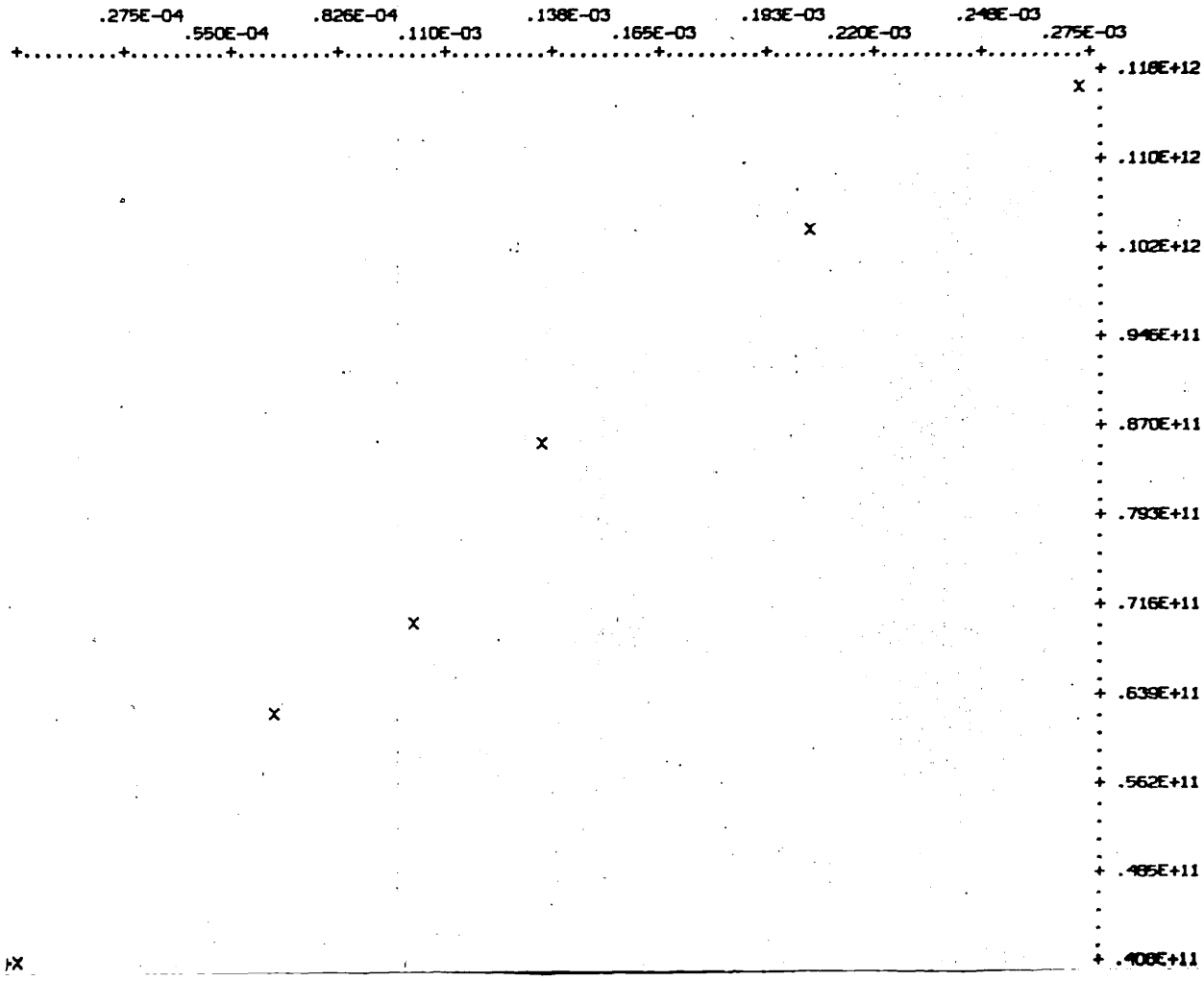

Figure 6.2

```
   T    D
385.0 48.8
   F1    F2       F3        I01        I1       I02       I2         P
 50.0   150.0     0.0      100.0      97.1     100.0     93.6      3.353
 50.0   200.0    50.0      100.0      88.7     100.0     84.2      4.169
 50.0   250.0   100.0      100.0      80.5     100.0     74.5      5.040
 50.0   300.0   150.0      100.0      76.2     100.0     70.3      5.824
 50.0   400.0   250.0      100.0      64.5     100.0     57.6      7.551
 50.0   450.0   300.0      100.0      58.4     100.0     51.5      8.336
 50.0   500.0   350.0      100.0      51.9     100.0     45.4      9.071
 50.0   550.0   400.0      100.0      45.8     100.0     39.5      9.897

VALUES OF Y=     .9052E+10   .1305E+11   .1898E+11   .2032E+11   .2782E+11   .3153E+11   .3466E+11   .3831E+11

VALUES OF X==  0.            .3440E-04   .6880E-04   .1032E-03   .1720E-03   .2064E-03   .2408E-03   .2752E-03

VALUES OF VBAR=   .2594E+03   .2608E+03   .2588E+03   .2613E+03   .2592E+03   .2608E+03   .2637E+03   .2636E+03

SLOPE =     .1039E+15


STANDARD DEVIATION =    .3378E+13


     Y-INTERCEPT =    .9918E+10
```

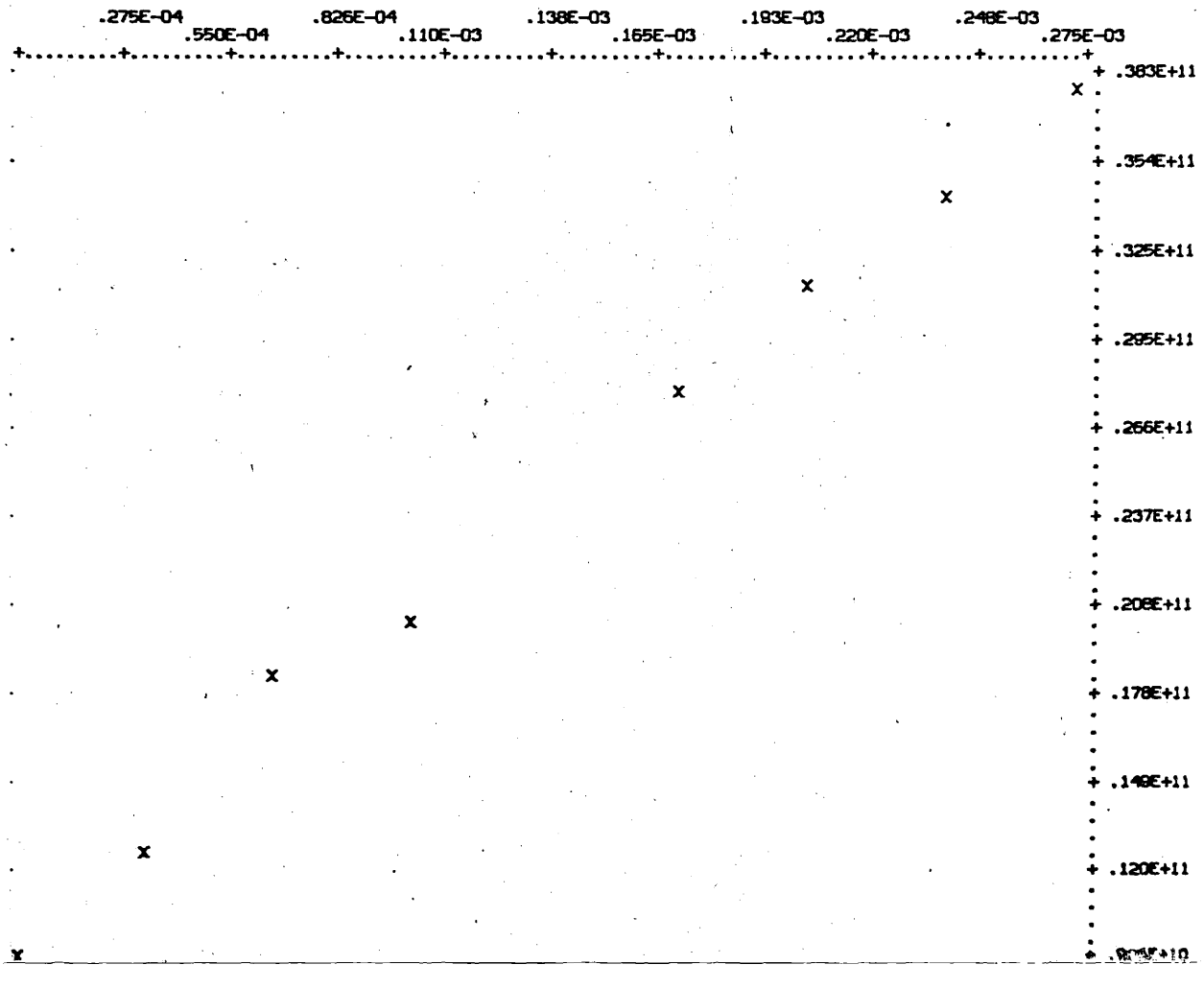

Figure 6.3

```
   T    D
500.0 48.8
   F1    F2     F3      I01      I1      I02      I2       P
 50.0   100.0    0.0    89.0     71.5    100.0    60.4     5.464
 50.0   150.0   50.0    92.5     48.5    100.0    38.0     7.486
 50.0   200.0  100.0    94.2    104.5    100.0    76.3     9.346
 50.0   250.0  150.0    95.6     75.4    100.0    50.6    11.151
 50.0   300.0  200.0    96.2     52.6    100.0    32.9    13.036
 50.0   350.0  250.0    96.8     40.6    100.0    24.3    14.950
 50.0   400.0  300.0    97.2     28.8    100.0    16.5    16.980

VALUES OF Y=    .1502E+11   .1662E+11   .1823E+11   .2200E+11   .2502E+11   .2661E+11   .2773E+11

VALUES OF X==   0.          .3440E-04   .6880E-04   .1032E-03   .1376E-03   .1720E-03   .2064E-03

VALUES OF Y=    .1502E+11   .1662E+11   .1823E+11   .2200E+11   .2502E+11   .2661E+11   .2773E+11

VALUES OF X==   0.          .3440E-04   .6880E-04   .1032E-03   .1376E-03   .1720E-03   .2064E-03

VALUES OF VBAR=   .1550E+03   .1509E+03   .1511E+03   .1519E+03   .1516E+03   .1511E+03   .1497E+03

SLOPE=   .6739E+14


STANDARD DEVIATION=   .4632E+13


INTERCEPT=   .1465E+11


STANDARD DEVIATION=   .5745E+09
```

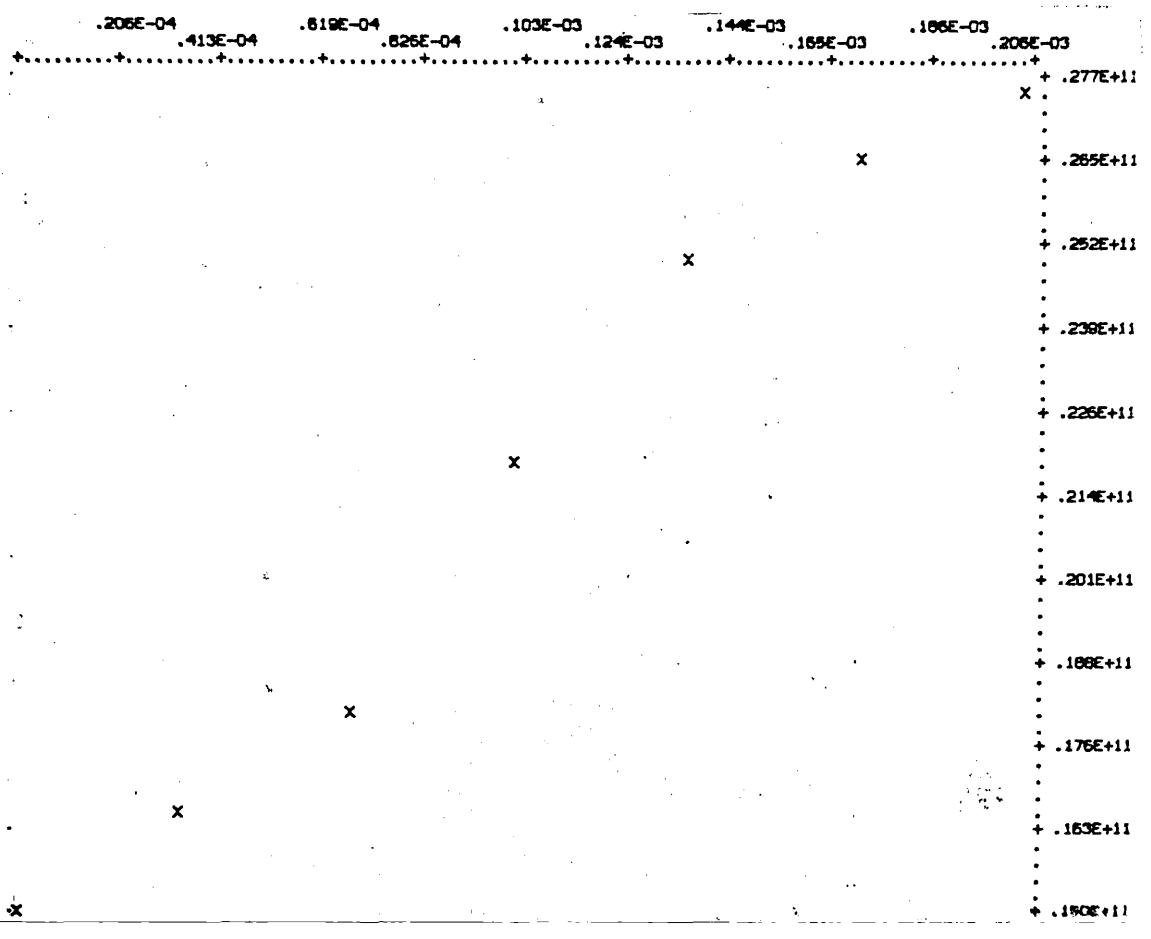

Figure 6.4

```
   T    D
196.0 48.8
   F1    F2       F3        I01       I1       I02       I2         P
 25.0   250.0     0.0     100.0      42.0     100.0     27.2      2.885
 25.0   300.0    50.0     100.0      30.1     100.0     15.6      3.358
 25.0   350.0   100.0     100.0      26.1     100.0     12.7      3.838
 25.0   375.0   125.0     100.0      22.8     100.0     10.3      4.115
 25.0   400.0   150.0     100.0      19.8     100.0      7.9      4.390
 25.0   450.0   200.0     100.0      15.8     100.0      4.9      4.908

VALUES OF Y=     .1154E+12   .1827E+12   .2060E+12   .2238E+12   .2556E+12   .3254E+12

VALUES OF X==  0.            .3440E-04   .6880E-04   .8600E-04   .1032E-03   .1376E-03

VALUES OF VBAR=   .2110E+03   .2143E+03   .2163E+03   .2152E+03   .2143E+03   .2143E+03

SLOPE=    .1412E+16


STANDARD DEVIATION=    .1308E+15


INTERCEPT=    .1170E+12


        DATA FOR 0+02+M=03+M
```

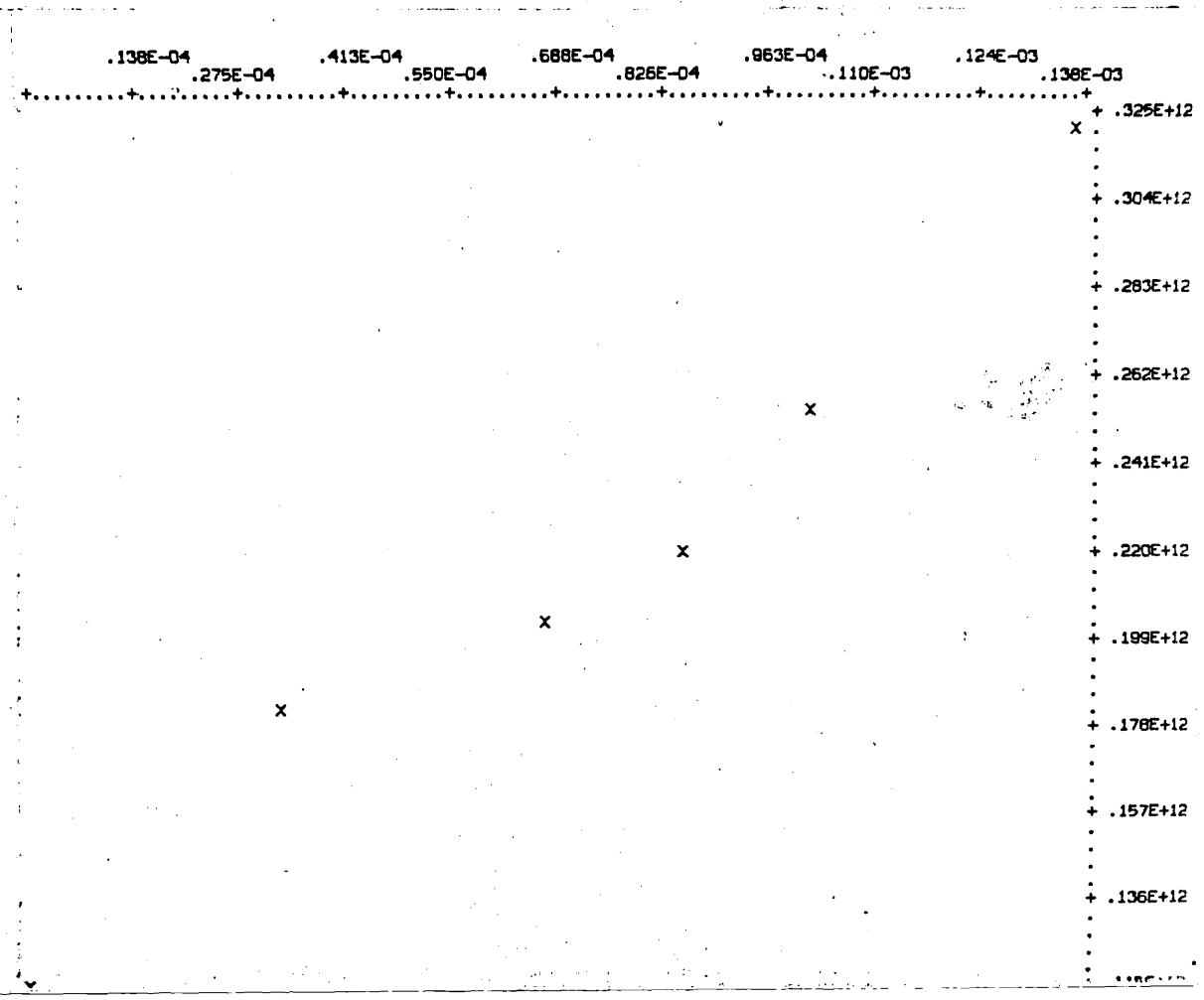

Figure 6.5

T D
400.0 48.8

F1	F2	F3	I01	I1	I02	I2	P
48.0	300.0	50.0	19.5	35.2	20.3	27.5	6.150
48.0	355.0	105.0	13.4	24.6	14.4	17.1	7.100
48.0	400.0	150.0	6.0	17.6	6.3	11.2	7.980
48.0	450.0	200.0	3.9	13.8	4.1	8.2	8.780
48.0	500.0	255.0	100.0	15.8	100.0	9.1	9.820

VALUES OF Y= .7060E+11 .1081E+12 .1203E+12 .1413E+12 .1301E+12

VALUES OF X== .3440E-04 .7224E-04 .1032E-03 .1376E-03 .1754E-03

VALUES OF VBAR= .2557E+03 .2564E+03 .2536E+03 .2563E+03 .2521E+0

SLOPE= .4364E+15

STANDARD DEVIATION= .1353E+15

INTERCEPT= .6846E+11

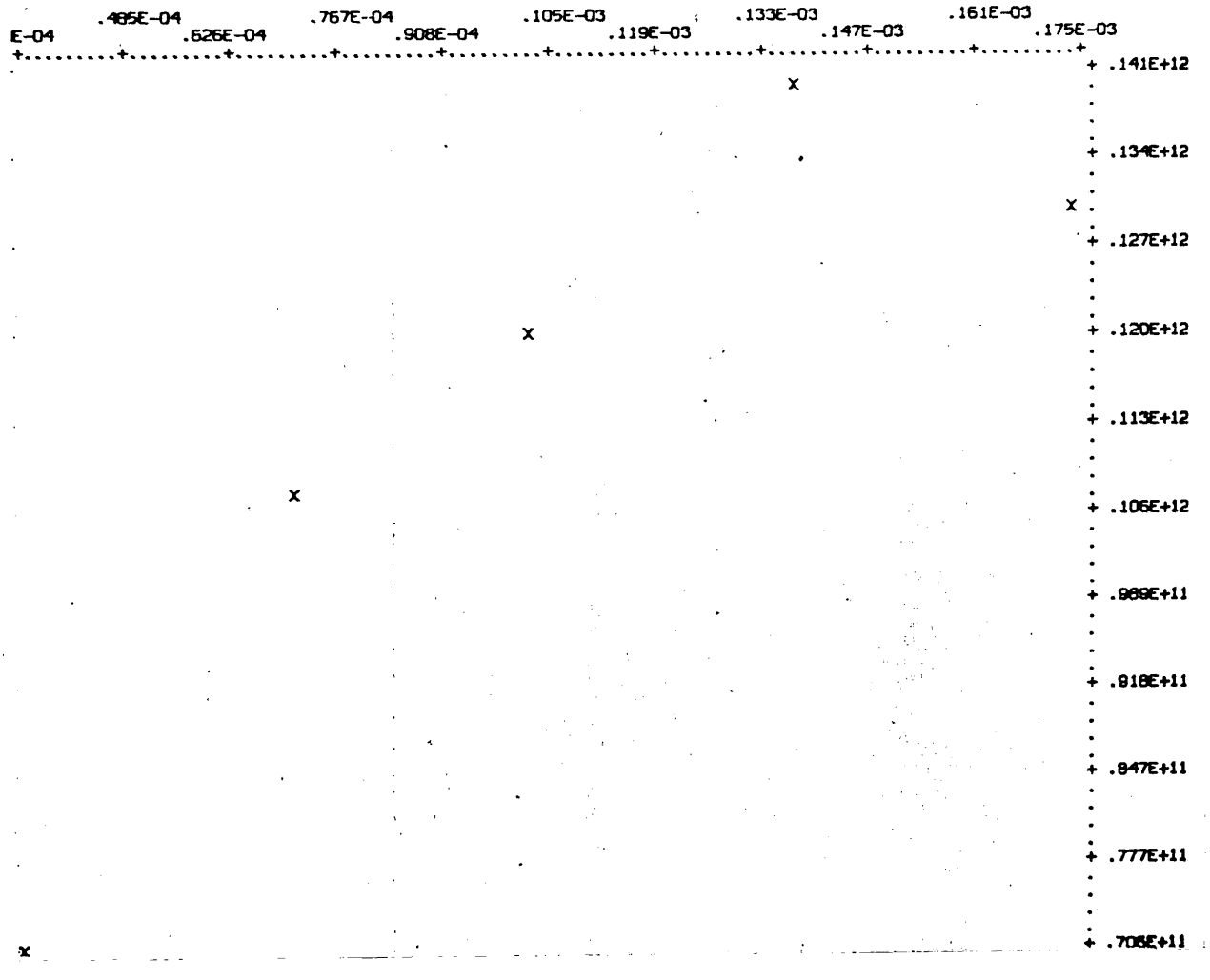

Figure 6.6

```
   T    D
500.0 64.4
   F1    F2       F3        I01        I1       I02       I2         P
 50.0   300.0     50.0     37.9       35.1      38.0      31.2      6.500
 50.0   350.0    100.0     29.9       30.1      30.1      25.4      7.500
 50.0   425.0    175.0     21.2       29.7      21.6      23.6      8.900
 50.0   450.0    200.0     18.6       42.8      19.0      34.5      9.300
 50.0   475.0    225.0     16.4       39.9      16.8      31.9      9.800
 50.0   500.0    250.0     14.7       39.2      15.2      30.4     10.300

VALUES 0F Y=     .3626E+11    .5162E+11    .7288E+11    .7099E+11    .7349E+11    .8447E+11

VALUES 0F X==    .3440E-04    .6880E-04    .1204E-03    .1376E-03    .1548E-03    .1720E-03

VALUES 0F VBAR=  .3041E+03    .3012E+03    .3014E+03    .3036E+03    .3026E+03    .3016E+03

SL0PE=    .3257E+15


STANDARD DEVIATI0N=    .3514E+14


INTERCEPT=    .2761E+11
```

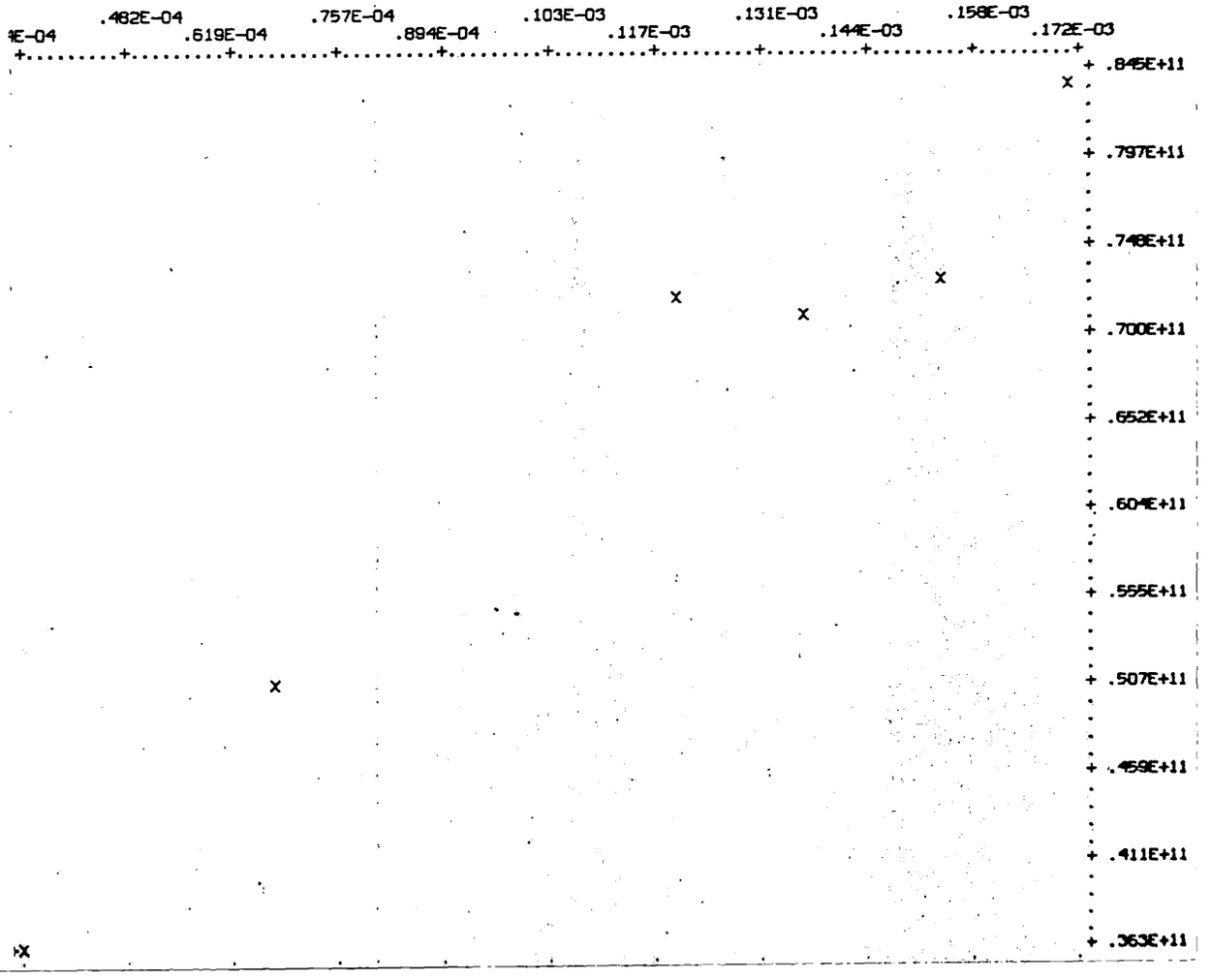

Figure 6.7

T	D						
196.0	48.8						
F1	F2	F3	I01	I1	I02	I2	P
50.0	250.0	50.0	9.8	13.1	14.2	10.3	3.219
70.0	250.0	70.0	12.2	16.5	16.8	13.2	2.815
90.0	250.0	90.0	11.8	15.9	17.1	12.2	2.799
110.0	250.0	110.0	11.8	14.4	16.8	10.5	2.688
130.0	250.0	130.0	11.8	12.9	16.8	9.5	2.572
150.0	250.0	150.0	12.5	12.5	17.5	8.5	2.498

VALUES OF Y= .7586E+11 .7868E+11 .9707E+11 .1120E+12 .1254E+12 .1282E+12

VALUES OF X== .3440E-04 .4816E-04 .6192E-04 .7568E-04 .8944E-04 .1032E-03

VALUES OF VBAR= .2063E+03 .2430E+03 .2689E+03 .2965E+03 .3271E+03 .3545E+0

SLOPE= .8650E+15

STANDARD DEVIATION= .8653E+14

INTERCEPT= .4335E+11

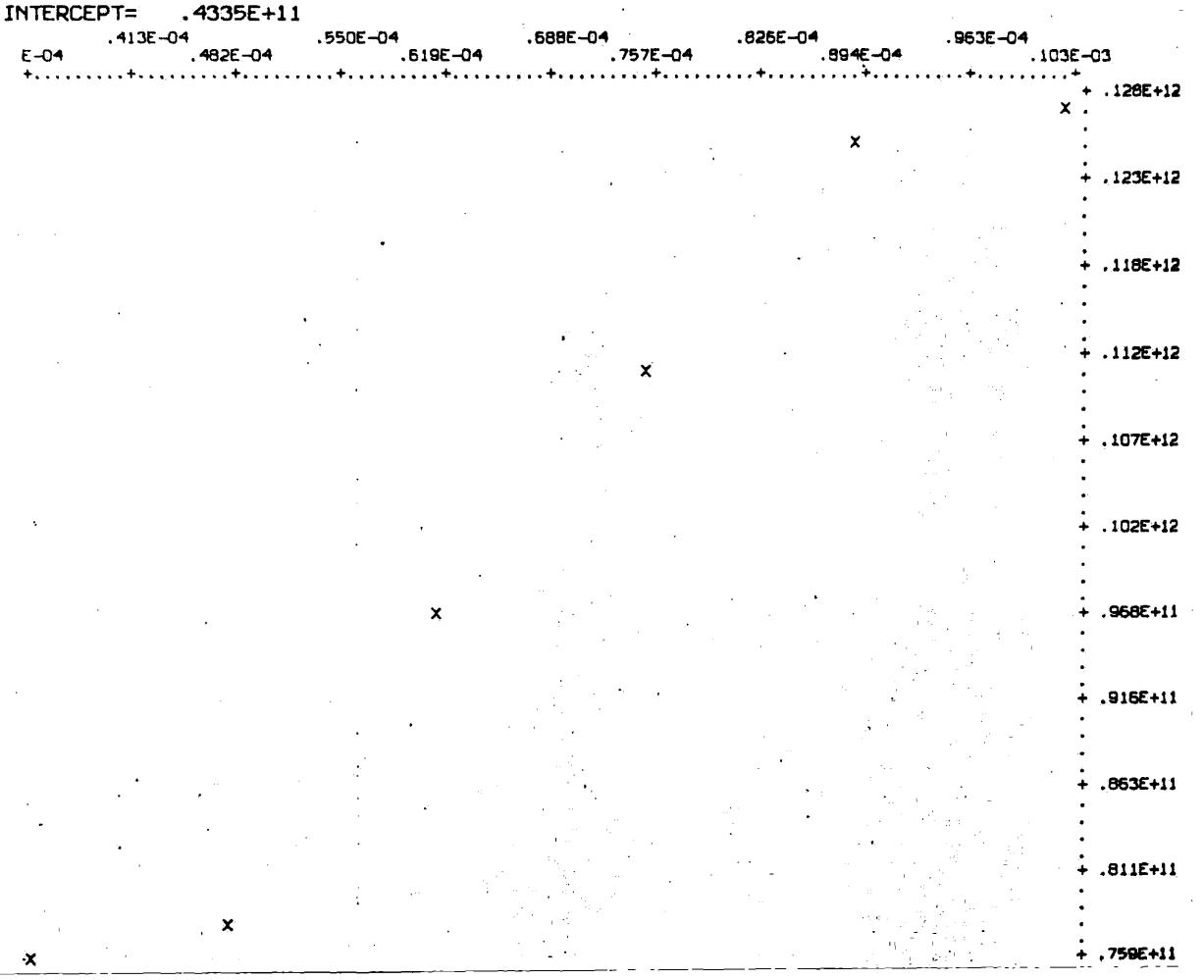

Figure 6.8

```
   T    D
385.0 48.8
   F1    F2       F3        I01        I1       I02        I2         P
100.0   150.0    100.0     100.0     103.9     100.0      73.6     4.121
130.0   150.0    130.0     100.0     132.7     100.0      76.2     4.746
160.0   150.0    160.0     100.0     123.1     100.0      57.7     5.316
190.0   150.0    190.0     100.0      82.9     100.0      34.5     5.772
220.0   150.0    220.0     100.0      82.7     100.0      28.0     6.216
250.0   150.0    250.0     100.0      56.7     100.0      14.9     6.847

VALUES OF Y=     .4472E+11   .5091E+11   .5456E+11   .5479E+11   .6032E+11   .6192E+11

VALUES OF X==    .6880E-04   .8944E-04   .1101E-03   .1307E-03   .1514E-03   .1720E-03

VALUES OF VBAR=   .2638E+03   .2566E+03   .2536E+03   .2562E+03   .2588E+03   .2540E+0

SLOPE=    .1584E+15


STANDARD DEVIATION=    .1865E+14


INTERCEPT=    .3546E+11
```

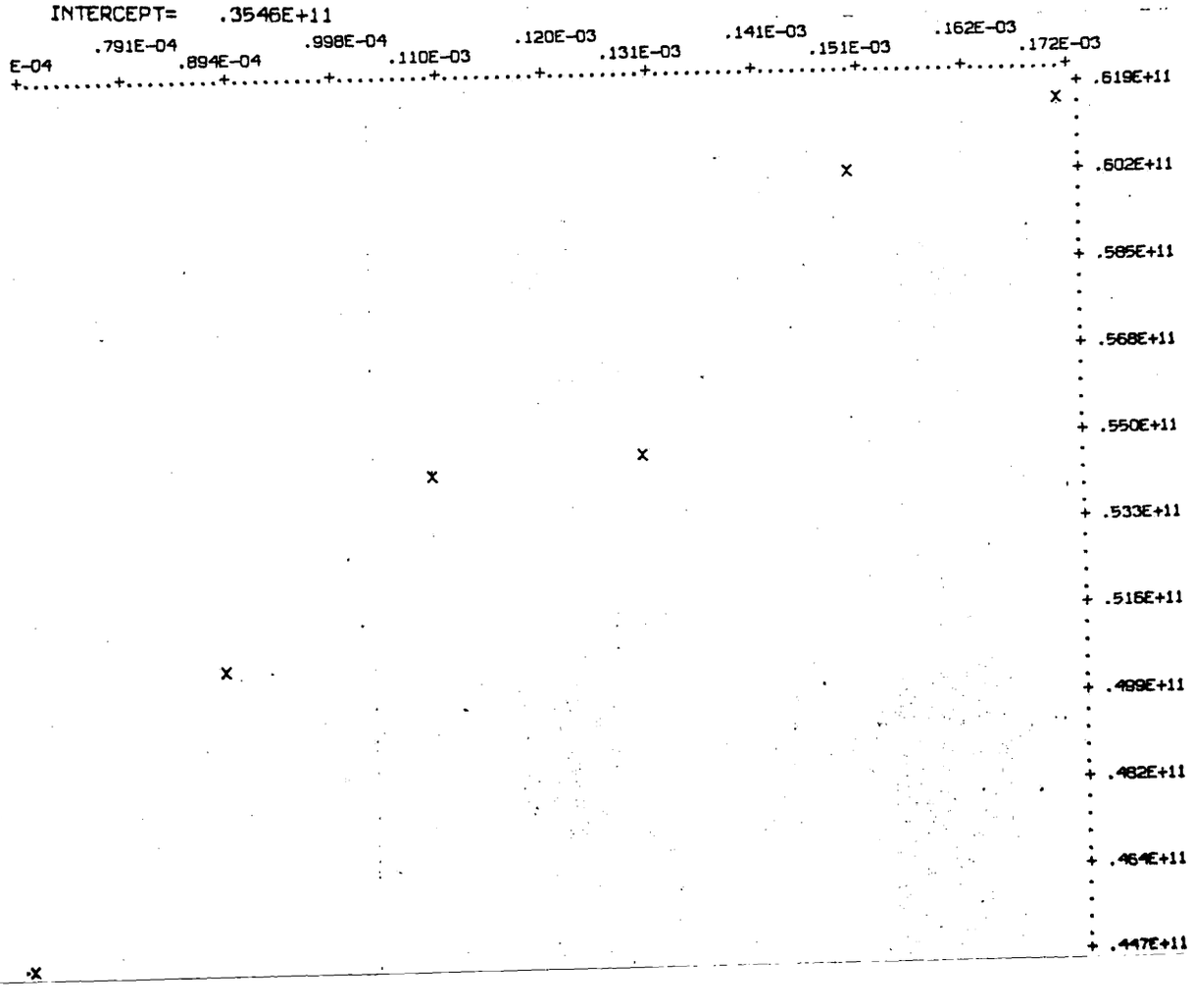

Figure 6.9

```
   T    D
500.0 48.8
   F1    F2      F3      I01      I1      I02      I2       P
 30.0   200.0    30.0    69.2    65.8    70.1    65.0    4.300
 70.0   200.0    70.9    54.4    53.4    55.6    50.9    5.100
 90.0   200.0    90.0    47.0    47.0    48.6    43.5    5.500
110.0   200.0   110.0    41.9    41.2    43.5    37.6    5.800
130.0   200.0   130.0    35.3    27.3    37.6    24.6    6.200
150.0   200.0   150.0    29.3    23.0    31.7    20.2    6.600

VALUES OF Y=     .1633E+11   .1882E+11   .2298E+11   .2277E+11   .2469E+11   .2638E+11

VALUES OF X==    .2064E-04   .4878E-04   .6192E-04   .7568E-04   .8944E-04   .1032E-03

VALUES OF VBAR=  .3021E+03   .2990E+03   .2978E+03   .3019E+03   .3006E+03   .2995E+03

SLOPE=    .1232E+15


STANDARD DEVIATION=    .1419E+14


INTERCEPT=    .1379E+11
```

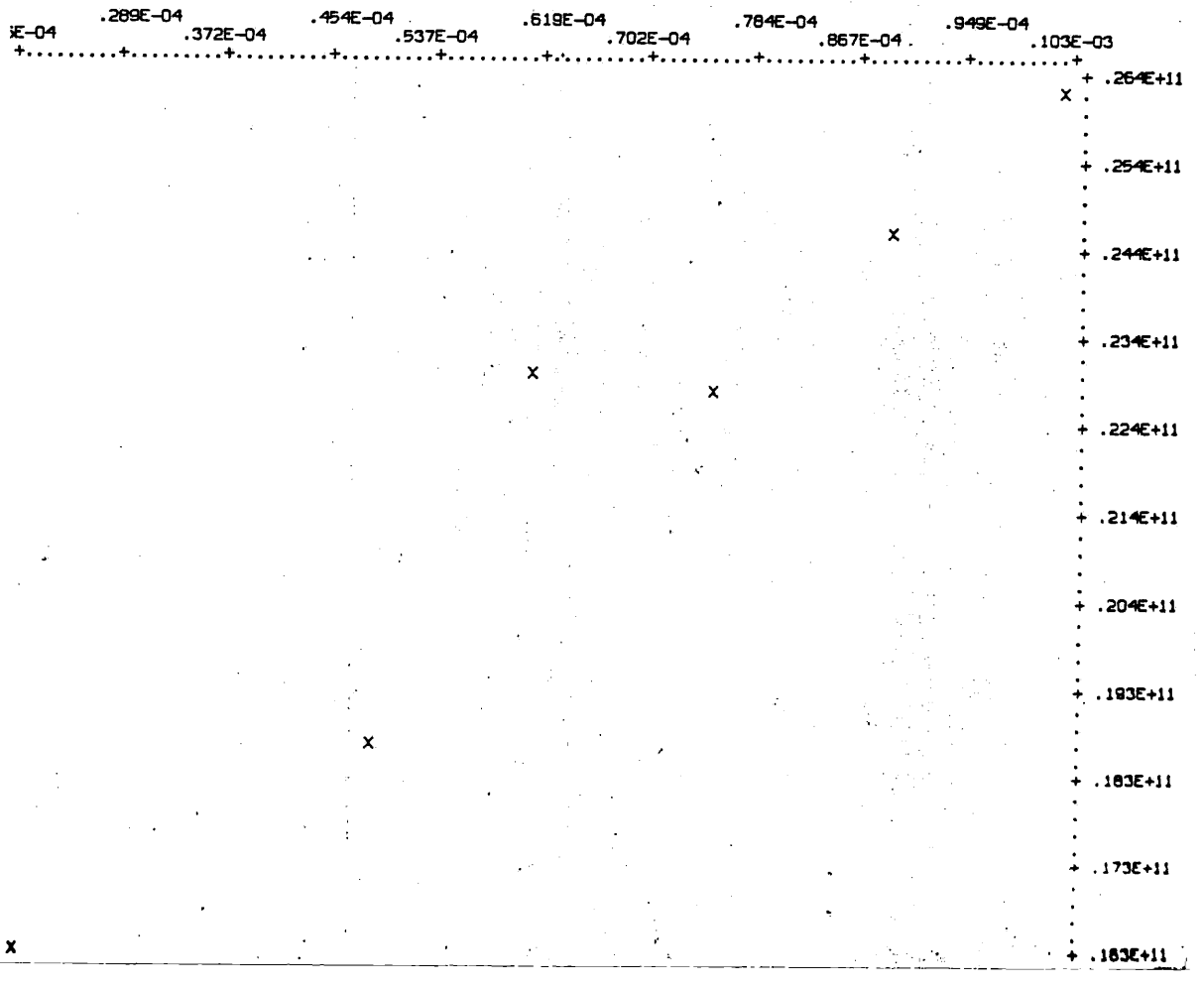

Figure 6.10

Arrhenius plots for $k_{1,M}$ (T=196-500K)

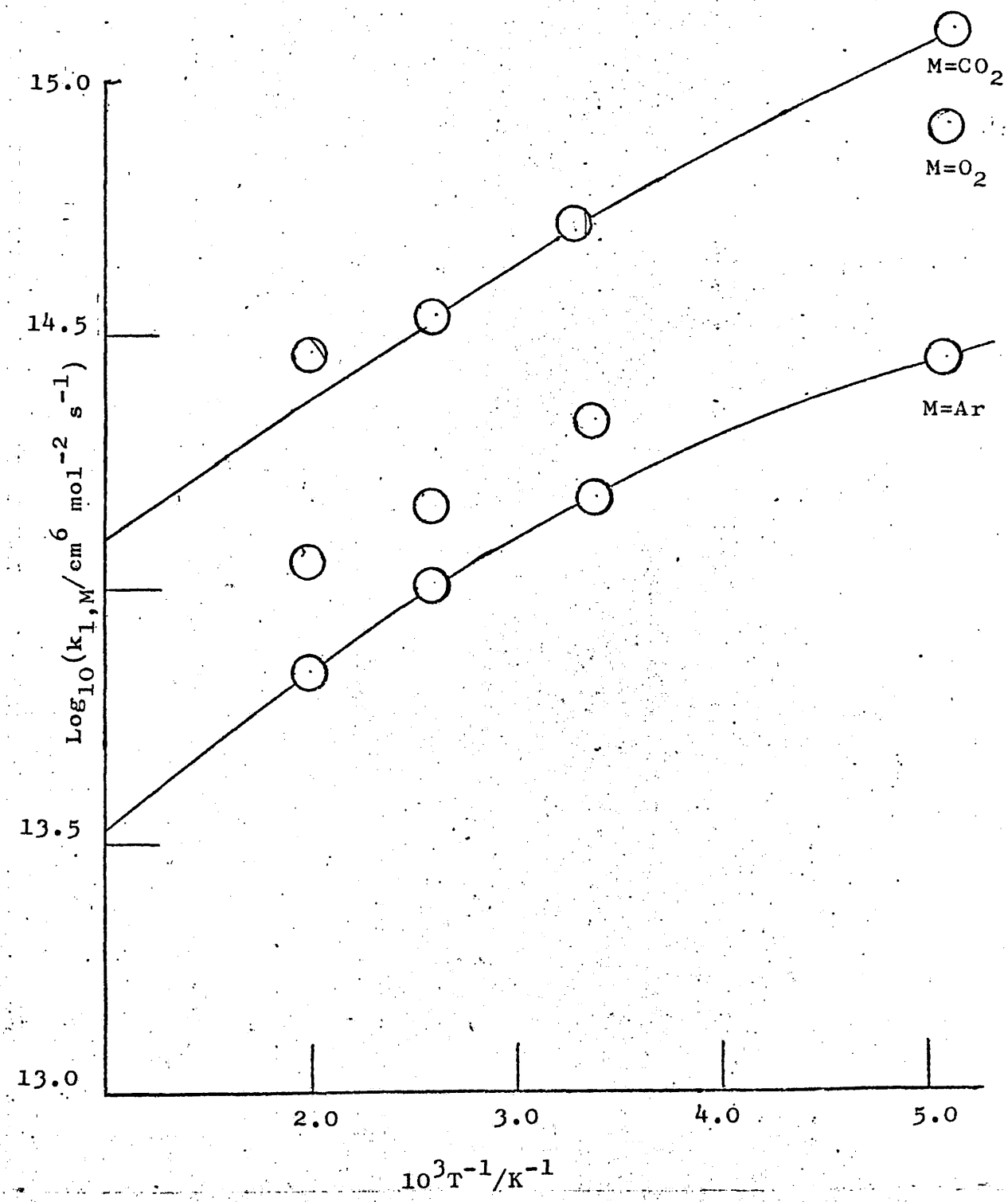

Figure 6.11

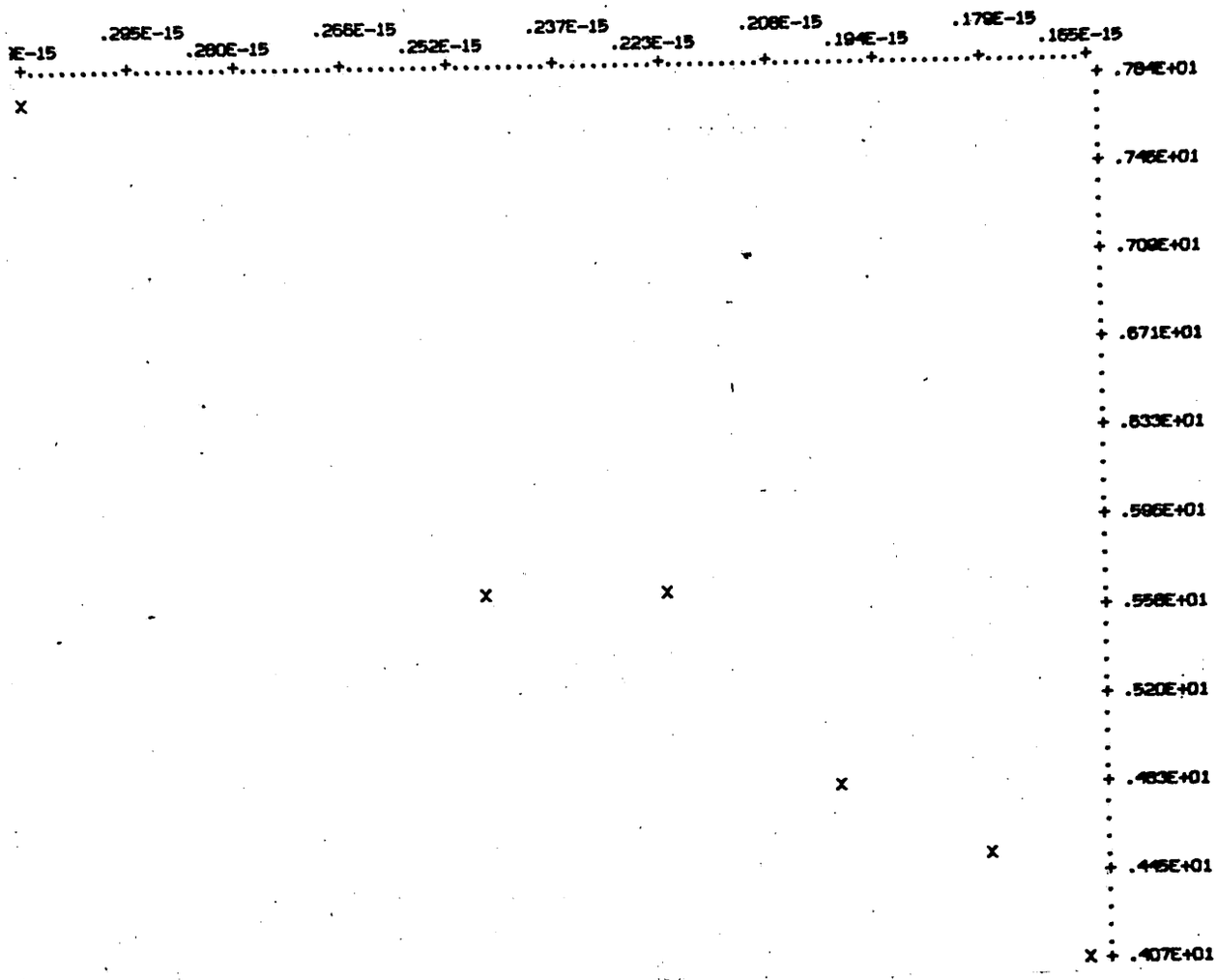
.295E-15
.280E-15
.268E-15
.252E-15
.237E-15
.223E-15
.208E-15
.194E-15
.179E-15
.165E-15
.784E+01
.746E+01
.709E+01
.671E+01
.633E+01
.596E+01
.558E+01
.520E+01
.483E+01
.445E+01
.407E+01

Table 6.2

M=Ar Summary of data for $k_{1,M}$ (196-500 K)

T/K	$k_{1,M}/10^{14}$ cm^6 mol^{-2} s^{-1}	$(k_w-k_w^*)/s^{-1}$	$(\gamma-\gamma^*)\times10^5$
196	2.84 ± 0.15	-0.48	-2.38
	2.88 ± 0.18	-0.49	-2.41
Mean	2.86 ± 0.17	-0.49	-2.39
295	1.46 ± 0.09		
	1.47 ± 0.34	0.64	2.52
	1.53 ± 0.11	-0.19	-0.77
Mean	1.49 ± 0.18		
385	1.04 ± 0.34	-0.12	-0.43
Mean			
500	0.65 ± 0.07	0.23	0.72
	0.72 ± 0.04	0.36	0.10
	0.67 ± 0.05	0.38	1.17
Mean	0.68 ± 0.05	0.33	1.00

Table 6.3

M=O_2 Summary of data for $k_{1,M}$ (196-500 K)

T/K	$k_{1,M}/10^{14}$ cm^6 mol^{-2} s^{-1}	$(k_w-k_w^*)/s^{-1}$	$(\gamma-\gamma^*)\times10^5$	k_w^*/s^{-1}
196	8.57 ± 0.46	-0.03	-0.14	0.98
	8.65 ± 0.86	-0.19	-0.97	-0.03
Mean	8.61 ± 0.66	-0.10	-0.56	-0.41
295	2.03 ± 0.18	-0.11	-0.45	
	2.27 ± 0.09	±0.04	+0.15	
	2.07 ± 0.23	-0.31	-1.22	
Mean	2.12 ± 0.16	-0.15	-0.61	
385	1.31 ± 0.47	1.49	5.20	
	1.58 ± 0.19	1.49	5.20	
Mean	1.45 ± 0.33	1.49	5.20	
500	1.23 ± 0.14	0.04	0.13	
	1.07 ± 0.24	0.04	0.14	
Mean	1.15 ± 0.20	0.04	0.13	

Table 6.4

M=CO_2 Summary of data for $k_{1,M}$ (196-500 K)

T/K	$k_{1,M}/10^{14}$ cm^6 mol^{-2} s^{-1}	$(k_w-k_w^*)/s^{-1}$	$(\gamma-\gamma^*)\times10^5$
196	14.1 ± 0.13	1.66	8.09
	15.8 ± 0.10	2.22	10.87
Mean	14.9 ± 0.12	1.94	9.48
295	5.08 ± 0.44	0.43	1.70
	5.01 ± 0.79	1.22	4.85
	5.91 ± 0.30	1.66	6.61
Mean	5.33 ± 0.51	1.10	4.39
400	2.64 ± 0.79	0.40	1.38
	4.36 ± 0.13	0.82	2.82
Mean	3.50 ± 0.46	0.61	2.10
500	3.26 ± 0.35	0.07	0.23
	2.83 ± 0.34	0.15	0.44
Mean	3.04 ± 0.35	0.11	0.33

plots for different pre-thermostatted residence times (at various V). These were always identical in decay rate. The total Ar flow was between 100 and 380×10^{-6} mol s^{-1} and $\bar{v}$ was 200 cm s^{-1}. The mean value of $k_{1,Ar}$ at 196 K (Fig. 6.1) was $2.86 \pm 0.16 \times 10^{14}$ cm^6 mol^{-2} s^{-1} (a summary of all determinations of $k_{1,Ar}$ at different temperatures is given in Tables 6.2-6.4).

Runs were then carried out (M=Ar) at 385 K when flow rate of Ar was varied between 100 and 500×10^{-6} mol s^{-1}. Blank corrections for this data were made (and also for runs at 500 K) to correct for flow perturbations and changes in the mean linear flow velocity caused by introduction of gases at the inlet jets. The blank determinations were carried out by adding a flow of Ar through J2 and J5 equivalent to the flow of reactant O_2 for each experimental point (i.e. one for each set of conditions, Section 3.3). The results are plotted in Fig. 6.2. However, the 'blanks' were found to be negligible and were not included in this case. The mean value of $k_{1,Ar}$ at 385 K is $1.01 \pm 0.05 \times 10^{14}$ cm^6 mol^{-2} s^{-1}. Three runs were also made in a similar manner at 500 K, (Fig. 6.3). The flow of Ar here was varied between 68 and 275×10^{-6} mol s^{-1} and the flow velocity ($\bar{v}$) maintained at 150 cm s^{-1}. The flow of discharge Ar was reduced to 68×10^{-6} mol s^{-1} to help reduce the gas stream flow velocity and to obtain a smaller 'background' recombination. The mean value for $k_{1,Ar}$ at 500 K using 'blank' corrections was $0.68 \pm 0.05 \times 10^{14}$ cm^6 mol^{-2} s^{-1}.

In a similar manner, runs were carried out for M=O_2,

Figs. 6.4, 6.5 and 6.6, for M=CO_2, Figs. 6.7, 6.8, 6.9. The final values of $k_{1,M}$ in the range 196-500 K are summarized (Tables 6.2-6.4), the accuracy is always better than $\pm$10% and in some cases $\pm$3%. The value of log $k_{1,M}$ was plotted (Fig. 6.10) as a function of 1/T according to the classical 'Arrhenius' equation for the determination of the activation energy and pre-exponential factor (A) and also (Fig. 6.11) as a function of $\log_{10}$ (T/300) for the determination of the temperature dependence of the reaction according to the form $k=AT^n$. This relationship is used when gas phase rate constants are not expressible in simple Arrhenius form. A simple 'least square' computer program was used to evaluate the constants. When M=Ar, the results agree well with those of Huie with the combined error limits (10-25%) but not with those of Clyne or Mulcahy. The measured temperature dependence is represented by:

$$k_{1,Ar}/cm^6\ mol^{-2}\ s^{-1} = (2.90\pm0.10)\times10^{13}\ \exp\left[(900\pm150)/RT\right]$$

$$R = 1.99\ cal\ K^{-1}\ mol^{-1}$$

or:

$$k_{1,Ar}/cm^6\ mol^{-2}\ s^{-1} = (1.49\pm0.04)\times10^{14}\ (T/300)^{(1.5\pm0.3)}$$

The temperature dependence, expressed in the form $k=AT^n$, is a good linear fit to the measurements, but the Arrhenius form is linear only if the extreme error limits of the measurements are used. The overall shape of the latter is curved with increasing activation energy (or slope) with decrease in temperature.

For M=O_2, CO_2, the values of $k_{1,M}/cm^6\ mol^{-2}\ s^{-1}$ are:

$$k_{1,CO_2} = (6.28\pm0.29)\times10^{14}\ (T/300)^{(1.7\pm0.3)}$$

$$k_{1,O_2} = (2.79\pm0.51)\times10^{14}\ (T/300)^{(2.2\pm0.5)}$$

or $$k_{1,CO_2} = (7.89\pm2.65)\times10^{13}\ \exp\left[(991\pm73)/RT\right]$$

$$k_{1,O_2} = (2.69\pm0.13)\times10^{13}\ \exp\left[(1248\pm137)/RT\right]$$

6.4 Heterogeneous Rate Constants (196-500 K)

From kinetic equation 3.3 used to determine the homogeneous rate constant $k_{1,M}$ at 295 K, $(k_w-k_w^*)$ was determined;

$(k_w-k_w^*) = \left[\text{Intercept} - \sum_M k_{1,M}F_M\right]\frac{F_{O_2}}{V^2}$, where the intercept is on the Y-axis for X=0. Also, the heterogeneous (surface) rate constants (196-500 K) can be determined by use of equation 3.5:

$$\frac{V}{V_R}\cdot\frac{F_{Ar}^*}{\Delta F_{Ar}}\ln\left[\frac{I^*2}{I^*1}\right] = k_w + \frac{2k_{2,NO}F_{NO}F_{Ar}}{V^2}\left[\frac{F_{Ar}+F_{Ar}^*}{F_{Ar}^*}\right]$$

where F_{Ar}^* = Flow of Ar through the discharge, F_{Ar} = Flow of Ar (M), and $\Delta F_{Ar} = F_{Ar} - F_{Ar}^*$.

Thus plots of L.H.S. against $\frac{F_{Ar}}{V^2}\left[\frac{F_{Ar}+F_{Ar}^*}{F_{Ar}^*}\right]$ can be used to obtain k_w as the intercept and $2F_{NO}k_{2,Ar}$ as the slope. From the slope, the mole fraction

$$X_{NO} = \frac{F_{NO}}{F_{NO}+F_{Ar}^*}$$

can be calculated assuming

$k_{2,Ar} = (3.27 \pm 0.42) \times 10^{15} \exp (594 \pm 35)/T \quad cm^6\ mol^{-2}\ s^{-1}$

given[80] for the range 217-500 K. An example has been given in Fig. 6.12, data in Fig. 6.4. The graph is accurately linear. These results are discussed in Section 8.

Figure 6.12

Plots for $k_{1,M}$ according to $k_{1,M}=AT^{n}$ (196-500 K).

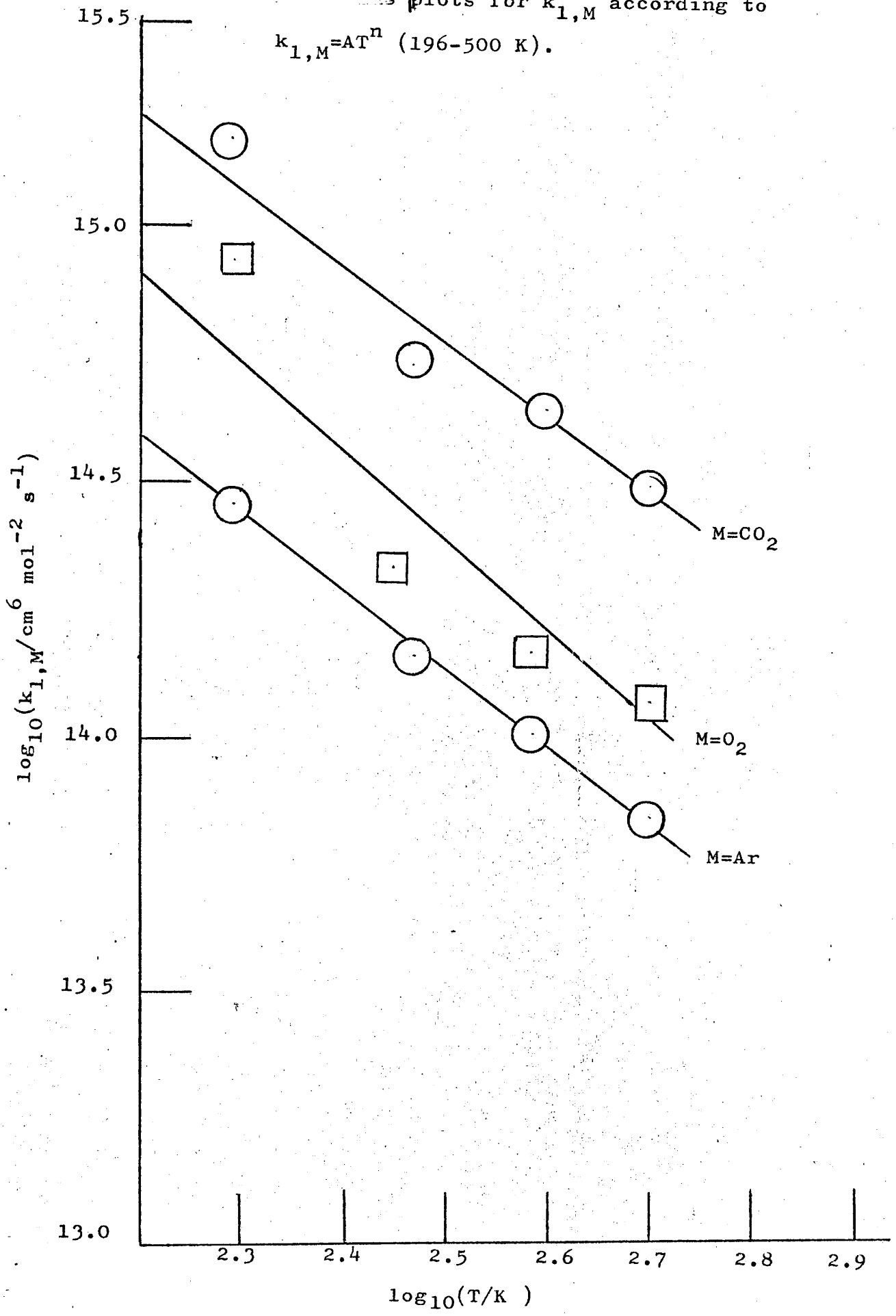

SECTION 7

The Experimental Determination of the Rate of the Homogeneous Reaction

$$O + SO_2 + M = SO_3 + M$$

at 295 K.

7.1 Introduction

This section describes the determination of the rate constant of the homogeneous gas reaction involving recombination of O with SO_2 at 295 K. In the first instance the reaction scheme was assumed, on the basis of earlier work to be

$$O + \text{wall} = \tfrac{1}{2}O_2 + \text{wall} \qquad \ldots(w)$$

$$O + NO + M = NO_2 + M \qquad \ldots(2)$$

$$O + NO_2 = NO + O_2$$

$$O + SO_2 + M = SO_3 + M \qquad \ldots(5)$$

The kinetic equation used for the studies viz:

$$\frac{V^3}{V_R}\ \frac{1}{F_{SO_2}}\ \ln\left[\frac{I1}{I2}\right] = \frac{V^2}{F_{SO_2}}\left(k_w^{SO_2} - k_w\right) + 2k_{2,SO_2}F_{NO} + k_{5,SO_2}F_{SO_2} + k_{5,M'}F_{M'} \qquad \ldots 7.1$$

(Since $I^*1 \triangleq I^*2$), where Ar is the added M' through the discharge and inlet jets ($M' \neq SO_2$), is exactly the same as equation 3.3 except that SO_2 becomes the reactant gas instead of O_2. The equation was slightly modified (see below) for $M=SO_2$. No interference from reaction (1) occured under the conditions used since $[O_2]$ was negligible. Three runs were carried out for M=Ar and two runs for $M=SO_2$ and the results of these are set out in Section 7.3. Preliminary work was carried out to establish first-order O-atom decay profiles in the presence of SO_2 for M=Ar (Section 7.2).

It is now generally thought that much of the SO_3 formed in the combustion products of sulphur containing fuels is formed as a result of reaction (5). However, due to the lack of kinetic data on the $O-SO_2-SO_3$ system, quantitative assessment cannot be made. In particular, the temperature coefficient of reaction (5) is unknown .

The reaction also plays a major role in the pollution of urban atmospheres (Section 1.3) by assisting in the formation of 'photochemical smog' eg. at Los Angeles, U.S.A. The rate of disappearance of O atoms in the presence of SO_2 has been studied by only a few teams of workers and for only a limited range of third bodies. Thus, Kaufman[7] obtained ($M=O_2$, T=295 K) $k_5=30\times10^{15}$ cm^6 mol^{-2} s^{-1} using a discharge-flow system. Thrush et al.[81] obtained ($M=O_2$, Ar, T=293 K) a value of $k_5=4.7\times10^{15}$ cm^6 mol^{-2} s^{-1} in good agreement with value of Allen and Cadle,[82] both using a flow-tube afterglow tecnique. However, Mulcahy[83] firstly reported (M=Ar, T=295 K) $k_5= 2.4\pm0.15\times10^{15}$ cm^6 mol^{-2} s^{-1} using the E.S.R.-stirred flow technique but later[84] reassigned a value (M=Ar) of 1.4×10^{15} cm^6 mol^{-2} s^{-1} using the same method and 1.0×10^{15} cm^6 mol^{-2} s^{-1} using afterglow detection at 300 K. He estimates that the best value is $1.1\pm0.3\times10^{15}$ cm^6 mol^{-2} s^{-1} and attributed the high values to a complex surface reaction involving SO_3. Adsorption of SO_3 by the wall was responsible for an increase in k_w, which therefore increased with increasing $[SO_3]$ in the gaseous phase. This caused k_w to vary sympathetically with the rate of reaction (5) in the flow stream and consequently, the apparent value

of k_5 was (a) too large and (b) dependent upon [O]. Both Mulcahy and Kaufman found difficulty in arriving at a stable surface condition. The mean value (M=Ar, T=295 K) of $k_5=2.46\pm0.21\times10^{15}$ cm^6 mol^{-2} s^{-1} reported here agrees reasonably well with Mulcahy's[83] earlier value; the higher values found by Thrush et al. and Allen and Cadle can be attributed to a secondary reaction $O + SO_3^* = SO_2 + O_2$ which would give an apparent rate constant of $2k_{5,Ar}$ at high [O], (Section 8).

Reports of work with other third bodies in the determination of $k_{5,M}$ are particularly sparse. No reports exist for M=He, N_2, CO or other third bodies, or of a report of the temperature coefficient. Mulcahy[84] obtained ($M=SO_2$, T=299 K) $10\pm4\times10^{15}$ cm^6 mol^{-2} s^{-1} in good agreement with the value ($M=SO_2$, NO_2, T=297 K) of 14×10^{15} cm^6 mol^{-2} s^{-1} by Jaffe and Klein[85] using photolytic methods. The value ($M=SO_2$, T=295 K) reported here is 14×10^{15} cm^6 mol^{-2} s^{-1}.

Thus, further accurate determinations are needed for different third bodies at 295 K and also for temperatures in the range 196-500 K.

7.2 Preliminary Work

Preliminary experiments were carried out in reaction system B using a microwave discharge to establish first-order atomic decay profiles over the full range of conditions and concentrations of reactant SO_2 to be used. These were carried out in exactly the manner described for decay profiles in the presence of added O_2 (Section 5.2) i.e. by adding

Figure 7.1

First Order decay profiles of atomic oxygen

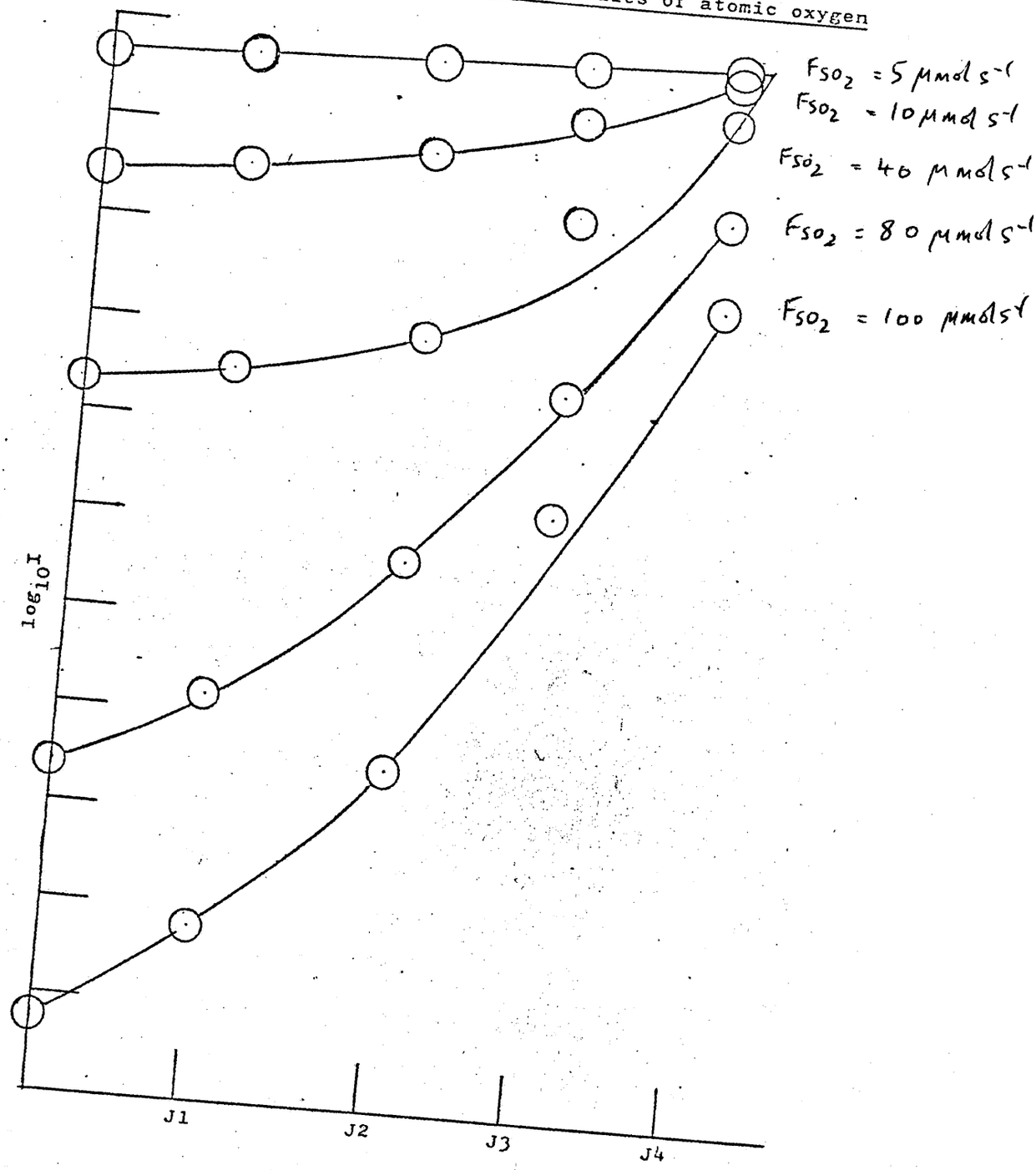

a measured flow of SO_2 through jets 1 to 5. A typical atomic decay profile in the presence of added SO_2 is shown in Fig. 7.1 and the data for this is given in Table 7.1. The SO_2 flow rate ranged from 0 to 70×10^{-6} mol s^{-1}, F_{Ar} was fixed at 170×10^{-6} mol s^{-1} and $\bar{v}$ was maintained at 400 cm s^{-1}. The plots deviate from linearity, curvature increasing gradually between points J5 and J3 and markedly beyond J3. This may be due to a change in kinetic order from third to second with increase of pressure, (Section 8). No further preliminary work was carried out.

7.3 The Rate of the Homogeneous Reaction:

$$O + SO_2 + M = SO_3 + M$$

This section contains experimental data obtained in system B for the determination of $k_{5,M}$. Three runs were carried out for M=Ar at 295 K and reproducibility was shown to be within the limits of standard deviation (i.e. 5-10%). The procedure was exactly the same as that described in Section 5.3 for $k_{1,M}$ ($M \neq O_2$) except that the reagent was now SO_2; this was further dried by passage through two fresh silica gel traps. F_{SO_2} was fixed at 10 or 14×10^{-6} mol s^{-1}, F_{Ar} ranged from 100 to 380×10^{-6} mol s^{-1} and $\bar{v}$ was maintained at 200 or 300 cm s^{-1}. $k_{5,Ar}$ was determined using equation 7.1, in the computer program the quantity F_{SO_2} replaced F_{O_2}. A typical set of experimental data (Run no. R1 Ar) is plotted in Fig. 7.2; a further run (R3 Ar) which gave $k_{5,Ar} = 3.1 \pm 0.5 \times 10^{15}$ cm^6 mol^{-2} s^{-1} was rejected for lack of

accuracy ($\pm$16%). These plots according to the equation 7.1 are curved, the slope decreasing from 3.0-3.6x10^{15} cm^6 mol^{-2} s^{-1} to 1.8-1.4 at higher values of F_{Ar}. This could be due to either: (a) a change of reaction order from overall third to second with increasing pressure or, (b) the attainment of a steady state concentration of SO_3 followed by rapid removal with O-atoms, these possibilities are fully discussed later (Section 8). in particular the way these plots helped to decide between (a) and (b). The mean value of $k_{5,Ar}$ = 2.46$\pm$0.21x10^{15} cm^6 mol^{-2} s^{-1}, this is compared with leterature values (Section 8).

In the determination of k_{5,SO_2} it was necessary to use the following equation for computation:

$$\frac{V^3}{V_R \Delta F_{SO_2}} \ln\left[\frac{I1}{I2}\frac{I02}{I01}\right] = 2k_{1,SO_2}F_{NO} + k_{2,Ar,}F_{Ar} + k_{2,SO_2}\sum F_{SO_2} \quad \ldots 7.2$$

where $\Delta F_{SO_2} = F_{SO_2} - F'_{SO_2}$, $\sum F_{SO_2} = F_{SO_2} + F'_{SO_2}$, F'_{SO_2} = 3.4x10^{-6} mol s^{-1} and I01, I02 are intensity readings for F'_{SO_2} added and are introduced as 'blank' corrections (these should be negligible at 295 K). The term involving ($k_w^{SO_2} - k_w$) disappears in the derivation of the above equation. The data (Table 7.1) was used in the computation. Δ x was chosen as the distance between jets J5 and J3 since the decay plots (Fig. 7.1) were approximately linear in this region. $\bar{v}$ was kept constant and the pressure was maintained in the range 1.5-2.3 torr. The plot according to the above equation for k_{5,SO_2} was of a parabolic shape and k_{5,SO_2} could not be determined.

Figure 7.2

T	P
295.0	48.8

F1	F2	F3	I01	I1	I02	I2	F
20.0	150.0	0.0	100.0	71.2	100.0	58.2	1.815
20.0	250.0	100.0	100.0	48.5	100.0	33.2	2.757
20.0	300.0	150.0	100.0	41.7	100.0	25.5	3.274
20.0	350.0	200.0	100.0	37.5	100.0	21.5	3.789
20.0	450.0	300.0	100.0	84.5	100.0	42.9	4.856
20.0	550.0	400.0	100.0	66.6	100.0	30.8	5.870

VALUES OF Y= .2165E+12 .4652E+12 .6001E+12 .6769E+12 .8032E+12 .9227E+12

VALUES OF X== 0. .6880E-04 .1032E-03 .1376E-03 .2064E-03 .2752E-03

VALUES OF VBAR= .3121E+03 .3263E+03 .3257E+03 .3254E+03 .3225E+03 .3236E+03

SLOPE = .2502E+16

STANDARD DEVIATION = .2578E+15

Y-INTERCEPT = .2841E+12

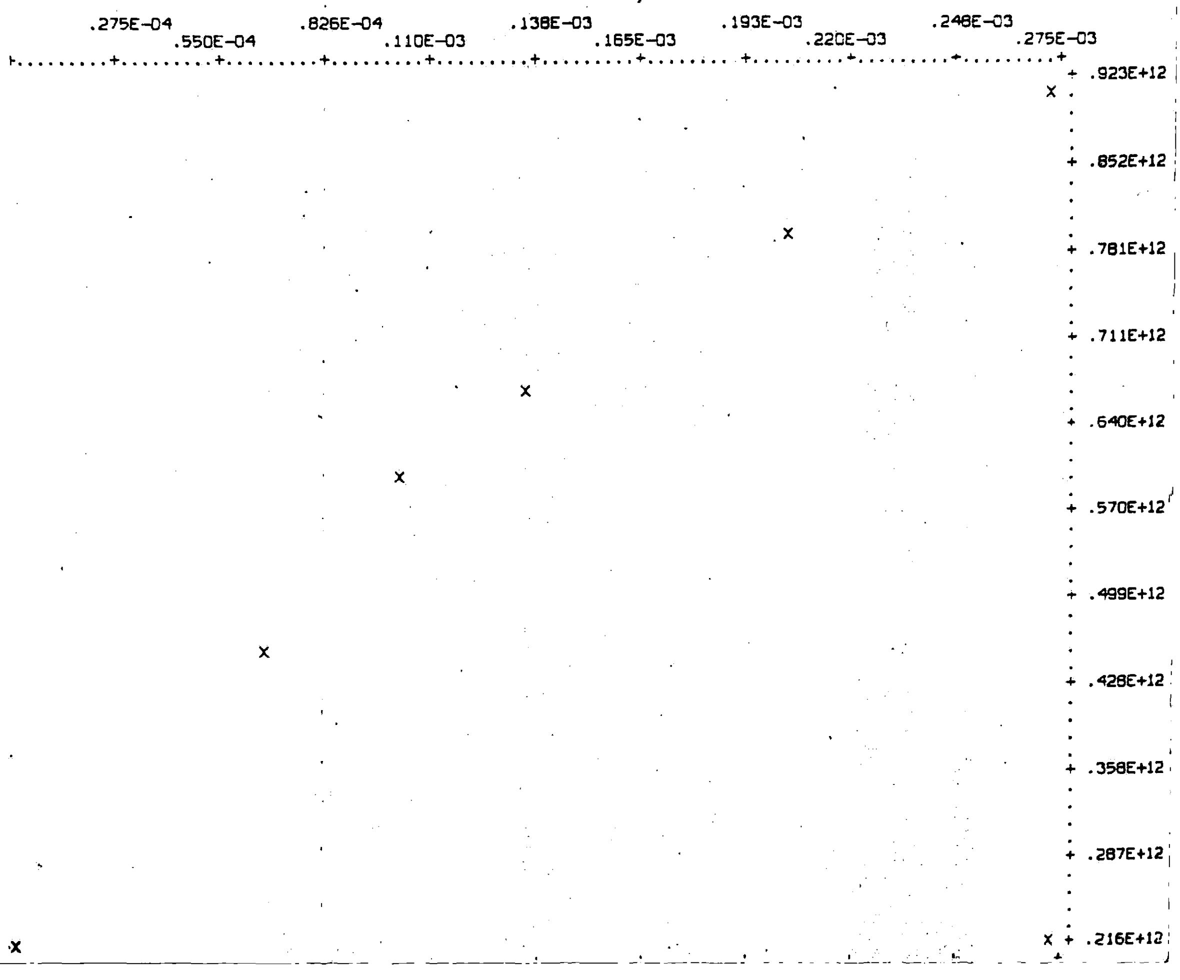

Experimental data to establish first order decay profiles in Fig. 7.1

	Intensity readings at					
$F_{SO_2}/10^6$ mol s^{-1}	J1	J2	J3	J4	J5	P/(Torr)
5	046.1	046.9	047.7	048.6	049.7	1.566
10	035.1	036.2	038.4	042.9	048.1	1.672
20	021.5	022.5	024.7	034.5	043.3	1.741
30	008.7	010.4	014.6	022.4	034.5	1.891
40	004.8	006.1	008.9	016.6	027.9	1.922
60	003.9	005.6	013.1	030.2	057.7	1.966
80	001.1	002.3	005.5	020.3	049.5	2.152
100	002.0	003.9	007.7	022.7	049.0	1.945

Table 7.1

SECTION 8

Discussion

Discussion

Experimental rate measurements at 295 K have been made for reactions (1) i.e. $O + O_2 + M \longrightarrow O_3 + M$ for various third bodies and the temperature dependence of the reaction (m=Ar, O_2, and CO_2) has been studied in the range 196-500 K. Rate constants of reaction (5) i.e $O + SO_2 + M \longrightarrow SO_3 + M$ have been made.

The results of determinations of $k_{1,M}$ for M=He, Ar, N_2, O_2, CO and CO_2 (Section 5.3) are summarized in Table 8.1 and the mean rate constants for these third bodies at 295 K compared with the results of other workers (since 1964) whose experimental systems excluded contaminants such as excited molecules or hydrogenous impurities (Sections 1.3 and 2.3). The present values lie generally in the middle of the range and agree well with those of Huie et al,[59] Stuhl and Niki,[61] and Kaufman and Kelso.[47] Agreement is to within 5-10% with these workers for the third bodies where a comparison is possible, and the estimated accuracy for the present work is 5-20%.

For M=CO, only two other values are presently available. The value of reference (61) is in good agreement with the present value but not with the value obtained by Meaburn et al,[76] even within combined deviations. The values obtained by pulse-radiolysis are 0.50% lower than the present

Figure 8.1

The temperature dependence of $k_{1,M}$ (M=Ar)

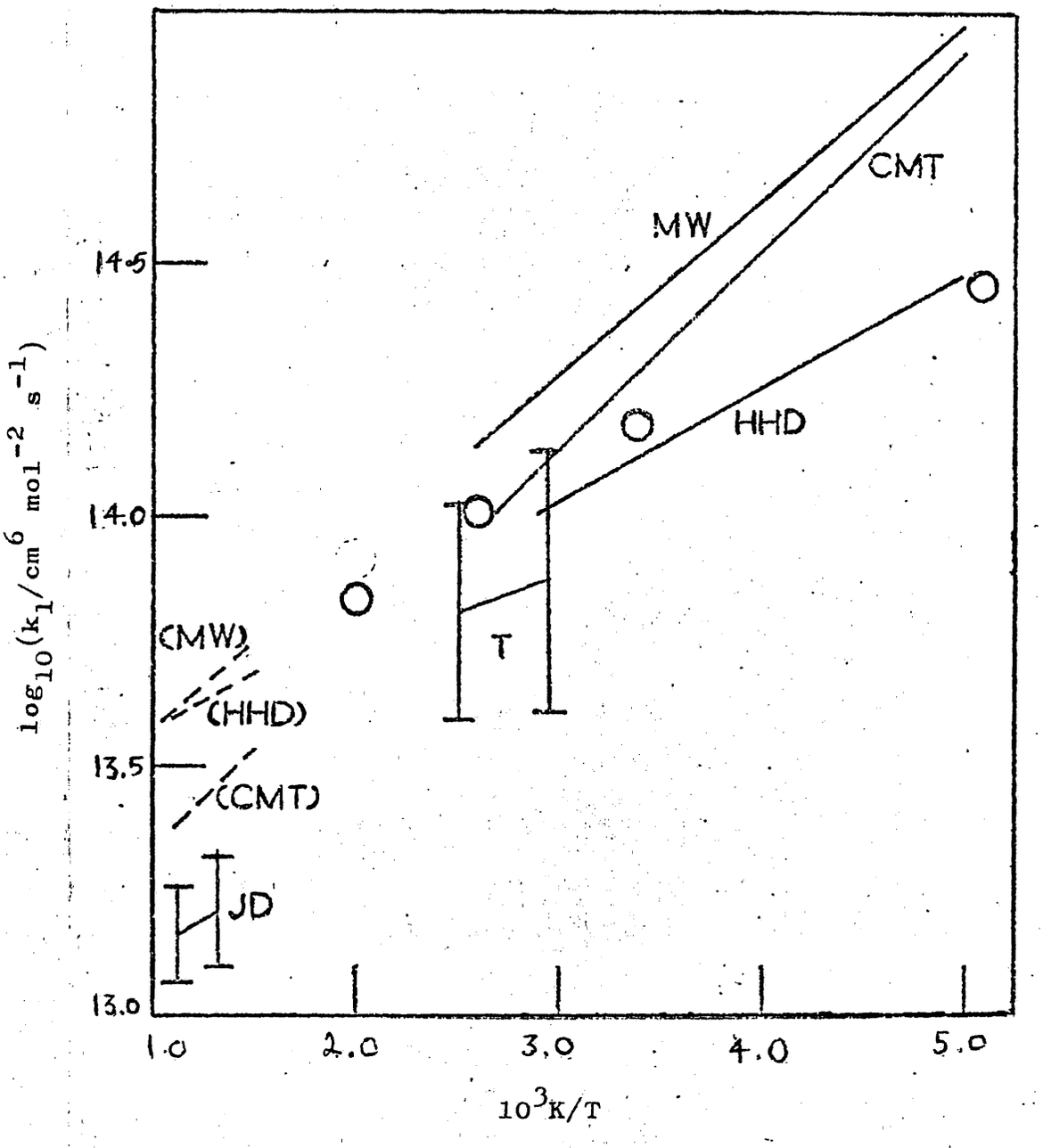

O This work

MW Mulcahy and Williams[50]

CMT Clyne, McKenney and Thrush[56]

T Thermal decomposition of ozone[12,16]

JD Jones and Davidson[14]

HHD Huie, Herron and Davis[59]

work. However, Bevan and Johnson[51] showed that the u.v. absorption bands of O_3 are distorted by vibrational excitation which may cause errors in the pulse-radiolysis method. Rosenburg and Trainor[86] found that there is vibrational excitation, following combination, in at least the ν_3 and ν_2 modes of ozone and that the partitioning of the product energy among the vibrational modes accounts for 50% of the 25 kcal mol^{-1} exothermicity of the recombination. Further, the measurements obtained by Bevan and Johnson[51] for $M=O_2$ and CO_2 are in excellent agreement (to within $\pm$6%) with the present results. The measurements obtained by Mulcahy and Williams[50] using the stirred-flow method are 30-80% higher than the present ones and no agreement within combined standard deviations are observed. Their results depend on the assumption of ideal mixing in their bulb reactor which, if in error, may explain why the results are higher than those of Clyne et al.[56] In both studies, heterogeneous wall reactions are also possible sources of error, (these errors have been eliminated in the present work) and the discrepancy in the temperature dependence (M=Ar) may be due to these errors. The value obtained by Clyne et al (M=Ar) is 20% above the value obtained here. Furthermore, Mulcahy generated oxygen atoms by pyrolysis of ozone. Incomplete dissociation of O_3 leads to the reaction $O + O_3 = 2O_2$ causing interference in the reactor; he also made corrections for reaction in the connecting tubes of the reactor. The most reliable alternative values are those obtained from the static method of Huie et al.[59] These measurements were conducted at higher total

Table 8.1

Values of $k_{1,M}/x10^{14}$ cm^6 mol^{-2} s^{-1} at 295 K.

$M=O_2$	M=Ar	M=He	$M=N_2$	M=CO	$M=CO_2$	Ref.
2.13	1.49	1.34	2.01	2.35	4.98	This work
1.35						12
0.45						22
	1.50					42
2.34	1.44	1.44	2.02		5.35	47
3.18	2.85	2.28			9.70	50
1.94	0.97				4.79	51
	1.58		2.52			52
	1.90					56
	1.31	1.19	2.03			59
	1.80	1.66				60
2.30			1.94	2.41		61
1.44				1.54	3.56	76
	0.83					91
	0.90	0.66			4.15	92

Relative Efficiencies of Third Bodies at 295 K.

He	Ar	N_2	O_2	CO	CO_2	Ref.
0.67	0.73	1.00	1.05	1.17	2.52	This work
0.83	0.71	1.00	1.07		2.58	12
0.87	0.64	1.00	1.13		2.46	11
0.71	0.71	1.00	1.16		2.65	47
0.59	0.64	1.00				59

Table 8.2

Confidence limits (95%) for $k_{1,M}/10^{14}$ cm^6 mol^{-2} s^{-1} for M=N_2,O_2,Ar,He,CO and CO_2 at 295 K.

N_2	O_2	Ar	He	CO	CO_2	Source
2.01±0.15	2.12±0.17	1.49±0.18	1.34±0.22	2.35±0.12	5.33±0.51	Present work
2.10±0.28	1.89±0.68	1.51±0.38	1.43±0.51	2.10±1.21	5.42±2.30	Table 8.1
2.13±0.42	1.86±0.81	1.51±0.30	1.45±0.74	1.98±5.57	5.51±3.30	Present work and Table 8.1 combined.

Table 8.3

Table 8.4

Recombination coefficients (γ) for oxygen atoms on various surfaces at 295 K.

Pyrex	Teflon	H_3PO_4	H_2SO_4	Ref.
0.02-0.1		0.02		This work
0.02				7
		0.05 (in pure O_2)		16c
0.12				24
0.02-0.5	0.01-0.04	0.04	0.02	94
0.03-0.05				95

pressures (50-500 torr) when wall recombination is negligible and at shorter time constants (10^{-3}-10^{-2} s). Agreement with their temperature dependence for M=Ar is satisfactory and within combined error limits of 10-25%. The third body efficiencies obtained in the present work relative to N_2 are compared with results other workers obtained where a range of three or more third bodies have been studied at 295 K (Table 8.2). The efficiencies compare well with those obtained in pyrolysis experiments, photolysis experiments and static methods. The efficiencies of Mulcahy et al[50] have been omitted since their rate constants are probably too high. Table 8.3 compares 95% confidence limits (calculated by standard statistical methods for small samples) for the data in Table 8.1 and for the three rate constants for each of the gases from the present data, after rejecting statistically improbable (<95%) values. The limits in the present data mask any systematic errors, unlike those for the data in Table 8.1, since the replicates were not completely independent. However, a comparison of the most probable values in Table 8.3 suggest that these errors are small (<10%) and are of the order of estimated instrumental errors.

A feature of the present method is that the effects of wall and other background reactions are eliminated, and the rate constants at 295 K show no trends with wall recombination

efficiency, which ranged from $1x10^{-5}$ to $12x10^{-5}$. However, most important is the result that the method distinguished between significant changes in surface recombination rate in the presence (γ) and absence (γ^*) of O_2 (Table 5.5). γ^* was reproducible ($\pm$25%) in the presence of a given third body on a clean pyrex tube but for different M was in the order He Ar, < N_2, O_2, < CO < CO_2. The results (Table 5.5) show that the introduction of O_2 reduced the efficiency by surface poisoning as first suggested by Benson.[54] This is also supported by the work on the $O+SO_2$ system. Oxygen may be strongly physically adsorbed on the wall by forces such as Van der Waal bonding hence poisoning the wall. The differences in γ and γ^* are probably due to the occurence of a surface reaction (in the presence of added O_2) occuring at the wall viz:

$$O + O_2 + \text{wall} = \overset{*}{O}_3 + \text{wall}$$

where $\overset{*}{O}_3$ is in a vibrationally excited state. Presumably, a small percentage of molecules are excited to higher states. Deactivation then would occur by cascading down the vibrational ladder to the ground state. Wall recombination clearly causes no significant errors in $k_{1,M}$ however, since the former varied by an order of magnitude at 295 K whereas the relative third body efficiencies are in close agreement with the static method of Huie where wall effects are absent. The measured values of γ are compared with those reported previously (Table 8.4). The value of $0.02x10^{-3}$ for an H_3PO_4 coated surface (in the presence of added O_2) agrees well with

the values of 0.05×10^{-3} for pure O_2 obtained by Kretschmer[16c] and with the value of 0.02×10^{-3} on pyrex of Kaufman.[7] Only Mulcahy[50] reports a value on Teflon which appears to be a slightly better poison than phosphoric acid. However, values of γ reported by different workers still vary by a factor of $10\text{-}10^2$. Results of determinations of the temperature dependence of reaction (1) following these facts are discussed below. The introduction of 'blank corrections' into the present flow-system (Section 3.3) to allow for background, wall effects and flow perturbations (which are not negligible above 300 K) was not considered in earlier determinations of $k_{1,M}$. It has already been shown (Section 6.4) how the 'blank' corrections were made and the 'surface' equation 3.5 used in reaction system B to determine $(k_{w_M} - k^*_{w_M})$ and $k^*_{w_M}$, the results (196-500 K) are given in Table 6.8. k^*_w (calculated for $M=O_2$, T=196 K) was very small (-0.413 ± 0.31 s^{-1}) and also independent of F_M; k^*_w would increase with F_M if k^*_w was significantly large, since V, V_R, F_{NO}, and $k_{2,M}$ are constant terms in equation 3.5. Thus the mole fraction of NO in the discharged gas stream can be accurately monitored by the present flow method (this is $\simeq 5 \times 10^{-4}$ p.p.m. for B.O.C. argon). For $M=O_2$, CO_2, Ar values of $(k_{w_M} - k^*_{w_M})$ are all small and do not interfere with the determination of k_1; in particular for $M=CO_2$, the terms $(k_{w_M} - k^*_{w_M})$ show a tendency to a negative temperature coefficient although more data is necessary for an accurate determination. This work on 'surface' rate constants using blank correction is believed to be the main

reason for the discrepancies which exist in values of $k_{1,M}$ as determined by earlier flow methods[7,47,50] and alternative static methods.[51,52,60,61] This work shows that wall effects are not a serious drawback of the flow method when allowances are made for their dependence on gas composition, and agreement with the best static methods can be expected over a wide temperature range and under very different conditions and time constant. This is significant for atomic reactions of higher kinetic order which are mainly studied by flow methods.

The measured temperature dependence of reaction (1) (M=Ar) is compared with the results of other workers (Fig. 8.1), including studies of the thermal decomposition of O_3 for M=Ar in the range 188-1000 K. The results agree with those obtained from the static measurements[59] within error limits of 10-25% but not with the results of flow measurements.[50,56] The present results, and those of Huie[59] can be represented satisfactorily by an equation of the form:

$$k_{1,Ar} = A(T/300)^n$$

where n is 1.50 ± 0.15 (for M=Ar). Combining the two sets of data, weighting each rate constant determination equally, gives $n = 1.54 \pm 0.25$ for M=Ar. The error limits corresponding

to the value of k_1 as determined by the earlier shock tube study of the dissociation of O_3 (750-900 K) by Jones and Davidson[14] are also apparent (Fig. 8.1). This value suggests a slightly greater value for n ($\doteq$1.9). However, the range of uncertainty in the generally accepted value of $\Delta H_f(O_3)$ = 34.8$\pm$0.4 kcal mol^{-1} at 273 K (and thus in K, the equilibrium constant of reaction 1) is too large to estimate a reliable value of n; all direct measurements of k_1 suggest that the lower limit of $\Delta H_f(O_3)$ at 273 K should be used in the calculation of k_1 from O_3 decomposition studies. The results obtained here and those obtained with the shock tube measurements are more consistent with a T^n dependence (Fig. 6.9) than for an Arrhenius form (Fig. 6.8). If the shock tube results were raised by a factor of 1.5, this work would extrapolate linearly for the T^n form and as a smooth curve for the Arrhenius form. However, the best value of n is probably close to 1.5 at low pressures since the value of n from Huie's data shows a tendency to decrease fron 1.9 to 1.5 as the total pressure decreases from 500 to 50 torr. This agreement between the results of Huie and the present work is conclusive evidence for the lower temperature dependence. The higher values of n (2.6-3.4) observed in flow systems previously were probably due to incomplete elimination of surface recombination and failure to distinguish between γ and γ^* and their dependence on gas concentration. In both flow studies, the mole fraction of O_2 was constant or approximately constant and the temperature dependence appears to increase with decreasing O_2. This suggests that

k_1 (M=Ar, CO_2) $\propto T^{-(1.8\pm0.3)}$.

Although earlier workers using flow studies[7,47,50] reported larger values of n, they also observed the same dependence for M=Ar and CO_2. Results of the temperature coefficient of reaction (1) for M=O_2 and CO_2 (196-500 K) by a direct method are reported here for the first time. If the low temperature results when M=O_2 have any meaning, since plots logk/logT and logk/$\frac{1}{T}$ are curves, then this suggests that different homogeneous or heterogeneous reactions are predominating at different temperatures. However, the nature of these processes are unknown at present.

The value of $k_{1,Ar}$ obtained can be expressed as:

$$k_{1,Ar} = 1.46\pm0.09\times10^{14} \left(\frac{295}{T}\right)^{1.5\pm0.3} \text{ cm}^6 \text{ mol}^{-2} \text{ s}^{-1}$$

The reverse of reaction (1), i.e. the rate of the dissociation reaction, can be considered as a unimolecular decomposition at its second order limit.[56] In the Hinshelwood-Rice-Rampsberger-Kassel (HRRK) theory,[87] a molecule is regarded as energised if the molecule contains at least the energy E^* required for reaction to occur, distributed in any way amongst its s normal vibrational modes. The full HRRK equation is:

$$\frac{k'}{k} = \left(\frac{1}{s-1}\right)! \int_0^\infty \frac{x^{s-1} e^{-x} dx}{1+K^{\ddagger}/k_{-1}[A]\left(\frac{x}{b+x}\right)^{s-1}}$$

where $x = \left(\frac{E-E^{*}}{RT}\right)$ $E = E_{Activation}$

and $b = \frac{E^{\ddagger}}{RT}$

k is the first order rate constant at high pressures

and k' is an overall rate constant for the scheme:

$$A + A \underset{-1}{\overset{1}{\rightleftharpoons}} \overset{*}{A} + A$$

$$\overset{*}{A} \xrightarrow[k^{2}]{} A^{\ddagger} \xrightarrow[k^{\ddagger}]{} \text{Products}$$

The activated complex $A^{\ddagger}$ (energy $E^{\ddagger}$) is one that is passing into the final state. An energised molecule is one that possesses sufficient energy to become an activated molecule.

At low pressures, at the second order limit $k_{-1}[A] \longrightarrow 0$, and for reaction to occur, then the rate of energisation to the energy state $\overset{*}{E}$, the HRRK equation reduces to:

$$k_{-1} = \frac{Z}{(s-1)} \left(\frac{\overset{*}{E}}{RT}\right)^{s-1} \exp\left(-\overset{*}{E}/RT\right) \quad \ldots. \; 8.1$$

which is the same as the Hinshelwood equation for an activated process. An essential feature of this theory is that the energy can flow freely between the various modes so that after sufficient time has elapsed the energy may pass into one particular mode; the molecule then decomposes. Lindeman pointed out that energisation and subsequent breakdown of the molecule are distinctly different processes but precisely what constitutes energisation has been treated in different ways.

On the contrary, Slater assumes that there can be no flow of energy between modes. Reaction occurs, not when the energy gets into a particular mode but, when the normal

vibrations come suitably into phase, so that a critical co-ordinate becomes sufficiently extended. Slater's definition of energisation is more stringent than Hinshelwood's because according to him, only those molecules which initially have the energy $\overset{*}{E}$ distributed in a particular manner among the degrees of freedom can undergo reaction. Slater's expression is approximately:

$$k_{-1} = Z\left(\frac{4\pi\overset{*}{E}}{RT}\right)^{(n-1)/2} \prod_{K} \mu_K \exp(-\overset{*}{E}/RT)$$

where n is the number of relevant normal modes in the reacting molecule, sometimes, owing to symmetry or degeneracy, less than the total number; μ is a quantity related to the 'amplitude factors' for various normal modes.

Over the temperature range considered here for reaction (1)(M=Ar), the equilibrium constant can be represented by the expression:

$$K = A \exp\left(\frac{-\overset{*}{E}}{RT}\right)$$ where A is independent of temperature.

The temperature dependence of the pre-exponential terms in the expressions for k_{-1} is therefore the same as that for k_1 which varies as $T^{-3/2}$. Since the collision number Z is proportional to $T^{\frac{1}{2}}$, the temperature dependence of the pre-exponential factor of k_{-1} is best fitted by a value of 2 for (s-1) or $\frac{1}{2}(n-1)$. The ozone molecule has 3 normal modes of vibration. The result for $k_{1,Ar}$ here is therefore compatible with the HRRK theory. However, some degrees of rotational freedom are required for Slater's theory. An earlier value by Clyne et al[56] of $k_{1,Ar} = 2.8\times10^{14}(T/273)^{-(3.4\pm0.8)}$ cm^6 mol^{-2} s^{-1} in a similar flow system to the present one was

incompatible with Slater's theory and only in agreement with the HRRK theory if rotational degrees of freedom also participate.

Tsang[79] recently carried out a detailed RRKM treatment comparing experimental rate data on decomposition and combination reactions involving ozone. For a computer vibrator model with external rotations active, calculation (M=Ar) leads to a temperature dependence of $T^{-(1.4\pm0.3)}$ and a collision efficiency of 0.18. Again the assumption of some rotational degrees of freedom were required by the Slater theory. This dependence is in excellent agreement with the value (M=Ar) reported here and also with that of Huie.[59] This agreement is considered to be conclusive evidence for the lower value of n in the temperature dependence equation.

Earlier values of $k_{5,M}$ for the reaction

$$SO_2 + O + M \longrightarrow SO_3 + M$$

have been reported (Section 7.1), the value obtained in this work (M=Ar, T=295 K) is $2.46\pm0.21\times10^{15}$ cm^6 mol^{-2} s^{-1}. This is about half the value obtained by Thrush[34] ($4.7\pm0.8\times10^{16}$ cm^6 mol^{-2} s^{-1}) using a similar discharge-flow method, and by Allen and Cadle[82] (4.8×10^{16} cm^6 mol^{-2} s^{-1}). Thrush used a kinetic method of analysis which eliminated parallel first order atomic oxygen reactions occuring in the flow tube.

This discrepancy is probably due to interference from wall effects of the type discussed below.

The present value is also in disagreement with that of Davis (2.6×10^{14} cm^6 mol^{-2} s^{-1}, using a reliable alternative flash photolysis-resonance fluorescence method) by an order of magnitude. His result may be influenced by heterogeneous reactions involving the walls of the reaction cell, and/or by formation of electronically excited O_2 molecules. Wall effects were eliminated in the present work by means of the kinetic equation (Section 7.1). Using an E.S.R.-stirred flow reactor, Mulcahy et al[83] reported a value of 2.4 ± 0.15 cm^6 mol^{-2} s^{-1} (T=295 K, M=Ar) in excellent agreement with the present value. Difficulties are encountered with E.S.R. flow reaction method since it depends on the assumption of ideal mixing in the bulb reactor. However, he[84] later reported the revised value $k_{5,Ar} = 1.1 \pm 0.3 \times 10^{15}$ cm^6 mol^{-2} s^{-1} which is about half the present value. $k_w^{SO_2}$ was found to depend on (i) the concentration of oxygen atoms; (ii) the initial condition of the reactor (viz. 'wet' or 'dry'); (iii) the concentration of SO_2 and (iv) the concentration of M. The values of $k_w^{SO_2}$ from plots for $k_{5,Ar}$ at 295 K increased ($1 \longrightarrow 5$ s^{-1}) with increase in the concentration of argon (F_{Ar}= 0-275$\times 10^{-6}$ mol s^{-1}). The results of preliminary experiments (Section 7.2) indicated (a) that the plots of $\ln[O]$ against t were curved, the slope decreasing with reaction time and decreasing $[O]$. These curves were obtained at constant concentration of argon and sulphur dioxide for a series of concentrations of sulphur dioxide. The slope at

high $[O]$ was approximately double that at low $[O]$ (Fig. 7.1); and (b) that the plots of equation (7.1) at constant F_{SO_2} to determine $k_{5,Ar}$ were also curved. At low flow rates of argon the slope was approximately double the slope at high F_{Ar}. Mulcahy et al[84] attributed the change in slope (also found by them) to a surface reaction with SO_3. Water was also present in their system (H_2SO_4 droplets were found on the surface) but was absent in the present system. Experiments with small ($\simeq 5\times10^{-6}$ mol s^{-1}) additions of SO_2 showed (Fig. 7.1) negligible decay of $[O]$ with time, thus showing that surface reactions were unimportant (only trace amounts of SO_3 would be required to be adsorbed on the surface to affect k_w, and the effect is independent of $[SO_2]$). Furthermore, as the concentration of SO_3 increases with reaction time, the slopes ($\ln[O]$ against time) in experiments would have to increase with reaction time. The measurements of $[O]$ in Mulcahy's work were not reproducible or stable whereas in this work intensity measurements were always reproducible and steady.

One possible scheme which can be postulated to explain these results is a possibility of a change in kinetic reaction order. For a third order recombination reaction,

$$O + SO_2(^1A) \underset{-1}{\overset{1}{\rightleftharpoons}} S\overset{*}{O}_3(^3A \text{ or } ^1A)$$

(* indicates vibrational excitation)

$$S\overset{*}{O}_3(^1A) + M \xrightarrow{2} SO_3 + M$$

whence

$$-\frac{d[O]}{dt} = \frac{k_1 k_2 [O][SO_2][M]}{k_{-1} + k_2[M]}$$

if $k_2[M] >> k_{-1}$, then $-\frac{d[O]}{dt} = k_1[O][SO_2]$

This possibilty was considered by Mulcahy, Steven and Ward[83] since k_{-1} might be small due to spin-reversal (a change in kinetic order[88] in the O + CO + M reaction occurs at ≏ 300 torr due to this effect). This scheme could explain the results of experiment (b) but not (a) since at constant $[SO_2]$ and $[M]$, plots of $\ln[O]$ against t would be linear.

An alternative approach would be the possibility of $S\overset{*}{O}_3$ not approaching a steady state under all conditions used in experiments (a) and (b). The scheme would be written:

$$O + SO_2(^1A) + M \overset{1}{\cong} S\overset{*}{O}_3 + M$$

$$O + S\overset{*}{O}_3(^3A) \overset{2}{\cong} SO_2 + O_2$$

whence $[S\overset{*}{O}_3]_{ss} = \frac{k_1}{k_2}[SO_2][M]$. If the steady state is achieved, then $-\frac{d[O]}{dt} = 2k_1[O][SO_2][M]$.

If not $-\frac{d[O]}{dt} = k_1[O][SO_2][M]$

Benson[54] showed that the steady state is achieved only when $[O]_o k_2/k_1[SO_2][M] > 1$, where $[O]_o$ is the initial $[O]$. $S\overset{*}{O}_3$ would need to be in the triplet state and k_2 would need to be 10^9-5×10^{10} $cm^3\ mol^{-1}\ s^{-1}$, whereas for singlet SO_3 formation, k_2 is only about 3×10^7 $cm^3\ mol^{-1}\ s^{-1}$ (cf. Mulcahy et al[84]). However, this scheme can be ruled out by experiments (a) since the slope would necessarily increase with increasing reaction time t (cf. Benson[54]).

The simplest possible scheme, to describe the results

of (a) (b) can, however, now be written;

$$O + SO_2 + M = S\overset{*}{O}_3 + M \qquad (1)$$

$$O + S\overset{*}{O}_3 = SO_2 + O_2 \qquad (2)$$

$$S\overset{*}{O}_3 + M = SO_3 + M \qquad (3)$$

whence $$\left[S\overset{*}{O}_3\right] = \frac{k_1[O][SO_2][M]}{k_2[O]+k_3[M]}$$

$$\therefore \quad -\frac{d[O]}{dt} = k_1[O][SO_2][M]\left\{\frac{2k_2[O]}{k_2[O]} + \frac{k_3[M]}{k_3[M]}\right\}$$

Now, if $k_2[O] >> k_3[M]$, i.e. $\frac{[O]}{[M]} >> k_3/k_2$, $-\frac{d[O]}{dt} = 2k_1[O][SO_2][M]$

but if $k_3[M] >> k_2[O]$ i.e. $\frac{[M]}{[O]} >> \frac{k_2}{k_3}$

then $$-\frac{d[O]}{dt} = k_1[O][SO_2][M]$$

If this latter condition holds under the conditions used in experiments (a) and (b), then the true rate constant $k_{5,Ar}$ (T=295 K) obtained here will be $1.23\pm0.1\times10^{15}$ cm^6 mol^{-2} s^{-1} in excellent agreement with the revised value of Mulcahy[84] but still five times higher than Davis' value. The reason for this discrepancy is unknown.

In one determination of k_{5,SO_2} at 295 K made (Section 7.3) according to kinetic equation 7.2 and the method described there, the plot was not linear but appeared parabolic. The reason for this is unknown at present.

However, the intercepts from the determinations of $k_{5,Ar}$ indicate a mean value of 1.3×10^{16} cm^6 mol^{-2} s^{-1} for

k_{5,SO_2} in excellent agreement with $1.0\pm0.4\times10^{16}$ cm^6 mol^{-2} s^{-1} obtained by Mulcahy et al. The present value is also close to the value $k_{5,SO_2} = 1.4\times10^{16}$ ($M=SO_2$ or NO_2) obtained by Jaffe and Klein[85] from photolytic experiments. This agreement is remarkable considering the great difference between the experimental techniques.

The important role played by reaction (1) in photochemical air pollution and in the chemistry of the stratosphere has been described (Section 1). Any assessment of the 'classical' Chapman[38] scheme depends critically on the value of k_2/k_3, following the O_3 concentration calculations in the stratosphere by Crutzen.[41] A new value[17] of k_3 has recently been determined ($k_3 = 1.05\times10^{-11}\exp -2170/T$ cm^3 mol^{-1} s^{-1}) and a new value of k_2 reported here. Previous calculations of concentrations of O_3 by the classical scheme led to considerably higher values than those observed and it was necessary to postulate catalytic destruction of O_3 by species such as NO_x or HO_x. However, the present value of k_2/k_3 is 2-3 times lower than previously assumed in regions of peak O_3 levels (30 km). Furthermore, recent calculation of diurnal NO_x levels are 5-20 times lower than earlier estimates in this region, mainly due to larger rate constants reported for reactions of the type $NO_x + HO_x$. A brief

reconsideration of the evidence for catalysis in view of these changes can now be made.

According to Crutzen[41] (Section 1), the production (P) and destruction (D) rates of O_3 are given by

$$\frac{d[O_3]}{dt} = 2J_A[O_2] - 2k_3C[O][O_3] = P - DC$$

where the catalytic coefficient (C) is unity in the absence of catalysis and $[O] = \frac{J_B[O_3]}{k_2[O_2][M]}$ to a satisfactory approximation.

The results for k_2, reported here, show that the requirement of catalysis is not invalidated by the use of lower values of the rates k_2/k_3, since the margins of error in the photolysis rate constants J_A/J_B, the assumed O_3 profile, and departure from equilibrium, is still unlikely to be so large above 30 km, according to Crutzen's arguments. Some of the more important catalytic chains to be considered are,

$$\text{Chain 1} \quad \begin{cases} O + NO_2 = NO + O_2 \\ NO + O_3 = NO_2 + O_2 \end{cases} \quad \ldots\ldots \quad (4)$$

$$\text{Chain 2} \quad \begin{cases} O + HO_2 = OH + O_2 \\ OH + O_3 = HO_2 + O_2 \end{cases} \quad \ldots\ldots \quad (5)$$

$$\text{or} \quad \begin{cases} O + HO_2 = OH + O_2 \\ O + OH = H + O_2 \\ H + O_2 + M = HO_2 + M \end{cases}$$

$$\text{Chain 3} \quad \begin{cases} O + OH = H + O_2 \\ H + O_3 = OH + O_2 \end{cases} \quad \ldots\ldots \quad (6)$$

$$\text{Chain 4} \quad \begin{cases} OH + O_3 = HO_2 + O_2 \\ O_3 + HO_2 = OH + 2O_2 \end{cases} \quad \ldots\ldots \quad (7)$$

which leads to

$$C = \left\{ \frac{1 + k_4[NO_2] + k_5[HO_2]}{k_3[O_3]} + \frac{k_6[H] + k_7[OH]}{k_3[O]} \right\}$$

The most important chains are chain 1 between 30-45 km and chain 2 above 40 km. NO_2 concentrations of only $1\text{-}3\times10^9$ molecules cm^{-3} are required to account for all the necessary catalysis between 20-40 km, which is a factor of 2-4 times larger than assumed in the estimation here, Experimental measurements in this range have been reported. However some catalysis by HO_x is required above 40 km. Thus, the catalysis theories are satisfactory with the most recently accepted rate constants and catalyst concentrations. (Notably $k_4 = 9.4\times10^{-12}(300/T)^{0.5}$, (Ref.89), $k_5 = 2.0\times10^{-11}$, $k_6 = 2.6\times10^{-11}$(Ref. 41), and $k_7 = 3.8\times10^{-12}\exp -1250/T$ cm^3 $molecules^{-1}$ s^{-1}(Ref. 90).

The modified and improved discharge-flow method described in this thesis opens up new areas of research. The kinetics and mechanism of the reaction:

$$O + CO + M = CO_2 + M$$

has been the subject of numerous investigations but results are in poor agreement with each other. Some investigators have found the reaction to be second order, while others, report it to be third order over a similar pressure range. Reported values for the rate constant are widely divergent and the reported activation energy ranges from -23.8 to 4.5 kcal mol^{-1}. Earlier work by Clyne and Thrush[8] has shown the relation $I = I_o[O][CO]$ (Section 2) to be valid where I_o which depends on the nature of M, is independent of total pressure in the low pressure region. The present method may be used to measure the rate constant with the following reservations:

a) since the reaction is of the order 10^2 times slower than the $O + O_2$ reaction, pressures of 15-30 torr must be used;

b) flow velocities of the order 50-100 cm s^{-1} and flows of CO 5-10 times higher than for $O + O_2$ measurements are needed;

c) a 'Chance OXI' filter is needed to isolate the u.v. light emission of the blue 'CO_2' glow (Section 2);

d) a discharge (Microwave or otherwise) must be developed capable of providing higher concentrations of $O(^3P)$ than are obtainable by the equipment and conditions described

(Section 2);

e) a carrier gas is needed free of nitrogen (to reduce the amount of air afterglow produced). This may be possible by passing the carrier over lithium metal.

Any wall effects reported by earlier workers using discharge-flow methods do not interfere with the present method. The above precautions will enable the O + CO system to be studied and to provide a reliable value for the rate constant and activation energy, thus helping to establish a 'classical' carbon-oxygen atmosphere for Mars and Venus.

A review of studies of the reaction:

$$O + SO_2 + M = SO_3 + M$$

(Section 7) emphasises the uncertainty in the overall mechanism; a problem which needs to be resolved. Furthermore no results for direct determination of the rate constant at 300 K for M=CO_2, He, N_2 O_2, CO, SO_2 exist at present. In particular, Davis quotes the relative efficiency of SO_2/He as 130 compared to the value 9.5 by Westenberg and de Haas. No direct determination of the temperature coefficient of the reaction has yet been attempted (reports indicate that it is positive). Studies of these reactions can readily be carried out by the present flow method by using smaller reactant gas (SO_2) flows and lower pressures (since the reaction is about 10 times faster at 300 K than the O + O_2 reaction). Difficulties due to water vapour and sulphuric acid droplets in the flow tube are absent in this flow system following the trapping apparatus used (Section 2 and 7).

This method, in general is widely applicable, since it

is suitable for continuous operation (eg. on-line monitoring of pollutants in the lower atmosphere and in the chemical engineering industry). Commercial flow systems can be used to analyse NO_x pollutants at present.

REFERENCES

References

1a G. Herzberg, Spectra of Diatomic Molecules, D. van Nostrand, 2nd. edition, 1951.

1b E. L. Bauer, A Statistical Manual for Chemists, 2nd. edition, Academic Press, (New York), 1971.

2 R. W. Wood, Phil. Mag., 1922, 44, 538.

3 K. F. Bonhoeffer, Z. Physik. Chem., 1925, 116, 391.

4 M. L. Spealman and W. H. Rodebush, J. Amer. Chem. Soc., 1935, 57, 1474.

5 A. G. Gaydon, Proc. Roy. Soc., 1944, 183A, 111.

6 W. D. McGrath and R. G. W. Norrish, Proc. Roy. Soc., 1957, 242A, 265.

7 F. Kaufman, Proc. Roy. Soc., 1958, 247A, 123.

8 M. A. A. Clyne and B. A. Thrush, Proc. Roy. Soc., 1962, 269A, 404.

9 A. Fontijn, A. J. Sabadell and R. J. Ronco, Anal. Chem., 1970, 42, 575.

9a A. Fontijn, C. B. Meyer and H. I. Schiff, J. Chem. Phys., 1964, 40, 64.

10 S. W. Benson and A. E. Axeworthy, J. Chem. Phys., 1957, 26, 1718.

11 E. Castellano and H. Schumacher, Z. Phys. Chem., 1962, 34, 198.

12 S. W. Benson and A. E. Axeworthy, J. Chem. Phys., 1965, 42, 2614.

13 D. Garvin, J. Amer. Chem. Soc., 1954, 76, 1523.

14 W. M. Jones and N. Davidson, J. Amer. Chem. Soc., 1962, 84, 2868.

15 A. Glissman and H. J. Schumacher, Z. Physik. Chem., 1933, 21B, 323.

16 J. A. Zaslowsky, H. B. Urbach, F. Leighton, R. J. Wnuk and J. Wojtowicz, J. Amer. Chem. Soc., 1960, 80, 2682.

16a L. Elias, E. A. Ogryzlo and H. I. Schiff, Can. J. Chem., 1959, 37, 1690.

16b D. S. Hacker, S. A. Marshall and M. Steinberg, J. Chem. Phys., 1961, 35, 1788.

16c C. B. Kretshner and H. L. Peterson, J. Chem. Phys., 1960, 33, 948.

17 J. L. McCrumb and F. Kaufman, J. Chem. Phys., 1972, 57, 1270.

18 F. S. Larkin and B. A. Thrush, Disc. Faraday Soc., 1964, 37, 112.

19 M. A. A. Clyne, B. A. Thrush and R. P. Wayne, Nature, 1963, 199, 1057.

20 W. D. McGrath and R. G. W. Norrish, Proc. Roy. Soc., 1958, 254A, 317.

21 M. A. A. Clyne and B. A. Thrush, Proc. Roy. Soc., 1963, 275A, 544.

22 P. D. Francis, Brit. J. Appl. Phys., 1969, 1717.

23 W. V. Smith, J. Chem. Phys., 1943, 11, 110.

24 J. C. Greaves and J. W. Linnett, Trans. Faraday Soc., 1959, 55, 1338.

25 V. Voevadskii and G. K. Lavrovskaya, Chem. Abs., 1949, 43, 1635.

26 F. Kaufman, Progression Reaction Kinetics, 1961, 1, 1.

27 S. Krongelb and M. Strandberg, J. Chem. Phys., 1959, 31, 1196.

28 J. A. Golden and A. L. Myerson, J. Chem. Phys., 1958, 28, 978.

29 J. E. Morgen and H. I. Schiff, J. Chem. Phys., 1963, 38, 1495.

30 I. M. Cambell and B. A. Thrush, Proc. Roy. Soc., 1967, 296A, 222.

31 H. W. Ford and N. Endow, J. Chem. Phys., 1957, 27, 1156.

32 F. Kaufman, N. J. Gerri and R. E. Bowman, J. Chem. Phys., 1956, 25, 106.

33 P. Harteck, G. Manella and R. R. Reeves, J. Chem. Phys., 1958, 29, 1333.

34 C. J. Halstead and B. A. Thrush, Proc. Roy. Soc., 1966, 295A, 363.

35 M. F. R. Mulcahy, J. R. Steven and J. C. Ward, J. Phys. Chem., 1967, 71, 2124.

36 R. S. Berry and P. A. Lehman, Ann. Rev. Phys. Chem., 1971, 22, 47.

37 P. A. Leighton, Photochemistry of Air Pollution, 1961. Academic Press, New York.

38 S. Chapman, Quart. J. Roy. Meteorol Soc., 1930, 3, 103.

39 B. G. Hunt, J. Geophys. Res., 1966, 5, 1385.

40 J. N. Pitts Jr., A. C. Lloyd and J. L. Spring, Chem. Brit, 1975, 11, 247.

41 P. J. Crutzen, J. Geophys. Res., 1971, 76, 7311.

42 H. Johnson, Science, 1971, August, 517.

43 J. Hampson, Nature, 1974, 250, 189.

44 A. F. Tuck, J. S. Fbot, E. L. Simmons and R. L. Newson, Nature, 1973, 244, 545.

45 A. E. A. Eggleton, R. G. Derwent, J. E. Lovelock and D. H. Pack, Nature, 1975, 255, 118.

46 G. Whittingham, Trans. Faraday Soc., 1948, 44, 141.

47 F. Kaufman and J. R. Kelso, Disc. Faraday Soc., 1964, 37, 26.

48 K. R. Jennings, Quart. Rev., 1961, 15, 237.

49 F. S. Larkin, Can. J. Chem., 1968, 46, 1005.

50 M. F. R. Mulcahy and D. J. Williams, Trans. Faraday Soc., 1968, 64, 59.

51 P. L. T. Bevan and G. R. A. Johnson, J. Chem. Soc. Faraday I, 1973, 69, 216.

52 T. G. Slanger and G. Black, J. Chem. Phys., 1970, 53, 3717, 3722.

53 R. A. Atkinson and R. J. Cvetanovie, J. Phys. Chem., 1971, 55, 659.

54 S. W. Benson, The Foundations of Chemical Kinetics, McGraw-Hill,

55 D. B. Hartley and B. A. Thrush, Proc. Roy. Soc., 1967, 296A, 520.

56 M. A. A. Clyne, D. J. McKenney and B. A. Thrush, Trans. Faraday Soc., 1965, 61, 2701.

57 D. R. Bates and M. Nicolet, J. Geophys. Res., 1950, 55, 301. .

58 L. Elias and H. Schiff, Private Communication with F. Kaufman, Ref. 26.

59 R. E. Huie, J. T. Herron and D. D. Davis, J. Phys. Chem., 1972, 76, 2653.

60 R. J. Donovan, D. Husain and L. J. Kirsch, Trans. Faraday Soc., 1970, 66, 2551.

61 F. Stuhl and H. Niki, J. Chem. Phys., 1971, 55, 3943.

62 J. Bradley, Chemical Applications of the Shock Tube, R.I.C. Lecture Series, 1963, 6.

63 M. A. A. Clyne and R. Walker, J. Chem. Soc., Faraday I, 1973, 1549.

64 K. R. Jennings and J. L. Linnet, Nature, 1958, 182, 597.

65 L. M. Arin and P. Warneck, J. Phys. Chem., 1972, 76, 1514.

66 K. F. Schuler and K. J. Laidler, J. Chem. Phys., 1949, 17, 1212.

67 A. A. Westenberg and N. de Haas, J. Chem. Phys., 1969, 50, 707.

68 G. J. Minkoff and C. F. H. Tipper, Chemistry of Combustion Reactions, Butterwoth's, 1962.

69 A. G. Gaydon and H. G. Wolfhard, Flames - Their Structure, Radiation and Temperature, 3rd. edition, 1970, 197.

70 A. A. Westenberg and R. Fristom, 10th International Symposium on Combustion, The Combustion Institute, 1965, 473.

71 E. M. Bulewicz, C. G. James and T. M. Sugden, Proc. Roy. Soc., 1956, 235A, 89.

72 A. A. Westenberg and R. Fristom, J. Phys. Chem., 1960, 64, 1393; 1961, 65, 591.

73 J. M. Brown and B. A. Thrush, Trans. Faraday Soc., 1967, 63, 630.

74 D. J. Horne and R. G. W. Norrish, Nature, 1967, 215, 1373.

75 H. L. Sandoval, R. Atkinson and J. N. Pitts, J. Photochem., 1974, 3, 325.

76 G. M. Meaburn, D. Perner, J. Lecalve and N. Borene, J. Phys. Chem., 1968, 72, 3920.

77 G. Dixon-Lewis, W. E. Wilson and A. A. Westenberg, J. Chem. Phys., 1966, 44, 2877.

78 F Kaufman and F. P. Del Greco, J. Chem. Phys., 1961, 35, 1895.

79 T. W. Tsang, International J. Chem. Kinetics, 1973, 5, 947.

80 J. V. Muhad and W. A. Payne, J. Chem. Phys., 1976, 65, 4830.

81 M. A. A. Clyne, C. J. Halstead and B. A. Thrush, Proc. Roy. Soc., 1966, 295A, 355, 363.

82 E. R. Allen and R. D. Cadle, Photochem. Photobiol., 1965, 4, 979.

83 M. F. R. Mulcahy, J. R. Steven, J. C. Ward and D. J. Williams, 12th. Symposium on Combustion, 1967.

84 M. F. R. Mulcahy, J. R. Steven and J. C. Ward, J. Phys. Chem., 1967, 71, 2124.

85 S. Jaffe and F. S. Klein, Trans. Faraday Soc., 1966, 62, 2150.

86 C. W. Von Rosenberg Jr. and D. W. Trainor, J. Chem. Phys., 1974, 61, 2442.

87 E. K. Gill and K. J. Laidler, Trans. Faraday Soc., 1959, 55, 753.

88 E. C. Y. Inn, J. Chem. Phys., 1973, 59, 5431.

89 P. P. Bernand, M. A. A. Clyne and R. T. Watson, 3rd. International Symposium on Gas Kinetics, Brussells, 1973.

90 R. C. Whitten and R. P. Turco, J. Geophys. Res., 1974, 79, 1302.

91 M. C. Sauer, J. Phys. Chem., 1967, 71, 3313.

92 M. C. Sauer and L. M. Dorfman, J. Amer. Chem. Soc., 1965, 87, 3801.

93 M. Bass and A. Broida, "Formation and Trapping of Free Radicals", Academic Press, London, 1960, Chapter 3.

94 M. F. R. Mulcahy, "Gas Kinetics", Nelson Press, 1973.

95 J. W. Linnett and D. G. H. Marsden, Proc. Roy. Soc., 1956, 234A, 489, 504.